TÉCNICO LISBOA

Dynamic Simulation of Biodiesel Washing Column

Manuel Peraboa Leite Ramalho Pinho

Thesis to obtain the Master of Science Degree in

Chemical Engineering

Supervisors: Dr. Ana Catarina Gouveia Braz
Dr. José Filipe Oliveira Granjo

Examination Committee

Chairperson: Prof. Sebastião Manuel Tavares da Silva Alves
Supervisor: Dr. Ana Catarina Gouveia Braz
Member of the Committee: Prof. Carla Isabel Costa Pinheiro

November 2021

Declaração

Eu, Manuel Peraboa Leite Ramalho Pinho, aluno do Instituto Superior Técnico nº 84472, autor da dissertação para obtenção do Grau de Mestre em Engenharia Química, com o título ”Dynamic Simulation of Biodiesel Washing Column” concedo ao Instituto Superior Técnico uma licença perpétua, mas não exclusiva, para utilizar esta dissertação para fins de ensino ou investigação e autorizo-o a inseri-la, bem como ao seu resumo alargado, em formato pdf, na sua página da internet, com endereço www.tecnico.ulisboa.pt de modo a permitir a sua divulgação junto de todos os que acedam àquela página, e, com o mesmo propósito de divulgação, a responder favoravelmente aos pedidos de instituições de ensino ou de investigação e Centros de Documentação ou Bibliotecas, remetendo-lhes aqueles mesmos ficheiros em formato pdf, mas fazendo uma expressa menção, seja na sua página na internet seja quando da remessa atrás referida, à obrigação de quem assim aceda àquela minha dissertação e respectivo resumo alargado em salvaguardar os meus direitos de autor sobre estes documentos, que me são conferidos pelo Código do Direito de Autor e dos Direitos Conexos.

Lisboa, a 3 de novembro de 2021

O aluno nº 84472

Acknowledgements

This project would not have been possible without the support of many people.

I would first like to thank my supervisors, Dr. Ana Catarina Braz and Dr. José Granjo, whose knowledge and expertise were crucial to the development of this thesis. Your guidance, patience, and availability were invaluable. I would like to express my sincere gratitude to Professor Carla Pinheiro for all the suggestions and guidance that pointed me in the right direction.

In addition, I would like to thank my parents for all the wise counsel, endless support and care throughout these years. I owe my accomplishments and success to you. To my sister, brother in law, niece and nephew, thank you for always cheering me up.

To my girlfriend, Mariana Cardoso, thank you for all the unconditional love and support. For believing in me during the most stressful and hardest times, and always staying by my side, thank you.

Last but not least, I am extremely grateful to my closest friends, Eduardo Gameiro, João Ribeiro, Rita Pereira and Rui Almeida. You made these last few years a lot more fun and bearable, even during late study nights.

Abstract

This work focuses on the development of a high-fidelity dynamic model of a biodiesel washing column and the implementation of a multivariable control system. Its development was motivated by an increasing occurrence of problems in these columns in industrial biodiesel production units when incorporating higher amounts of waste cooking oil and other low-quality fatty materials. This incorporation causes the formulations of raw oil to change significantly, requiring more process flexibility and adequate control systems to maintain the product within strict quality standards and prevent operational problems. To understand the phenomena occurring inside the washing columns and suggest some corrective measures, a rate-based model of an extraction column was developed in gPROMS® ModelBuilder, describing in detail the mass transfer occurring and the hydrodynamics of the system. The model was validated against data from an industrial unit.

A 2 $\times$ 2 control system was then implemented in Simulink®, consisting of two PI controllers and two decouplers to minimise closed-loop interactions. The behaviour of the extraction column was simulated for the following scenarios: change in biodiesel composition; contamination in biodiesel inlet; and change in glycerol concentration in the washing water. The impact of these disturbances on the column hydrodynamics (e.g., the flooding percentage, phase inversion) and product quality was observed. Finally, the performance of the system in open-loop, closed-loop, and closed-loop with decouplers was compared.

Keywords

Biodiesel, Liquid-liquid extraction, Multivariable control, Rate-based model

Resumo

Neste trabalho é desenvolvido um modelo dinâmico detalhado de uma coluna de lavagem de biodiesel e implementado um sistema de controlo multivariável. O seu desenvolvimento deveu-se à verificação da crescente ocorrência de problemas nestas colunas, nas unidades industriais de biodiesel, ao incorporar maiores quantidades de óleos alimentares usados e outras matérias primas de baixa qualidade. Esta incorporação gera alterações significativas na composição do óleo por processar, exigindo uma maior flexibilidade no processo e, simultaneamente, sistemas de controlo adequados de modo a manter o produto dentro de rigorosos padrões de qualidade e evitar problemas operacionais. Para compreender os fenómenos que ocorrem dentro das colunas de lavagem e sugerir algumas medidas corretivas, foi desenvolvido em gPROMS® ModelBuilder um modelo ”rate-based” de uma coluna de extração, descrevendo em detalhe os fenómenos de transferência de massa e a hidrodinâmica do sistema. O modelo foi validado com dados de uma unidade industrial.

Em seguida, foi implementado em Simulink® um sistema de controlo 2×2, consistindo em dois controladores PI e dois desacopladores de modo a minimizar as interações em cadeia fechada. O comportamento da coluna de extração foi simulado para os seguintes cenários: alteração na composição do biodiesel; contaminação do biodiesel não lavado; e alteração na concentração de glicerol na água de lavagem. Foi observado o impacto destas perturbações na hidrodinâmica da coluna (percentagem de inundação e inversão de fase, por exemplo) bem como na qualidade do produto. Finalmente, foi comparado o desempenho do sistema em cadeia aberta, cadeia fechada, e cadeia fechada com desacopladores.

Palavras Chave

Biodiesel, Extração líquido-líquido, Controlo multivariável, Modelo ”rate-based”

Contents

List of Figures

List of Tables

List of Publications and Communications

Part of the work contained in this thesis has been:

- Presented as a poster entitled ”Dynamic Simulation of Biodiesel Washing Column” at the ”Advanced Process Modelling Forum 2021”
- Preliminarily accepted for a poster communication entitled ”Control of an industrial packed extraction column for biodiesel washing” at the ”32nd European Symposium on Computer-Aided Process Engineering” that will take place in Toulouse from June 12nd and 15th, 2022.
- Incorporated in a manuscript of book chapter for the book series ”Computer Aided Chemical Engineering” that is to be submitted for peer review no later than November 15th, 2021.

Acronyms

Abbreviations

CC	Cohen-Coon
CFPP	Cold Filter Plugging Point (K or °C)
CtN	Cetane Number
CN	Condition Number
CP	Cloud Point (K or °C)
CV	controlled variables
DV	disturbance variables
FAME	Fatty Acid Methyl Esters
FFAs	Free Fatty Acids
GM	Gain Margin
GHG	Greenhouse Gases
IFSH	integrated framework of simulation and heuristics
IMC	Internal Model Control
IAE	Integral of the absolute value of the error
ISE	Integral of the squared error
ITAE	Integral of the time-weighted absolute error
MV	manipulated variables
PM	Phase Margin (°)
PP	Pour Point (K or °C)
PWC	plantwide control
RGA	Relative Gain Array
SVA	Singular Value Analysis
UCO	used cooking oils
ZN	Ziegler-Nichols

Greek Symbols

α	flow channel angle in packed bed (°) or parameter used to determine viscosity
β	parameter used to determine viscosity
χ	phase inversion parameter
ε	void fraction of packed bed (-)
γ	parameter used to determine viscosity
μ	dynamic viscosity ($Pa \cdots$)
ϕ	fractional volumetric hold-up (-)
ψ_{mF}	resistance coefficient for single-pahse flow (-)

ρ density (kg/m^3)

σ interfacial tension (N/m)

ξ parameters used to calculate viscosity

Constants

g Gravitational Constant 6.67408$\times 10^1 1$ $m^3 kg^{-1} s^{-2}$

R Ideal Gas Constant 8.314 $J/(molK)$

Latin Symbols

a_I specific contact area (m^2/m^3)

a^M, b^M, c^M parameters of the modified Misek correlation

A_k, B_k, C_k parameters to calculate the molar volume

$A_{1k}, B_{1k}, C_{1k}, A_{2k}, B_{2k}, C_{2k}$ parameters to calculate the viscosity

a_p specific packing surface area (m^2/m^3)

a_w specific wall surface (m^2/m_3)

$B_{1,k}, B_{2,k}$ temperature dependency correlation parameters ($kmol/m^3$ and K^-1)

C concentration (kg/m^3)

$C_{1i}, C_{2i}, C_{3i}, C_{4i}, C_{5i}$ constants for the DIPPR viscosity model

d diameter (m)

d_{32} Sauter mean drop diameter (m)

$\mathscr{D}$ diffusivity coefficient ()

d_{in} column internal diameter (m)

E axial dispersion coefficient

f_0, f_1 optimised constants to calculate the viscosity

$\%Fl$ flooding percentage

H_{so} dimensionless group proportional to coalescence velocity

k mass transfer coefficient (m/s)

K partition coefficient

L height (m)

$L_{\textbf{dead-zone}}$ height of the dead-zone (m)

$L_{\textbf{int}}$ interface level (m)

$L_{\textbf{packing}}$ height of the packing (m)

$m_{dc}^{\textbf{vol}}$ slope of the equilibrium line between two phases

m mass transfer direction parameter

MW molar weight

N_C weighted-average number of carbon atoms

N_{cs} number of carbons of the short-chain alcohol

N_{DB} weighted-average number of double bonds

$N_{\textbf{frag}}$ number of fragments in the component

n number of groups/molecules

P dimensionless group to calculate Re

P_c critical pressure (Pa)

Q correction term

q function of the absolute temperature

$Re_{\textbf{Stokes}}$ Reynolds number

s_0, s_1 optimised constants to calculate the viscosity

t time (s)

T_c critical temperature (°C)

T_f flash point (°C)

T_r reduced temperature (°C)

u_t terminal velocity of a droplet

$U_{\textbf{FAME}}$ total unsaturated FAME content (wt %)

V superficial phase velocity (m/s)

V_c critical volume (m^3)

V_{cF} flooding velocity (m/s)

V_L molar volume (m^3/mol)

$V_{\textbf{slip}}$ slip velocity (m/s)

V_{so} slip velocity at low dispersed-phase flow rate (m/s)

V_i interstitial phase velocity (m/s)

Δv molar group

x molar fraction

We Weber number

w mass fraction

$\bar{w}_s$ middle rising or falling velocity of single velocity in packing bed (m/s)

z coordinate

Z_m^{RA} critical compressibility factor

Subscripts and Superscripts

avg average

c,C continuous phase

d,D dispersed phase

i,j component

in inlet

out outlet

mix mixture

p particle

f phase

L light phase

H heavy phase

k group of components

org,organic organic phase

aq,aqueous aqueous phase

***** equilibrium

1

Introduction

Contents

1.1 Background

Biodiesel, Fatty Acid Methyl Esters (FAME), is a widely marketed biofuel produced from the transesterification of vegetable oils, frying oils, animal fats, or from the esterification of fatty acids.

Biodiesel's ability to find new uses for fats and oils makes it an ideal biofuel, reducing emissions of carbon dioxide, total hydrocarbon, and particulate matter of 15 % for a 20 % biodiesel incorporation blend (B20) compared to petroleum [1, 2]. Other environmental benefits regarding the usage of biodiesel include reduction of lifecycle Greenhouse Gases (GHG) emissions from 66 to 94 % when compared to petroleum diesel [3] — the carbon dioxide released from the biodiesel combustion is offset by the carbon dioxide absorbed during the growth of the feedstock [4]. For example, the production of biodiesel from soybean oil, instead of low-sulphur diesel from crude oil diesel, generates less 78 % carbon dioxide, less 79 % wastewater and less 96 % hazardous waste [3].

The positive impacts of biodiesel are not only environmental but also economic. Second and third generation biofuels can be produced using marginal land, having a significant potential to reduce GHG emissions as well [5, 6]. Additionally, the biofuel industry can provide new labour and market opportunities for domestic crops [5–7], reducing a country's dependency on crude oil imports and supporting agriculture [5, 7], add value to the feedstock, increase the number of rural manufacturing jobs, increase income in taxes, and investments in new plants and equipments [7].

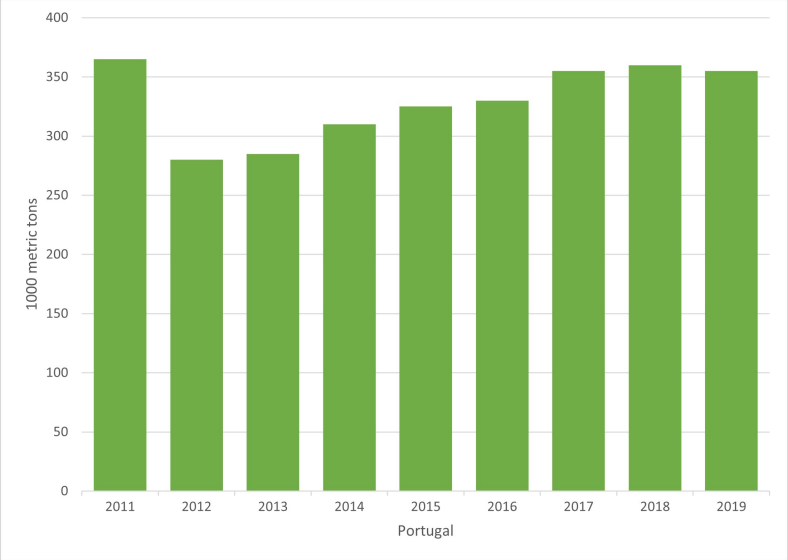

Figure 1.1: Biodiesel annual production in Portugal (1000 metric tons) from 2011 to 2019 [8].

The environmental and economic importance of biodiesel has resulted in an increased production in recent years. The biodiesel production in Portugal has been growing, Figure 1.1, and between 2013 to 2019 had an average annual growth rate of 4.07 % [8]. This growth is even more pronounced worldwide, with an average annual growth rate of 7.84% from 2013 to 2019 [8], as it can be seen in Figure 1.2.

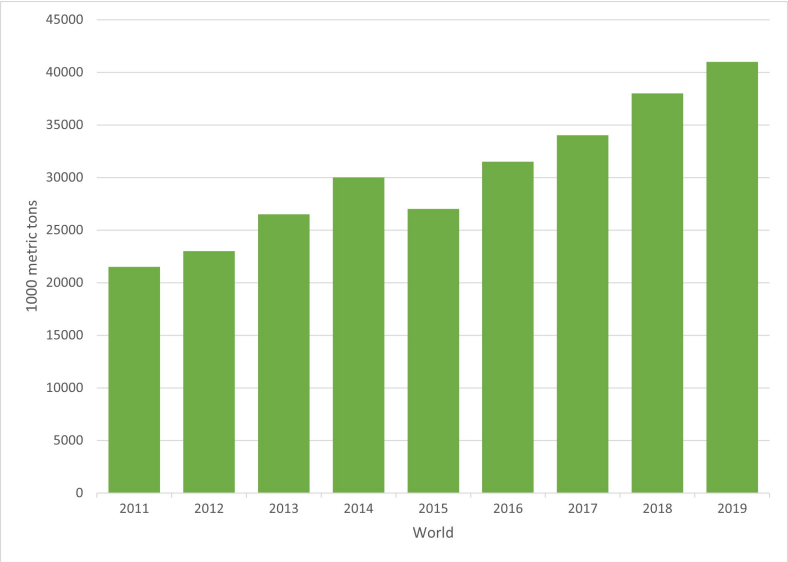

Figure 1.2: Biodiesel annual production worldwide (1000 metric tons) from 2011 to 2019 [8].

However, there are some drawbacks to this alternative fuel. The cost of feedstock is a major economic factor in the viability of biodiesel production, which is usually about 75 – 80 % of the total operating cost [7]. Also, using these oils to produce biodiesel instead of using them for alimentary purposes is ethically questionable.

The incorporation of used cooking oils (UCO) can greatly reduce the total manufacturing cost of biodiesel, since it is 2.5 to 3.5 times cheaper than virgin vegetable oils [7]. Hence, the quantity of UCO used as feedstock in the European Union has been growing in the last years [9, 10], see Figure 1.3.

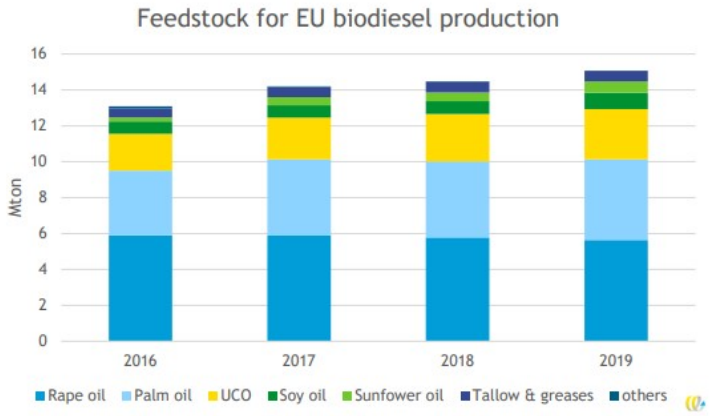

Figure 1.3: Feedstock for EU biodiesel production (in Mton) [9].

The usage of UCO adds value to waste cooking oil that otherwise would have to be processed.

1.2 Biodiesel Production

Biodiesel production processes can be divided in three main steps:

1. Feedstock pretreatment
2. Reactions
3. Product Purification

Starting with the pretreatment, this stage involves reducing the quantity of water, phospholipids, suspended particles, polymers, and Free Fatty Acids (FFAs) [11]. Water is removed because it promotes the formation of soaps during alkaline transesterification, which then can solidify and clog lines that result in forced shutdowns [11]. Phospholipids, polymers and particulates in oil feedstock impact negatively on the biodiesel production process as they promote the destruction of the catalyst and can also hinder phase separation of oil/glycerol phases. Refining removes the phospholipids and FFAs from the crude oil [12]. This is a crucial step because some phospholipids are strong emulsifiers that will inhibit the separation of the soaps, and lower the yield in neutral oil, during the alkali neutralization step. Additionally, phospholipids will also react with water and form insoluble sediments that are undesirable. Following the refining process is the bleaching process. Here the main objective is to remove the color pigments from the oil as well as remove the remaining soap, phospholipids, trace metals and sulphur compounds [12].

After the pretreatment is the reaction section. Biodiesel is produced by the transesterification of triglycerides with short-chain alcohols in the presence of a catalyst, as presented in Figure 1.4. This

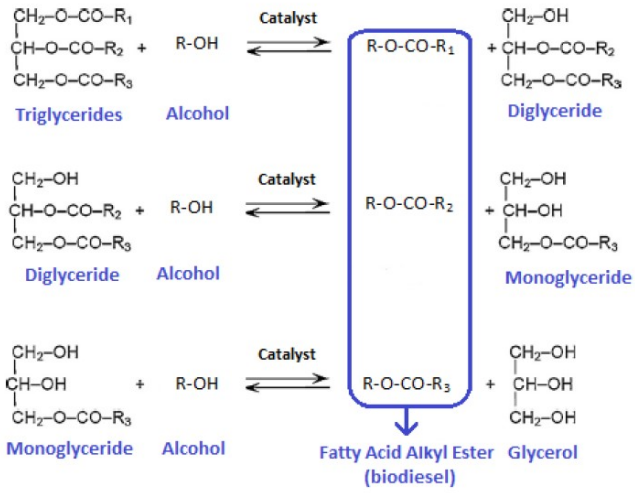

Figure 1.4: Transesterification reaction [13].

catalyst can either be homogeneous or heterogeneous, and its nature acidic, alkaline or enzymatic. Homogeneous catalysts can minimise the mass transfer resistance, when compared to heterogeneous

catalysts, however their separation is more laborious. Focusing on the nature of the catalyst, the most used ones are alkaline, usually made of sodium hydroxide (NaOH) and potassium hydroxide (KOH) that are easily soluble in methanol [13]. These catalysts have higher reaction rates than acidic ones, resulting in higher biodiesel yields achieved in shorter reaction times. On the other hand, they are more sensitive to feedstock purity, particularly to low grade fats that contain higher concentrations of FFAs and water. A block diagram of the alkaline biodiesel production process is illustrated in Figure 1.5.

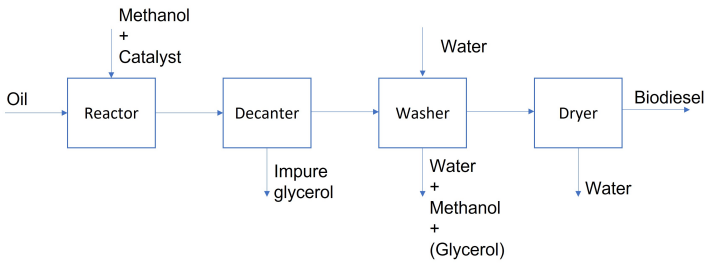

Figure 1.5: Block diagram of the alkaline biodiesel production process.

Finally, after the transesterification reaction, the biodiesel must be purified to reduce the concentration of glycerol, methanol and water. The post reaction processing focusses on the recovery of the esters from the reaction mixture and the necessary refining to meet the quality specifications ASTM D6751 or EN14214 [13, 14]. The first step is usually the ester/glycerol separation. Here, the difference in densities between the ester and glycerol phases is the driving force of this separation, which happens because the fatty acid alcohol esters and glycerol are sparingly mutually soluble [12]. However, the presence of methanol in one or both phases affects the solubility of ester in glycerol and vice versa. This step is typically achieved in decanters, centrifuges or hydrocyclones [12].

After removing the majority of the glycerol, the biodiesel is washed. Water washing is a simple and efficient method that produces biodiesel with high purity. Here, water is added to the esters to eliminate the remaining glycerol, methanol, catalyst (if the transesterification had an homogeneous catalyst) and any soaps that might have formed during the reaction due to their solubility in water [13]. The usage of warm water (between 45 to 60 °C) prevents the precipitation of saturated fatty acid esters [12], and also retards the formation of emulsions with the usage of a gentle washing action [14]. This step can be achieved with a liquid-liquid extraction column.

Lastly, the biodiesel needs to be dehydrated. Usually this operation is accomplished with a dryer. This system operates at a highly reduced pressure that allows the water to evaporate at much lower temperatures. This is a crucial measure since high temperatures can darken the fuel which is a sign that the polyunsaturated methyl esters are polymerizing. In order to reduce the amount of wastewater produced, equipments such as molecular sieves and silica gels can be used to remove the water instead of the ester washing and drying operations.

1.3 Problem Statement

A recent trend in the biodiesel industry is the increasing incorporation of waste cooking oil and other low-quality fatty materials, motivated by economic and regulatory factors. This trend causes the formulations of raw oil to change significantly, requiring more process flexibility and adequate control systems to maintain the product within strict quality standards and prevent operational problems. In the homogeneous alkali processes, currently the most common in the industry, the separation stage includes the water washing of biodiesel to extend the removal of glycerol, methanol, and acylglycerols [15, 16]. This operation is accomplished in an extraction column. In practice, subtle changes in the oil composition (i.e., incomplete reaction, soaps, or fine solids in suspension) can promote the formation of stable emulsions that need to be handled before causing shutdowns and extra manufacturing costs. Consequently, a high-fidelity dynamic model of the extraction column is valuable for control and troubleshooting.

1.4 Objectives

The objectives of this work are the development of a high-fidelity dynamic model of an industrial extraction column capable of capturing key physical phenomena occurring in this equipment unit; the validation of the extraction column model with industrial data; and lastly, the implementation of a robust control system to keep the product within quality standards, and to prevent operational problems.

1.5 Structure of the Thesis

This thesis is divided into five chapters. The first chapter is the introduction of the work with a focus on the biodiesel industry. Entering the second chapter, the focus of the thesis shifts towards liquid-liquid extraction, where the developed model is described, and afterwords in the third chapter, its validation is presented and also a sensitivity analysis is shown. Chapter four consists of the control of the extraction column, where the different control systems are presented and compared with each other. Finally, chapter five is the conclusion and a perspective for future work is shown.

2

Model Development

Contents

In this chapter, the packed column model is presented. First, an overview of a liquid-liquid extraction column is shown with an emphasis on biodiesel washing processes. The most common mathematical approaches used to model these columns is presented and the rate-based model is further analysed since it was the one used. Finally, the used correlations to predict the equilibrium, mass-transfer and hydrodynamic behaviour of the column are shown.

2.1 Liquid-liquid Extraction Column

Liquid-liquid extraction operations require equipment that promotes the contact between two liquid phases in order to guarantee an efficient solute transfer [17]. This is accomplished by dispersing one liquid (the dispersed phase) into the other (the continuous phase), which increases the specific area for mass transfer. The higher-density liquid enters at the top and is usually the continuous phase, while the lower-density fluid enters at the bottom of the stage/column and is the dispersed phase.

Liquid-liquid extraction columns can be static or pulsed. The former rely on gravity and density difference to function, however, for systems with similar densities and high interfacial tensions the latter are recommended. The most used static columns are sieve-tray, packed, and atomization columns. Scheibel, Kühni, and rotating disc columns are the three most used pulsed columns. The static columns have the following advantages: they can have larger diameters for higher productivity, and are simpler to operate; and disadvantage: lower mass transfer efficiency (for the atomization columns), specially for systems with low viscosities ($<$ 5 cP) and low interfacial tensions (between 0.003 and 0.02 N/m) [17]. The pulsed columns usually have a higher mass transfer efficiency due to an improved dispersion that results from the mechanical agitation of the fluids. Liquid-liquid extraction columns are the most used and efficient equipment for biodiesel washing.

A thorough understanding of the extraction column requires an understanding of the different physicochemical mechanisms that occur during extraction, see Figure 2.1.

Succinctly, some crucial aspects of these phenomena will be presented [18]. The phase equilibrium shows the difference of equilibrium and local composition of the components, which is a measure of the maximum driving-force for mass transfer and the limit of extraction. The droplets in static extractors result from the dispersed phase flowing through the atomisers in column trays. Droplet diameter indicates the interfacial area available for mass transfer, coalescence velocity, and also the efficiency of the internal circulation of the solutes in the droplets. Holdup is defined as the volumetric fraction of the dispersed phase inside the extractor.

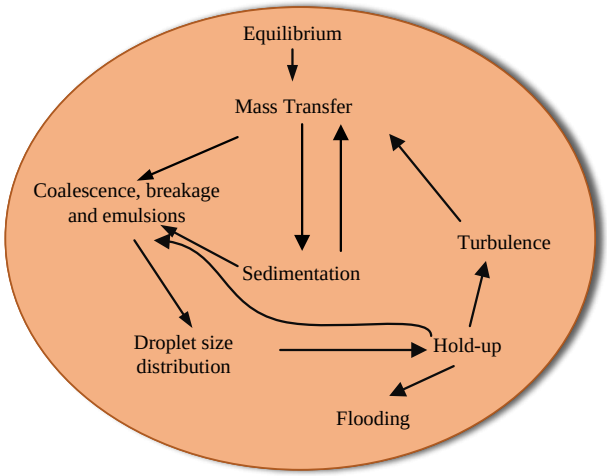

Figure 2.1: Scheme of the main phenomena related to extraction and their relations.

The coalescence of droplets can occur through collision or absorption and produces a larger droplet that could be present in a settled layer, droplet aggregate or isolated droplets. The formation of unstable emulsions is a key factor to have an efficient mass transfer during extraction, and then followed by a quick coalescence to guarantee liquid-liquid separation after extraction. That is, there should be a balance between the coalescence and breakage velocities.

2.2 Mathematical Approaches

There are different mathematical approaches to model a liquid-liquid extraction column, three of which are briefly explained in this section.

2.2.1 Equilibrium-based

The equilibrium-based is a stagewise model. Here, the column is described as a series of completely mixed stages and the mathematical equations are developed based on the principle of mass conservation applied to each stage [19]. These equations, when combined together for a counter-current cascade of stages (see Figure 2.2), are called the MESH equations. These were developed by Wang and Henke (1966) [20], and are a rigorous method to describe phase-equilibria in a column that can be modified and applied to a liquid-liquid extraction column [20, 21].

There are three main approaches for the equilibrium-based approach [20], these are the following: 1. Phase equilibrium is achieved at each stage; 2. There are no chemical reactions; 3. Complete separation of the two liquid phases.

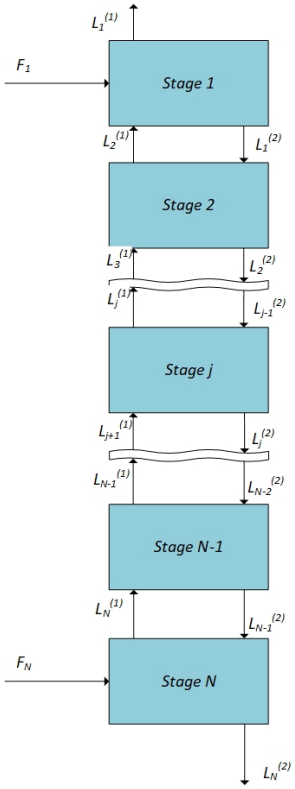

Figure 2.2: General counter-current cascade of *N* stages.

2.2.2 Rate-based

Rate-based models also use mass and heat transfer phenomena to describe the process.

The energy and mass conservation equations for each phase are connected by energy and mass balances at the interface, which is assumed to be at thermodynamic equilibrium. The differential equations are numerically integrated for the total packed height [22]. Phase-equilibrium only occurs at the interface, with mass and energy transfer being described with rate equations and transfer coefficients. Figure 2.3 illustrates the interface mass transfer phenomenon. It is assumed that all resistance to mass and energy transfer is located adjacent to the phase boundary.

With this model, the hydrodynamics of the column can be described by a broad variety of correlations for the holdup, flooding, coalescence velocity, interfacial area, and interface level, for example.

It is assumed that each phase is completely mixed in each segment [23].

According to [19], the differential models that describe liquid-liquid extraction columns can be classified as pseudo-homogeneous or population balance dispersion models. These models are obtained by formulating differential conservation equations for the continuous and dispersed phases inside a column. The mentioned methods differ in describing the dispersed phase.

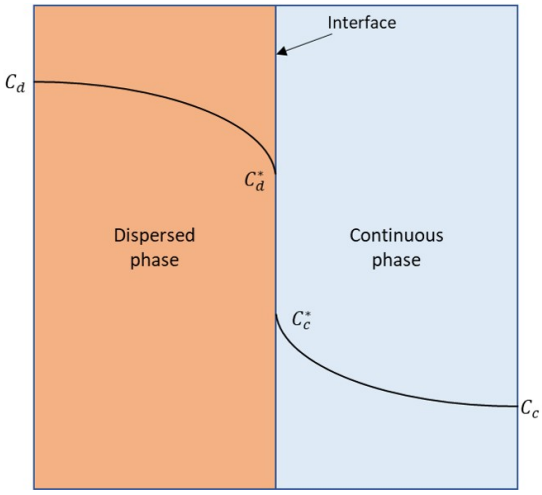

Figure 2.3: Concentration profiles in the region close to the interface during interphase mass transfer.

The pseudo-homogeneous dispersion model can be applied to single phase and dispersed multi-phase systems and it is based on the principles of physico-chemical laws. The system, exemplified in Figure 2.4, is represented as a continuum with the dispersed phase treated as pseudo-homogeneous [19].

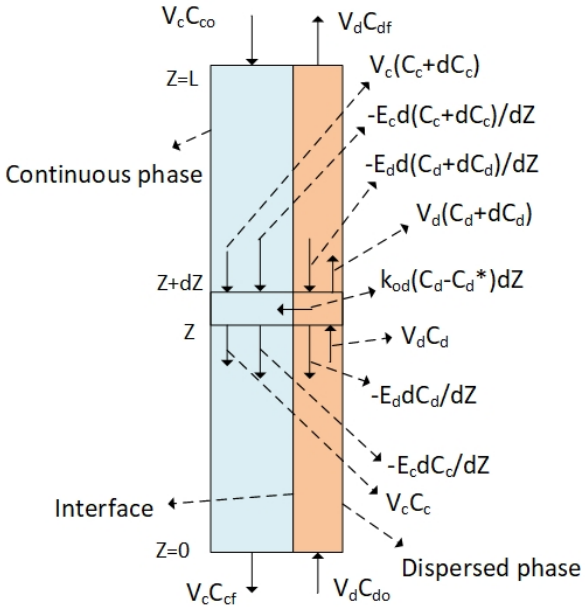

Figure 2.4: Pseudo-homogeneous dispersion model.

2.2.3 Population Balance

Population balance modelling is based on population balance equations, which are expressed by a set of integro-partial differential equations to describe the behaviour of a population of particles [24] and its environment from the behaviour of single particles in their local environments [25]. The population is described by the density of a suitable extensive variable, usually the number of particles (drops in this case) but sometimes by other variables such as mass or volume of these particles [25]. The drop population balance model for an extraction column is illustrated in Figure 2.5.

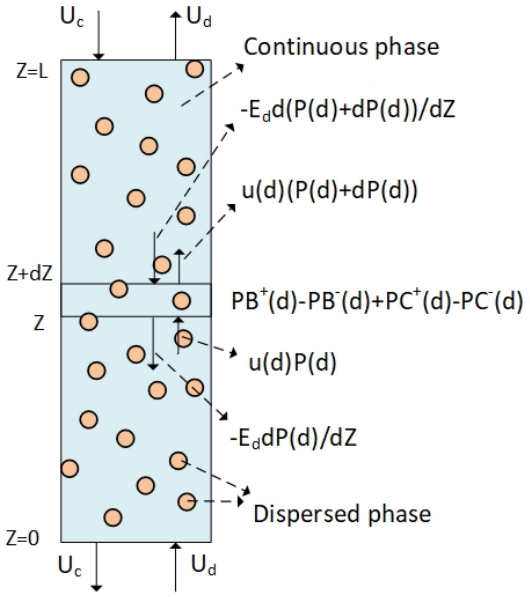

Figure 2.5: Differential drop population model for a column.

This type of model can be characterised with: 1. Hydrodynamic Equations: that describe the continuous phase with a plug-flow model, the dispersed phase flowrate through a differential equation of drop breakage and coalescence; 2. Drop Transport Equations: describing each drop individually, for a given diameter and height, and also accounts with the influence of the other drops; 3. Axial Mixing: equations that require experimental data for both phases; 4. Drop Breakage: describes the breakage rate of drops; 5. Drop Coalescence: describer the coalescence phenomenon due to random collision and due to absorption.

2.3 Model Development of the Extraction Column

A simplified diagram of the packed column is illustrated in Figure 2.6. Here, the higher-density liquid, water, enters at the top of column, while the lower-density fluid, biodiesel, enters at the bottom. In this system biodiesel is the dispersed phase so its droplets rise through the column always in contact with

the continuous-phase, water. The droplets build up and form the interface where mass transfer occur, as explained before. The washed biodiesel leaves the column at the top and then goes to the drying unit in the plant, while the washing water that leaves the column needs to be treated.

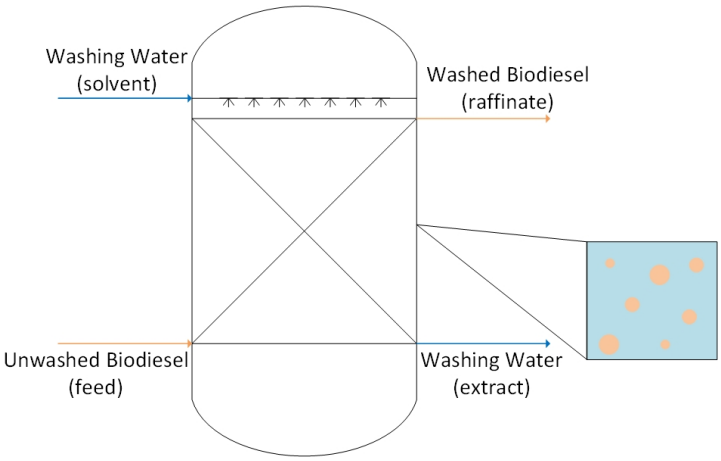

Figure 2.6: Simplified example of the packed liquid-liquid extraction column for the system biodiesel/water with a section of the column.

For the construction of this dynamic model, the following assumptions and simplifications were adopted [22]:

- Type of model: The rate-based model is considered to be the most appropriate approach to model this system. The equilibrium-based approach corrected with packing efficiencies is not adequate to describe multicomponent systems, and the complexity of mass transfer and hydrodynamic phenomena is not accurately simulated.

- Column Operation: The column operates adiabatically and the heat balances were not considered since it was only interesting to analyse the impact of temperature on the solubilities of the solutes.

The list of parameters and variables used in this section is presented in Table 2.1.

Table 2.1: Lis of parameters and variables used to describe the model.

Parameters	Variables
a_I, a_p, a_w	C_c, C_d
d_{in}, ε, u_d^{in}, u_c^{in}	ϕ_c, ϕ_d
C_c^0, C_d^0, C_c^{in}, C_d^{in}	E_c, E_d
g, R	V_c, V_d, V_{ic}, V_{cF}, V_{dF}
μ_w	k_{od}, k_c, k_d
L_{packing}, $L_{\text{dead-zone}}$	ρ_c, ρ_{mix}, μ_c, μ_d
D, Vol	m_{dc}^{vol}
m, α, ψ_{mf}	V_{slip}, V_{so}
q, N_C, N_{DB}, U_{FAME}	D_c
CtN_{BDF}, T_f, CP, PP, $CFPP$	V_{so}, H_{so}, P
a_i^M, b_i^M, c_i^M	Re, Re_{stokes}, Re_{cdp}
T, T_c, T_r	σ
MW_i, V_{Li}, n_{ik}, A_k, B_k, C_k, N_{frag}	u_t
B_{1k}, B_{2k}	We_c
Z_m^{RA}, P_c, V_{Li}^{Rackett}	L_{int}
N_k, A_{1k}, B_{1k}, C_{1k}, A_{2k}, B_{2k}, C_{2k}	$\bar{w}_s$, $\%Fl_C$, $\%Fl_D$
ξ_1, ξ_2, α, β, γ	χ, ρ_L, ρ_H, μ_L, μ_H, ϕ_L, ϕ_H
f_0, f_1, s_0, s_1	K_i, w_i^{aq}, w_i^{bd},
C_{1i}, C_{2i}, C_{3i}, C_{4i}, C_{5i}	x_i, ρ_{mix}, μ_{mix}, x_{fi}, μ_{fi}
A_{w0}, q_i, Q_k	
X, K	
c_{diff_i}, V_{A_i}	

2.3.1 Equations

The general unsteady state mass balance equations for the continuous and dispersed phases are represented in Equations 2.1 and 2.2, respectively [19].

$$\frac{\partial(C_c\phi_c)}{\partial t} = V_c\frac{\partial(C_c)}{\partial z} + E_c\phi_c\frac{\partial^2(C_c)}{\partial z^2} - k_{od}a_I(C_d^* - C_d) \tag{2.1}$$

$$\frac{\partial(C_d\phi_d)}{\partial t} = -V_d\frac{\partial(C_d)}{\partial z} + E_d\phi_d\frac{\partial^2(C_d)}{\partial z^2} + k_{od}a_I(C_d^* - C_d) \tag{2.2}$$

Where z is measured in the direction of flow of the dispersed phase; the subscripts c and d refer to the continuous and dispersed phases, respectively, V is the superficial phase velocity (m/s), E is the axial dispersion coefficient (m^2/s), a_I is the specific contact area (m^2/m^3), ϕ_d is the volume fraction

holdup, ϕ_c is $1 - \phi_d$ and k_{od} is the overall mass transfer coefficient based on the dispersed phase (m/s). Gayler and Pratt (1957) showed that backmixing of the dispersed phase does not occur [26]. Forward dispersion, however, is observed and happens due to differing droplet sizes and velocity but because of high coalescence and breakage rate in packed columns this is not as important as continuous phase backmixing [26]. Thus, $E_d = 0$.

The boundary conditions for this system are:

- $z = 0$

$$C_d^{in} u_d^{in} = \phi_d V_d C_d \tag{2.3}$$

$$\frac{\partial(\phi_c V_c C_c)}{\partial z} = 0 \tag{2.4}$$

- $z = L$

$$\frac{\partial(\phi_d V_d C_d)}{\partial z} = 0 \tag{2.5}$$

$$C_c^{in} u_c^{in} = \phi_c V_c C_c + E_c \frac{\partial(\phi_c C_c)}{\partial z} \tag{2.6}$$

These boundary conditions are the result from material balances across the system's boundaries and it is assumed that dispersion occurs only between $z = 0^+$ and $z = L^-$ [27].

The initial conditions are:

$$0 = V_c \frac{\partial(C_c)}{\partial z} + E_c \phi_c \frac{\partial^2(C_c)}{\partial z^2} - k_{od} a_I (C_d^* - C_d) \tag{2.7}$$

$$0 = -V_d \frac{\partial(C_d)}{\partial z} + E_d \phi_d \frac{\partial^2(C_d)}{\partial z^2} + k_{od} a_I (C_d^* - C_d) \tag{2.8}$$

For Equations 2.1 and 2.2, the volume fraction holdup was calculated with Equation (2.14) and the axial dispersion coefficient for the continuous phase was obtained with the Becker Axial Mixing Model correlation [18] for structured packed columns, Equation (2.9).

$$\frac{E_c \rho_c}{\mu_c} = (405.1 \mathrm{Re}_c^{0.798} + 27.7 \mathrm{Re}_d^{0.914}) \left(\frac{d_{\mathrm{in}}}{100}\right)^{1.178} \tag{2.9}$$

Where d_{in} is the column internal diameter (cm),

$$\mathrm{Re}_c = \frac{V_{ic} \rho_c}{\mu_c (a_p + a_w)}$$

$$a_w = \frac{4}{d_{\mathrm{in}}}$$

$$\text{Re}_d = \frac{V_{ic} d_p \rho_c}{\mu_c}$$

V_{ic} is the interstitial velocity of the continuous phase (m/s), a_w is the specific wall surface (m^2/m^3), ρ_f is the density of phase f calculated in subsection 2.4.2 and μ_f is the dynamic viscosity of phase f whose correlations are presented in subsection 2.4.3. The relation between V_{ic} and V_c is given by:

$$V_{ic} = \frac{V_c}{\varepsilon(1-\phi_d)} \tag{2.10}$$

The overall mass-transfer coefficient was calculated with the following equation:

$$\frac{1}{k_{od}} = \frac{1}{k_d} + \frac{m_{dc}^{\text{vol}}}{k_c} \tag{2.11}$$

where $m_{dc}^{\text{vol}} = dC_d/dC_c$ is the slope of the equilibrium line expressed in volumetric concentration units and exemplified in Figure 2.7, k_d and k_c are the dispersed- and continuous-phase film coefficients, respectively, and were calculated with Equations 2.12 (the Handlos and Baron model), and 2.13 for non-rigid drops in packing columns. V_{slip} is the slip velocity [18].

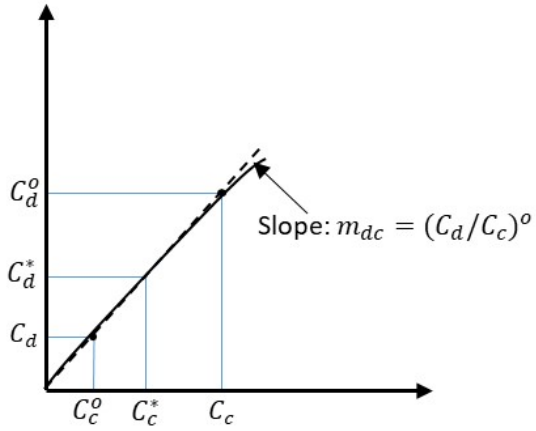

Figure 2.7: Slope m_{dc}.

In Figure 2.7, the superscript o denotes equilibrium.

$$k_d = \frac{0.00375 V_{\text{slip}}}{1 + \mu_d/\mu_c} \tag{2.12}$$

$$k_c = 0.698 \left(\frac{\mathscr{D}_c}{d_p}\right) \left(\frac{d_p V_{\text{slip}} \rho_c}{\mu_c}\right)^{0.5} \left(\frac{\mu_c}{\rho_c \mathscr{D}_c}\right)^{0.4} (1-\phi_d) \tag{2.13}$$

The diffusivity coefficient, $\mathscr{D}$ was estimated with the correlation present in subsection 2.4.5.

2.3.2 Holdup and Interface Level

Holdup, ϕ_D, in packed columns is known as the volume of the dispersed phase expressed as a fraction of the void space in the packed section [18].

This variable can be predicted using the slip velocity concept, presented by Gayler *et al.* (1953), which is defined as the dispersed phase droplet velocity relative to the moving continuous phase [26].

For a static extractor, the holdup can be calculated using the following expression [18]:

$$\phi_d = \frac{V_d[cos(\pi \frac{a_p d_p}{2}/4)]^{-2}}{\varepsilon[V_{so}\text{exp}(\frac{-6\phi_d}{\pi}) - \frac{V_c}{\varepsilon}(1-\phi_d)]} \tag{2.14}$$

where the subscripts c and d are relative to the continuous and dispersed phases, respectively, V_{so} is the slip velocity at low dispersed-phase flow rate (m/s), V is the liquid velocity (m/s), a_p is the specific packing surface area (m^2/m^3), d_p is the Sauter mean drop diameter and ε is the void fraction. The equations needed to calculate these variables are presented below.

Table 2.2: Equations to calculate the slip velocity, V_{so} in static extractors.

Equations to calculate V_{so}	Conditions
$V_{so} = \frac{\Delta\rho g d_p^2}{18\mu_c}$	$Re_{\text{Stokes}} < 2$
$V_{so} = \frac{Re\mu_c}{d_p\rho_c}$	$Re_{\text{Stokes}} > 2$

$$\text{Re}_{\text{Stokes}} = \frac{\rho_c \Delta\rho g d_p^3}{18\mu_c^2} \tag{2.15}$$

Table 2.3: Correlations to calculate Re.

Correlations to calculate Re	Conditions
$\frac{Re}{P^{0.149}} = 0.94H_{so}^{0.757} - 0.857$	$H_{so} \leq 59.3$
$\frac{Re}{P^{0.149}} = 3.42H_{so}^{0.441} - 0.857$	$H_{so} > 59.3$

$$P = \frac{\rho_c^2 \sigma^3}{\mu_c^4 g \Delta\rho} \tag{2.16}$$

$$H_{so} = \left(\frac{4d_p^2 g\Delta\rho}{3\sigma}\right)\left(\frac{\mu_w}{\mu_c}\right)^{0,14} P^{0,149} \tag{2.17}$$

Where μ is the liquid viscosity (Pa·s), μ_w is the reference viscosity of water (Pa·s), ρ is the liquid density (kg/m^3), σ is the interfacial tension (N/m) estimated in subsection 2.4.4, g is the gravitational acceleration of 9,807 m/s^2 and P and H_{so} are dimensionless groups. The terminal velocity of a droplet, u_t, is given by:

$$u_t = \frac{\mu_c Re}{\rho_c d_p} \tag{2.18}$$

It is important to note that when H_{so} is higher than 59.3, the terminal velocity stops increasing with the diameter because of the deformation of the droplets. If the diameter continues to increase, the flow becomes more oscillatory and irregular, shown in Figure 2.8. This phenomenon negatively impacts the movement of the droplet and promotes the formation of aggregates in the dispersion zone of the column, leading to backmixing and lower separation efficiencies. On the other hand, smaller droplets have a similar behaviour as rigid spheres ($H_{so} < 2$) with no internal circulation, which undermines the advantages of having a high interfacial area available for mass transfer (see Figure 2.8). So, the ideal Sauter mean diameter of the droplets of the dispersed phase should be large enough to guarantee a decent terminal velocity, and small enough to ensure a high interfacial area for mass transfer.

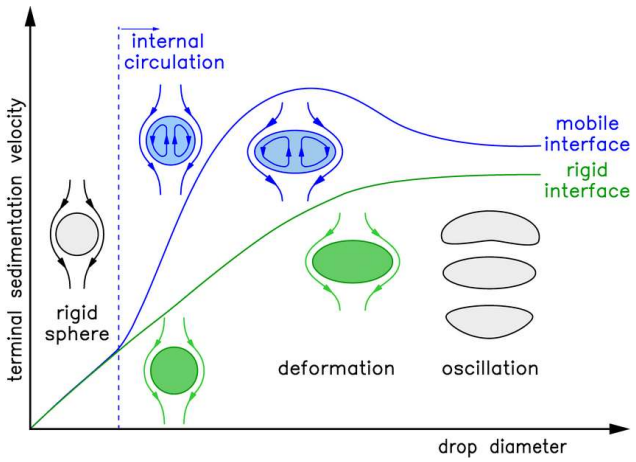

Figure 2.8: Terminal velocity of a droplet relative to its diameter [28].

The Sauter mean diameter of the drop, d_p, is obtained with Equation (2.19) for structured packing [18].

$$d_p = 0.12 \frac{4}{a_p} \mathrm{We}_c^{-0.5} \mathrm{Re}_{c_{dp}}^{0.15} \tag{2.19}$$

where

$$\mathrm{Re}_{c_{dp}} = \frac{4\rho_c V_{\mathrm{slip}}}{\mu_c a_p}$$

$$We_c = \frac{4\rho_c V_{\text{slip}}^2}{\sigma a_p}$$

V_{slip} and V_{so} have the following relation:

$$V_{\text{slip}} = V_{so} exp\left(\frac{-6\phi_d}{\pi}\right) cos\left(\pi \frac{a_p d_p}{2}/4\right) + \left(cos\left(\pi \frac{a_p d_p}{2}/4\right)\right) V_c \tag{2.20}$$

The interface level, L_{int}, is calculated with Equation (2.21).

$$L_{\text{int}} = L_{\text{packing}} + 1.6 - \frac{\phi_L \text{Vol}}{0.9\pi(D/2)^2} L_{\text{dead-zone}} \tag{2.21}$$

where L_{packing} is the height of the packing, 1.6 meters is the height at which the biodiesel enters the column, ϕ_L is the fraction of the light phase (biodiesel), Vol is the volume of the column, D is the diameter of the column, and $L_{\text{dead-zone}}$ is the height of the dead-zone.

2.3.3 Flooding

To calculate the flooding velocity of the continuous phase, V_{cF}, Equation (2.22) was used [18].

$$V_{cF} = \frac{0.178\varepsilon V_{so}}{1 + 0.925(V_{dF}/V_{cF})(1/[cos(\pi a_p d_p/8)]^2)} \tag{2.22}$$

The dispersed phase flooding velocity, V_{dF}, was calculated with Equation (2.23) [29].

$$\frac{V_{dF}}{\bar{w}_s} = \frac{\varepsilon}{m}\left[1 - \left(\frac{V_c}{\bar{w}_s}\right)^{0.6}\right]\left[1 - \frac{\left[1 - \left(\frac{V_c}{\bar{w}_s}\right)^{0.6}\right]}{m}\right]^{m-1} - \frac{V_c}{\bar{w}_s}\frac{\frac{1}{m}\left[1 - \left(\frac{V_c}{\bar{w}_s}\right)^{0.6}\right]}{1 - \frac{1}{m}\left[1 - \left(\frac{V_c}{\bar{w}_s}\right)^{0.6}\right]} \tag{2.23}$$

Where $\bar{w}_s$ is the middle rising or falling velocity of single droplet in packing bed (m/s) and is calculated with the following expression

$$\bar{w}_s = 0.8 \cdot \cos(\alpha) \cdot \psi_{mF}^{-1/6}\left(\frac{4\varepsilon/a_p}{d_{32}}\right)^{1/4}\left(\frac{d_{32}\Delta\rho g}{\rho_c}\right)^{1/2} \tag{2.24}$$

and m is a parameter that depends on the mass transfer direction. In this case $m = 1.5$ since the solutes are going from the dispersed to the continuous phase [29]. In Equation (2.24), α is the flow channel angle in packed bed with a value of 45 ° and ψ_{mF} is the resistance coefficient for the continuous phase with a value of 0.710 (Montz-Pak Plastic C1-300, similar to C3) [29].

To calculate the flooding percentage for each phase, Equation (2.25) was used for the continuous phase and Equation (2.26) for the dispersed phase.

$$\%Fl_C = \frac{V_c}{V_{cF}} \times 100 \tag{2.25}$$

$$\%Fl_D = \frac{V_d}{V_{dF}} \times 100 \tag{2.26}$$

2.3.4 Phase Inversion Parameter

There is another variable that should be considered to analyse this system. An indicator of phase behaviour is crucial to identify and avoid this situation from happening, because once it happens it is not easily reversed since the new condition corresponds to a more stable configuration [18]. This indicator, χ, is given as:

$$\chi = \frac{\phi_L}{\phi_H}\left(\frac{\rho_L \mu_H}{\rho_H \mu_L}\right)^{0.3} = \frac{\phi_L}{1-\phi_L}\left(\frac{\rho_L \mu_H}{\rho_H \mu_L}\right)^{0.3} \tag{2.27}$$

where

$\chi < 0.3$	light phase always dispersed
$\chi = 0.3 – 0.5$	light phase probably dispersed
$\chi = 0.5 – 2.0$	either phase can be dispersed, phase inversion may occur
$\chi = 2.0 – 3.3$	heavy phase probably dispersed
$\chi > 3.3$	heavy phase always dispersed

The subscripts L and H refer to the light and heavy phases.

2.3.5 Quality parameters of biodiesel

The quality parameters of biodiesel are explained and calculated here. With the calculation of these parameters, it is possible to evaluate the performance of the model.

2.3.5.A Cetane Number

The Cetane Number (CtN) of a diesel engine fuel is a measure of ignition delay, that is, the time period between the start of injection and the first pressure increase during combustion of the fuel [30]. Higher cetane fuels will have shorter ignition delay periods than lower cetane fuels [31]. This number was calculated using eq. (4.9) [32].

$$\mathrm{CtN_{BDF}} = 3.930 N_{\mathrm{C}} - 15.936 N_{\mathrm{DB}} \tag{2.28}$$

Where N_C and N_{DB} are the weighted-average number of carbon atoms and the weighted-average number of double bonds.

2.3.5.B Flash Point

Flash point is the minimum temperature at which fuel produces enough vapour to cause ignition resulting to flame generation. Biodiesel has a average flash point of 150 °C, higher than diesel fuel (55 – 66 °C) [33]. This temperature was calculated with Equation (2.29) [32].

$$T_f = 23.362N_C + 4.854N_{DB} \tag{2.29}$$

2.3.5.C Low-Temperature Flow Properties

Cloud Point (K or °C) (CP), Pour Point (K or °C) (PP) and Cold Filter Plugging Point (K or °C) (CFPP) are significant properties to be analysed when the fuel is going to be used in cold regions, they indicate the low-temperature application capability of biodiesel [34, 35].

Starting with the CP, this indicator is the minimum temperature at which the first crystal formation starts, it was calculated according to Equation (2.30) [32].

$$\text{CP} = 18.134N_C - 0.790U_{FAME} \tag{2.30}$$

Where U_{FAME} is the total unsaturated FAME content (wt %).

The PP is the lowest temperature below which a liquid loses its flow characteristics [34], which was calculated with Equation (2.31).

$$\text{PP} = 18.880N_C - 1.000U_{FAME} \tag{2.31}$$

Finally, the CFPP is defined as the minimum temperature at which a given volume of pure (unblended) biodiesel, referred to as B100, still passes through a standardised filter within 60 seconds [33]. It was calculated using Equation (2.32) [32].

$$\text{CFPP} = 18.019N_C - 0.804U_{FAME} \tag{2.32}$$

2.4 Properties Estimation and Correlations

2.4.1 Solubility Correlation

One crucial parameter that determines the extent to which the components in two liquid phases are distributed at equilibrium is the partition or distribution coefficient [20]. In practical terms, the miscibilities can be expressed as mass fractions, and using a modified Misek correlation [27] that accounts for the effect of temperature,T, Equation (2.33) is obtained:

$$\ln K_i = \ln \frac{w_i^{\text{bd}}}{w_i^{\text{aq}}} = a_i^M w_i^{\text{aq}} + \frac{b_i^M}{T} - c_i^M \tag{2.33}$$

where K_i is the partition coefficient of component i for a mass fraction basis; a_i^M, b_i^M, and c_i^M are the parameters of the modified Misek correlation; variable w_i^{bd} is the mass fraction of component i in biodiesel, and w_i^{aq} is the mass fraction of component i in the aqueous phase. The parameters were estimated from solubility data gathered by an industrial partner.

2.4.2 Density

To calculate the density of the mixture (see Equation (2.34)), Kay's mixing rules (Equations 2.35 and 2.36) were used to account with the molar weights and molar volumes of biodiesel [36], the fraction of the acylglycerols [37] and the molar volumes of glycerol, water and methanol [38]. The impact of the polarity of components such as glycerol and methanol was not considered, thus using an ideal mixing rule (Kay), since the concentrations of these compounds in both phases are low.

$$\rho_{\text{mix}} = \frac{MW_{\text{avg}}}{V_L^{\text{mix}}} \tag{2.34}$$

$$V_L^{\text{mix}} = \sum_i^m V_{L_i} x_i \tag{2.35}$$

$$MW_{\text{avg}} = \sum_i^m x_i MW_i \tag{2.36}$$

Where ρ_{mix} is the density of the mixture, MW_{avg} is the average molar weight of the mixture, V_L^{mix} is the molar volume of the mixture, V_{L_i} is the molar volume of the set of compounds i, x_i is the mole fraction of the set of compounds i and m is the total number of sets of compounds.

The GCVOL Group Contribution Method was used to compute the biodiesel density. This method uses a group contribution method to predict the molar volumes of liquids. It has the advantage of being a completely predictive model based only on the molecular structure of the compound. Research has shown that accurate descriptions of fatty ester densities could be achieved with this model, hence

its application on this work. The molar volume of liquid i, $V_{L_i}^{\text{GCVOL}}$, is calculated using the following expression:

$$V_{L_i}^{\text{GCVOL}} = \sum_k n_{ik} \Delta v_k \tag{2.37}$$

where n_{ik} is the number of group k in molecule i and Δv_k is the molar group k. Its temperature dependence is given by the following equation:

$$\Delta v_k = A_k + B_k T + C_k T^2 \tag{2.38}$$

where *T* is the absolute temperature that can vary between the melting and the normal boiling points if it is used to predict the density of solvents. A_k, B_k and C_k are parameters from Elbro et al. [36].

The fragmented approach by Zong was used to estimate the fraction of acylglycerols. Here the liquid molar volumes of triglycerides are calculated from the fragment composition and the fragment parameters, Equation (2.39).

$$V_{L_i}^{\text{Zong}} = \sum_k N_{\text{frag,k}} V_k^l(T) \tag{2.39}$$

The Van Krevelen equation, 2.40, was used to calculate the temperature dependency for the liquid molar volume of fragment k.

$$V_k^l = \frac{1 + B_{2,k} T}{B_{1,k}} \tag{2.40}$$

where $V_{L_i}^{\text{Zong}}$ are the liquid molar volumes of triglycerides (m^3/kmol), V_k^l is the liquid molar volume contribution of fragment (m^3/kmol), $N_{\text{frag,k}}$ is the number of fragment k in the component, $B_{1,k}$ (kmol/m^3) and $B_{2,k}$ (K^{-1}) are the temperature dependency correlation parameters of fragment k and T is the temperature (K). The parameters $B_{1,k}$ and $B_{2,k}$ for the glycerol fragment and the saturated fatty acid fragments with carbon numbers ranging from 4 to 18 were regressed against available literature experimental density data. This methodology was used due to its capabilities of systematic correlation and accurate estimation of thermophysical properties of triglycerides, oils and fats. The fragment-based methodology, when used with proper mixing rules, showed superior predictions over commonly used functional group contribution methods.

The molar volumes of the remaining compounds, i.e. glycerol, methanol, and water, were estimated with Equation (2.41) [38].

$$V_{L_i}^{\text{Rackett}} = \frac{R T_c (Z_m^{RA})^{1+(1-T_r)^{2/7}}}{P_c} \tag{2.41}$$

Where Z_m^{RA} is the critical compressibility factor $= V_c P_c / RT_c$, V_c is the critical volume, T_c is the critical temperature, P_c is the critical pressure and T_r is the reduced temperature $= T/T_c$.

2.4.3 Viscosity

To estimate the dynamic viscosity of biodiesel, Grunberg-Nissan model was used [39]

$$ln(\mu_{\text{mix}}) = \sum_{i=1}^{n} x_i ln(\mu_i) \tag{2.42}$$

where x_i is the mole fraction of component i and μ_i is the dynamic viscosity of component i. However, the values of the viscosities for different biodiesel fractions come from different sources. For the fatty species, the viscosity (mPa·s) was calculated with the following expression:

$$ln(\mu_i) = \sum_k N_k \left(A_{1k} + \frac{B_{1k}}{T + C_{1k}} \right) + \left[MW_i \sum_k N_k \left(A_{2k} + \frac{B_{2k}}{T + C_{2k}} \right) \right] + Q \tag{2.43}$$

where N_k is the number of groups k in molecule i, MW is the component molecular weight that multiplies the "perturbation term", A_{1k}, B_{1k}, C_{1k}, A_{2k}, B_{2k} and C_{2k} are parameters obtained from the regression of experimental data, k represents the groups of component i and Q is a correction term expressed as

$$Q = \xi_1 q + \xi_2 \tag{2.44}$$

where ξ_1 and ξ_2 are related to each class of compounds and q is a function of the absolute temperature (K):

$$q = \alpha + \frac{\beta}{T + \gamma} \tag{2.45}$$

where α, β and γ are optimised parameters obtained by regression of data that is presented in Ceriani et al. (2011) [39]. The effect of functional groups on the dynamic viscosity is corrected by the term Q according to the total number of carbon atoms N_c in the molecules. In Equation (2.46), ξ_1 is a function of N_c and is applicable to all compounds and stated as follows:

$$\xi_1 = f_0 + N_c f_1 \tag{2.46}$$

where f_0 and f_1 are optimised constants. N_{cs} represents the number of carbons of the short-chain alcohol that reacted with the fatty acid to produce the fatty ester. The term ξ_2 describes the differences between the viscosity of isomer esters at a given temperature and is dependent on the number of carbons of the substitute fraction, N_{cs}, as seen in Equation (2.47).

$$\xi_2 = s_0 + N_{cs} s_1 \tag{2.47}$$

Where s_0 and s_1 are optimised constants. Equation (2.47) is mostly used to account for the effect of the alcoholic fraction present in fatty esters.

The viscosity of glycerol, water and methanol was calculated with DIPPR liquid viscosity model from Aspen Plus® [40].

$$ln(\mu_i) = C_{1i} + C_{2i}/T + C_{3i} ln(T) + C_{4i} T^{C_{5i}} \tag{2.48}$$

Where C_{1i}, C_{2i}, C_{3i}, C_{4i} and C_{5i} are constants.

2.4.4 Interfacial Tension

The interfacial tension in liquid systems is a phenomenon that occurs at the contact surface of partially immiscible components, forming an interface. This results from a change in the adhesion force field of the molecules of the conjugated phases near the interface, thus creating a region with different characteristics from the bulk of those phases. To estimate the interfacial tension of the system Equation (2.49) for a ternary mixture was used [41].

$$\sigma = \frac{K\ R\ T\ X}{A_{w0} \text{exp}(X)(\sum_i^{\text{aqueous}} x_i^{\text{org}} q_i + \sum_i^{\text{organic}} x_i^{\text{aq}} q_i + \sum_i^{\text{organic}} x_i^{\text{sol}} q_i^{\text{sol}})} \tag{2.49}$$

Where R is the ideal gas constant (JK^{-1}mol^{-1}), T is the temperature (K), x is the mole fraction, x_{sol} is the mole fraction of solute in the organic phase, richer in the solutes, A_{w0} is the van der Waals surface area of a standard segment of 2.5 $\times$ 10^5 m^2/mol, q is a measure of molecular surface area and is given by

$$q_i = \sum_k n_{ik} Q_k$$

where n_{ik} is the number of occurrences of group k in molecule i and Q is a factor of surface area of group k [42]. The constant X is given by

$$X = -ln\left(\sqrt{(\sum_i^{\text{aqueous}} x_i^{\text{org}} + \sum_i^{\text{organic}} x_i^{\text{aq}} + \sum_i^{\text{organic}} x_i^{\text{sol}})^2}\right)$$

and K is an empirical constant with a value of 0.9414 [41]. This equation with the empirical constant returned satisfactory results for a large number of ternary systems [41]. This model is not the most accurate in estimating the interfacial tension of a certain system, however, it returns values with similar precision, requires less computational power and, therefore, it was chosen.

2.4.5 Diffusivity Coefficient

To calculate the effective diffusion coefficient, $\mathscr{D}$, the Wilke and Chang method (1955) was used, Equation (2.50) [43].

$$\mathscr{D}_f = 7.4 \times 10^{-8} \frac{\left[\sum_{i=1}^{n} (x_{f_i} c_{\text{diff}_i} MW_i) - x_{f_i} c_{\text{diff}_i} MW_i\right]^{0.5} T}{\mu_f V_{A_i}^{0.6}} \tag{2.50}$$

Where x_{f_i} is the mole fraction of component i in phase f, c_{diff_i} is the association parameter for the solvent, μ_f is the viscosity of phase f and V_{A_i} is the molar volume of component A.

3

Model Validation and Sensitivity Analysis

Contents

In this chapter, the equilibrium model of the column is validated with industrial data. A sensitivity analysis is also performed to evaluate the hydrodynamic behaviour of this model. Firstly, the quality parameters of biodiesel are presented, that is, the Cetane Number, flash point and low-temperature flow properties. The model validation focus on the impact of the working conditions on the process, while the sensitivity analysis shows the effects of contamination, interface level, liquid atomisation and density on the model. A systematic approach is presented in order to keep the process under desired conditions in case of contamination. The rate-base model was implemented in steady-state, i.e. the partial derivatives with respect to time are zero (Chapter 2, page 16). The simulations for the packed column model were run in gPROMS® ModelBuilder.

3.1 Quality Parameters

These quality parameters were presented in Chapter 2 (page 22) and are shown in Table 3.1.

Table 3.1: Quality parameters of biodiesel.

Quality Parameters	
CtN (vol%)	54.9
T_f (°C)	161.3
CP (°C)	0.03
PP (°C)	-2.2
CFPP (°C)	-3.2

The CtN has a plausible value that implies shorter ignition delay periods [31,44], a flash point slightly above average (150 °C) [33], the CP is lower than usual for UCO (9 °C) but within a common interval for FAME (-3 to 7 °C) [45], the PP is close to the average value for UCO of -3 °C, and finally the CFPP is marginally higher than the average value (-6 °C) [45]. The model accurately estimated these properties.

3.2 Estimation of Solubility Parameters

The parameters of the modified Misek model (Equation (2.33), page 24) were estimated from data obtained from laboratory experiments for different values of temperature, solvent to feed ratio and inlet flowrate of biodiesel. The final estimate of these parameters is presented in Table 3.2.

Table 3.2: Modified Misek model parameters estimated from the regression of solubility data.

Parameters	Glycerol	Methanol	Water	FAME
a_i^M	-113.2855	32.4798	1.3428	-4.8327
b_i^M	-968.2514	364.9632	1338.4886	-7.7095
c_i^M	0	3.3022	11.0598	0.5374

$\ln K_i = \ln w_i^{bd}/w_i^{aq} = a_i^M w_i^{aq} + b_i^M/T - c_i^M$

The effect of the solvent to feed ratio, S/F, at 45 °C for UCO in the solubility of the solvents is illustrated in Figure 3.1. It is possible to observe that the partition coefficients, K_i, of glycerol, methanol and FAME increase with S/F while the K_i of water decreases. Figure 3.2 illustrates the effect of the temperature on the solubility of the solutes with S/F =13.5 %. Increasing the temperature will increase the solubility of methanol in water while the solubility of glycerol and water in biodiesel decrease. The solubility of FAME in the aqueous phase has a marginal decrease.

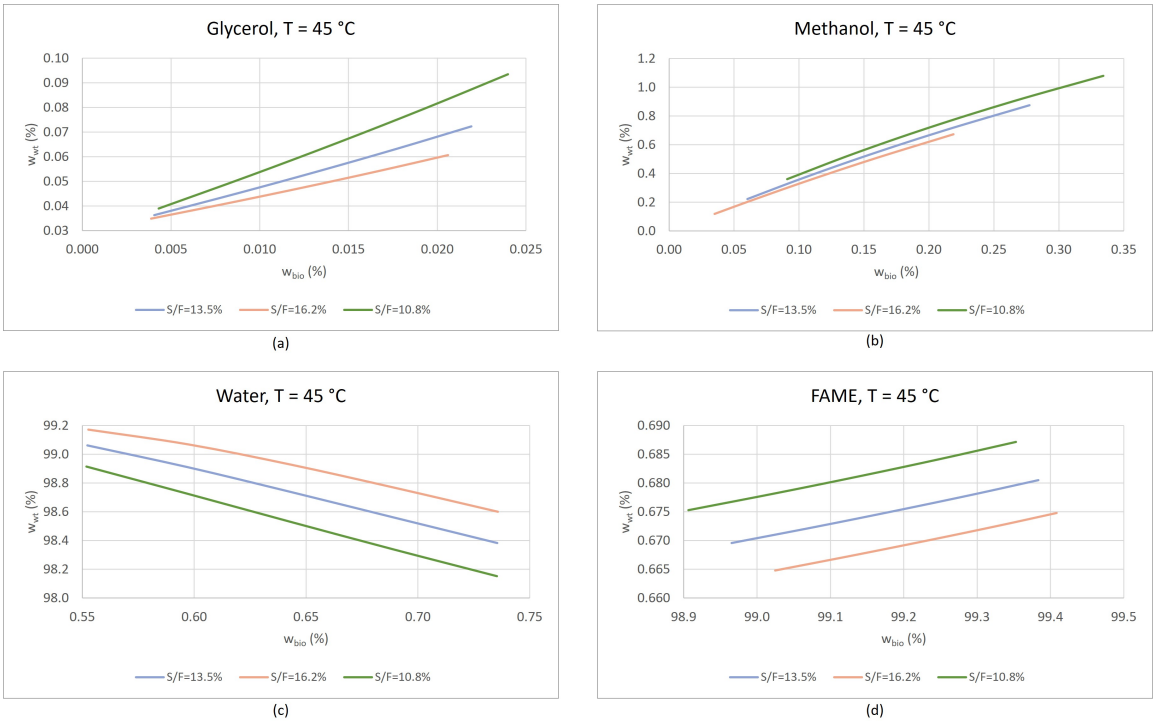

Figure 3.1: Effect of the solvent to feed ratio at 45 °C in the concentration profiles of (a) glycerol, (b) methanol, (c) water, and (d) FAME in biodiesel and washing water for used cooking oil.

Figures 3.3 and 3.4 reflect the impact of the different oils in the solubility of the glycerol. It is possible to conclude that the ester profiles have a small impact on the solubility of the solvents.

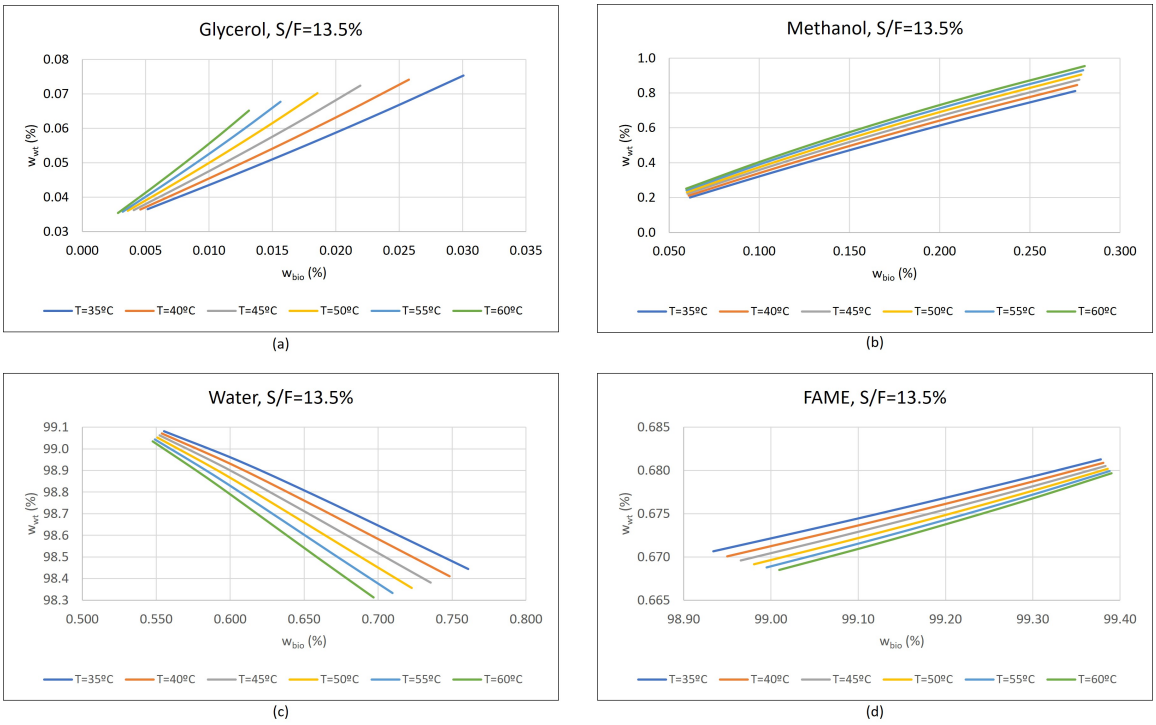

Figure 3.2: Effect of the temperature with $S/F = 13.5$ % in the concentration profiles of (a) glycerol, (b) methanol, (c) water, and (d) FAME in biodiesel and washing water for used cooking oil.

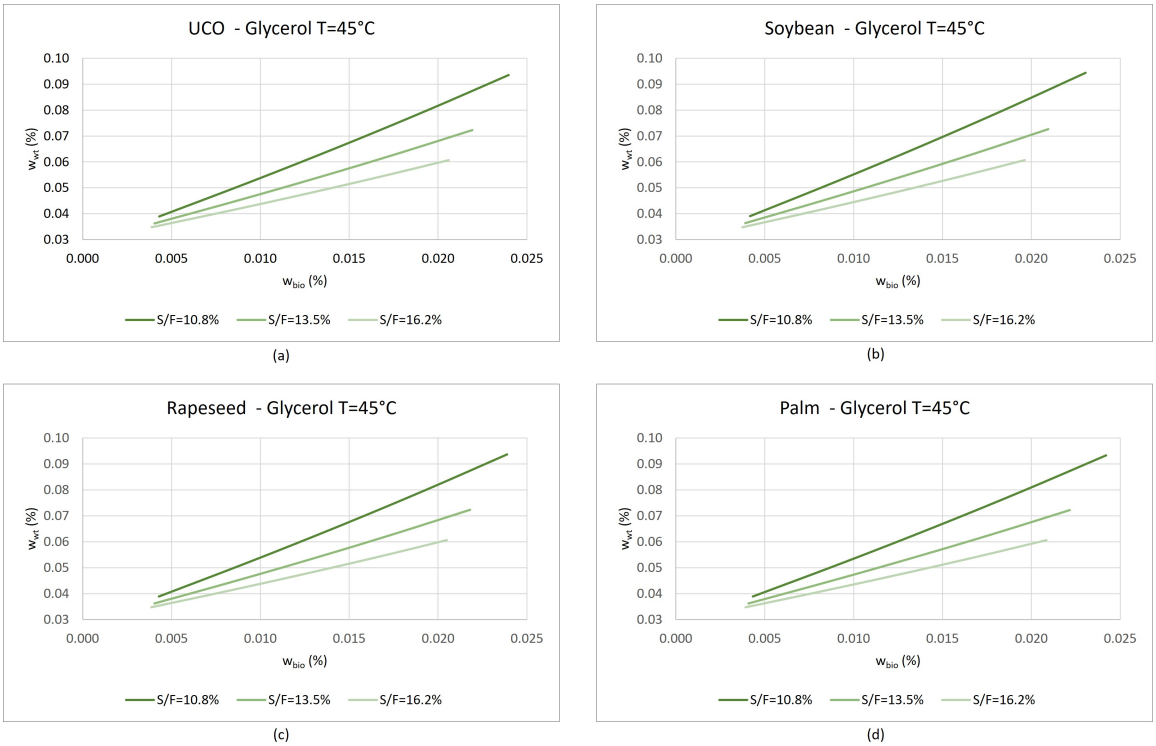

Figure 3.3: Effect of the solvent to feed ratio at 45 °C in the concentration profiles in biodiesel and washing water for (a) UCO, (b) soybean oil, (c) rapeseed oil, (d) and palm oil.

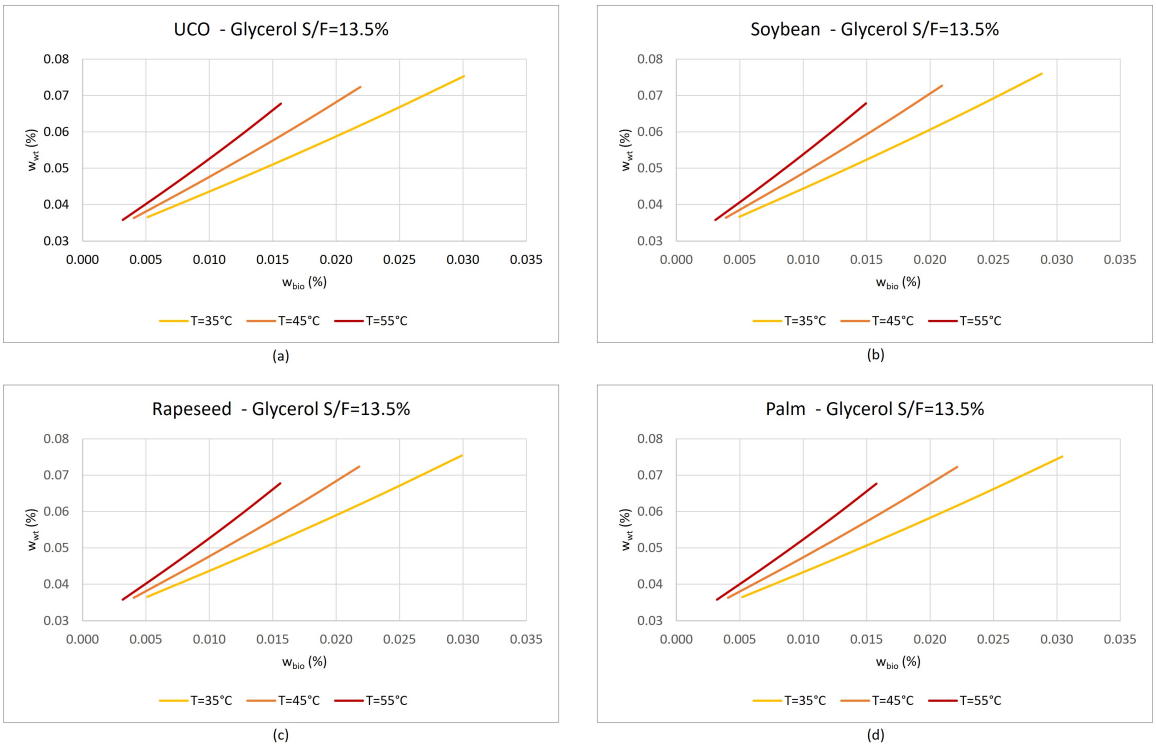

Figure 3.4: Effect of the temperature for $S/F = 13.5$ % in the concentration profiles in biodiesel and washing water for (a) UCO, (b) soybean oil, (c) rapeseed oil, (d) and palm oil.

3.3 Model Validation

To evaluate the mass transfer model, the packed column was simulated in steady-state with different solvent to feed ratios and temperatures and the results were compared with the studies conducted by the industrial partner. Figures 3.5 to 3.8 illustrate the concentration profiles of both phases in the column for glycerol, methanol, water and FAME for different S/F at 45 °C. In these Figures the unwashed and washed biodiesel, and washing water from the experimental studies are represented with markers and are positioned in their values at the top and bottom of the column. It is possible to say that the model predictions are fairly accurate, particularly for glycerol and methanol. Here, the increase in the solvent to feed ratio has the same impact as observed above, validating the model.

The effect of temperature on the solubilities of the solvents is shown in Figures 3.9 to 3.12. Here, only the values for 45 °C and 55 °C are compared since the working conditions are usually between this interval. The relative errors for the composition of washed biodiesel are 46.1 % for glycerol, 31.4 % for methanol, 29.7 % for water, and 0.2 % for FAME.

Again, the model satisfactorily predicted the solubility of the solvents in biodiesel. Increasing the temperature has the same effect as mentioned above.

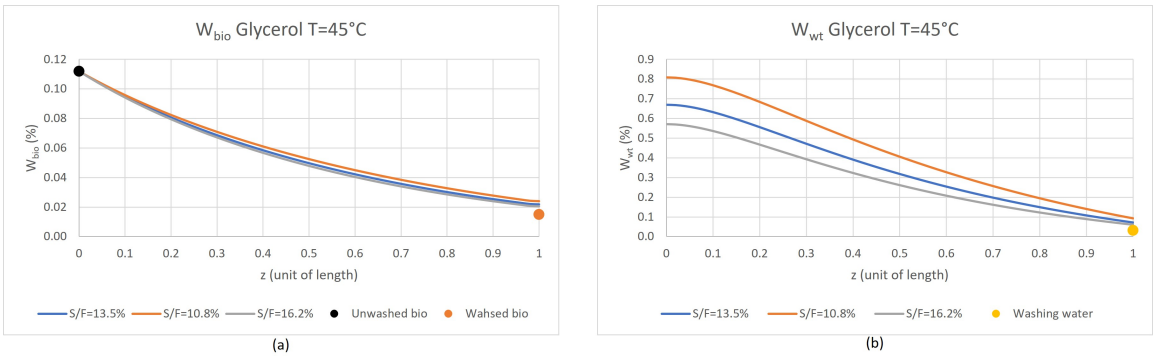

Figure 3.5: Glycerol concentration profile in (a) biodiesel and (b) washing water for different solvent to feed ratios compared with typical process values (markers).

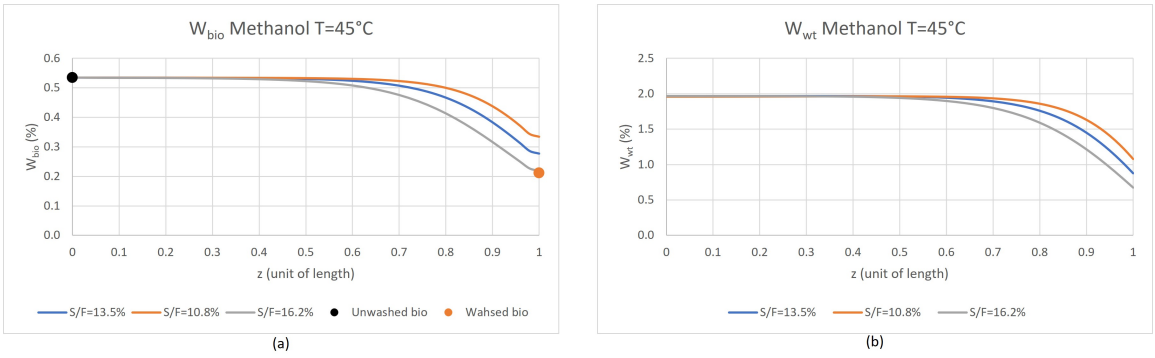

Figure 3.6: Methanol concentration profile in (a) biodiesel and (b) washing water for different solvent to feed ratios compared with typical process values (markers).

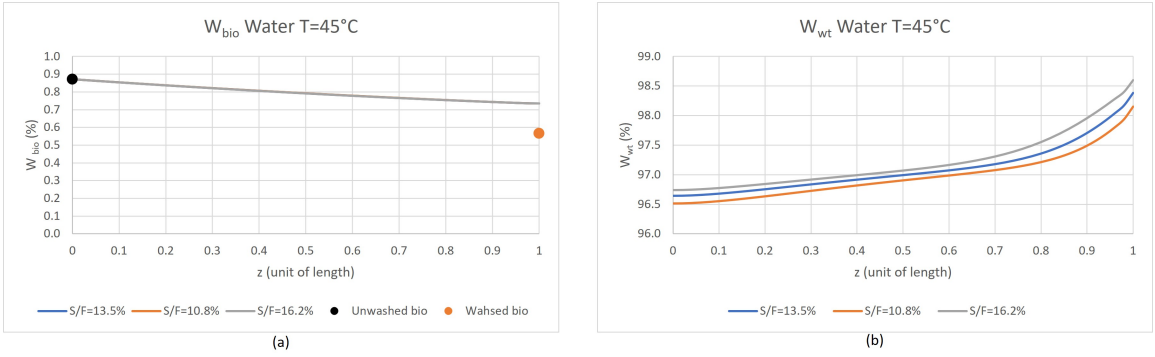

Figure 3.7: Water concentration profile in (a) biodiesel and (b) washing water for different solvent to feed ratios compared with typical process values (markers).

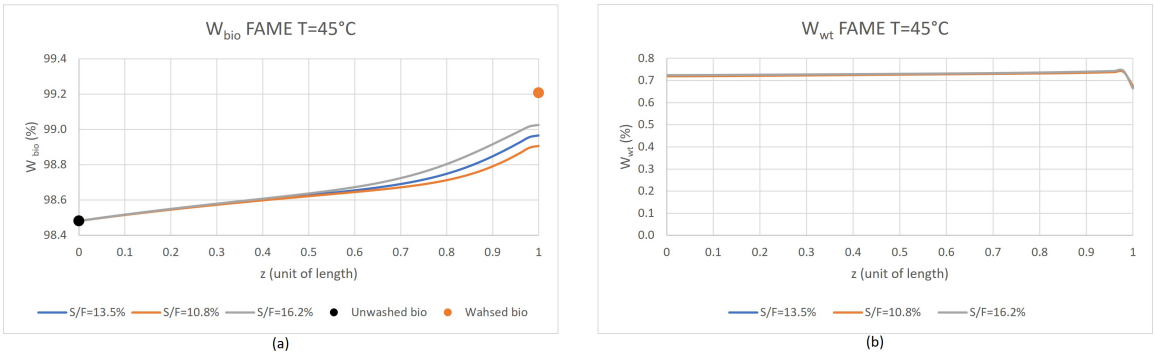

Figure 3.8: FAME concentration profile in (a) biodiesel and (b) washing water for different solvent to feed ratios compared with typical process values (markers).

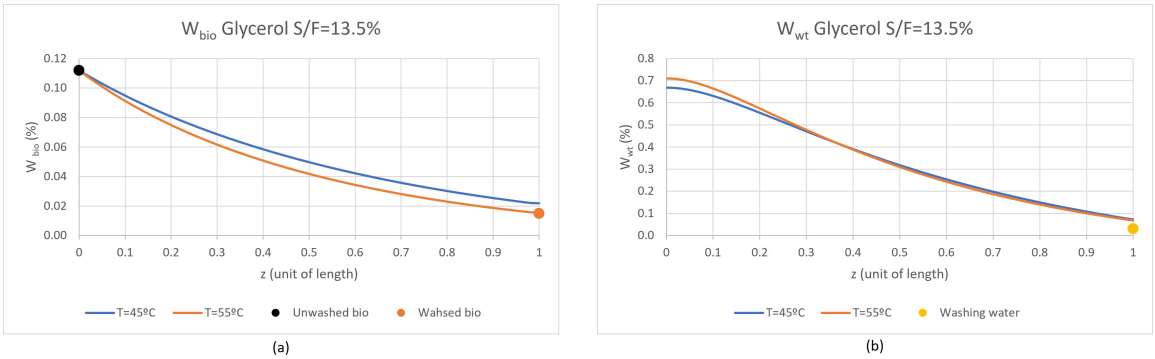

Figure 3.9: Glycerol concentration profile in (a) biodiesel and (b) washing water for different temperatures compared with typical process values (markers).

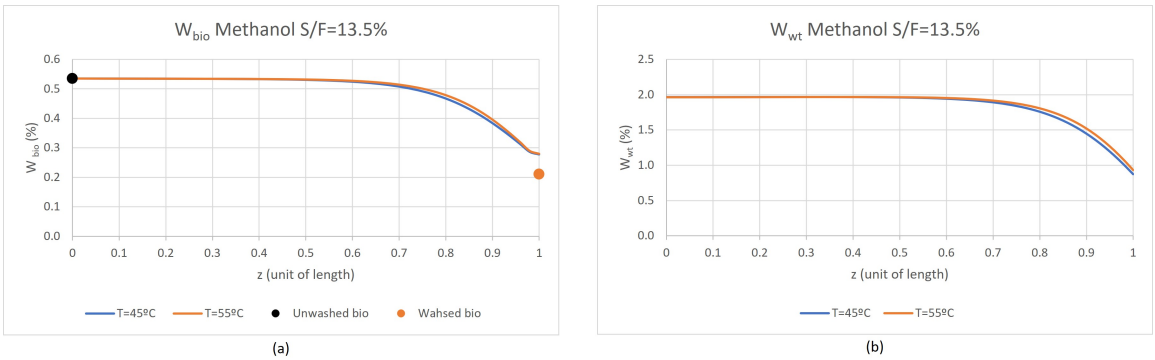

Figure 3.10: Methanol concentration profile in (a) biodiesel and (b) washing water for different temperatures compared with typical process values (markers).

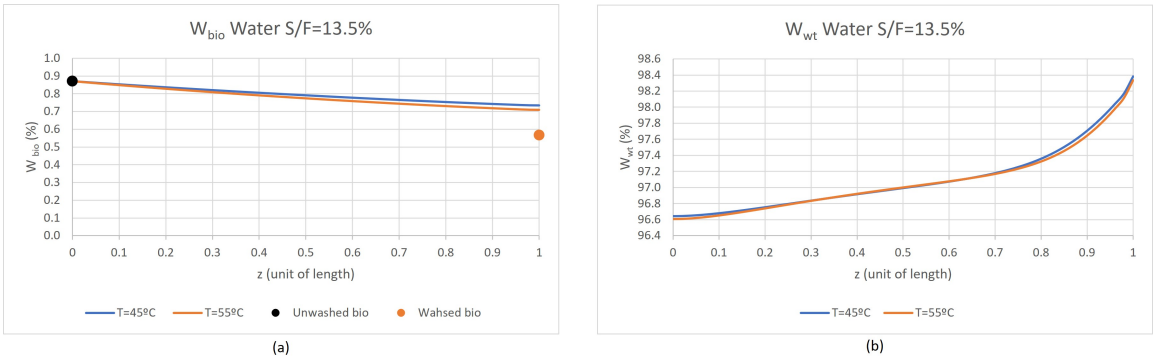

Figure 3.11: Water concentration profile in (a) biodiesel and (b) washing water for different temperatures compared with typical process values (markers).

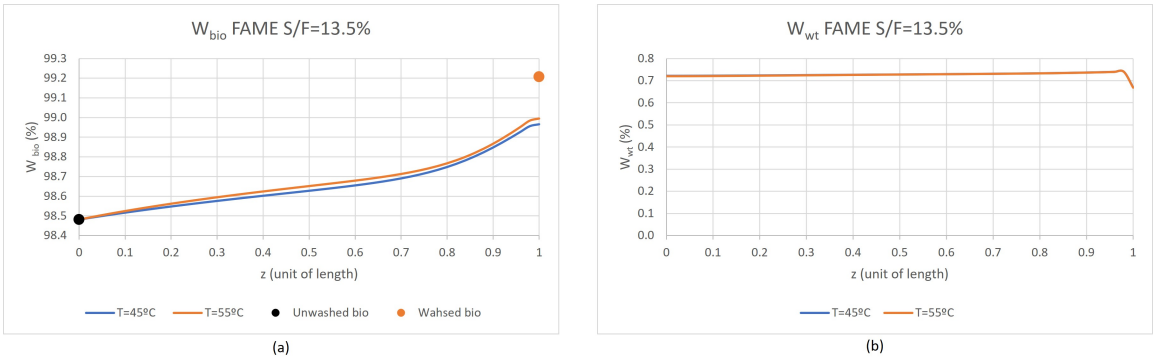

Figure 3.12: FAME concentration profile in (a) biodiesel and (b) washing water for different temperatures compared with typical process values (markers).

Finally, Figure 3.13 illustrates the impact of different ester concentration profiles in the solubility of glycerol in both phases. The different oils have barely no effect on the solubility of glycerol in biodiesel and, even though there is some difference in the composition profile of glycerol in the aqueous phase, the washed biodiesel has approximately the same composition of glycerol. Thus, using different oils will not significantly impact the process, which was already verified industrially.

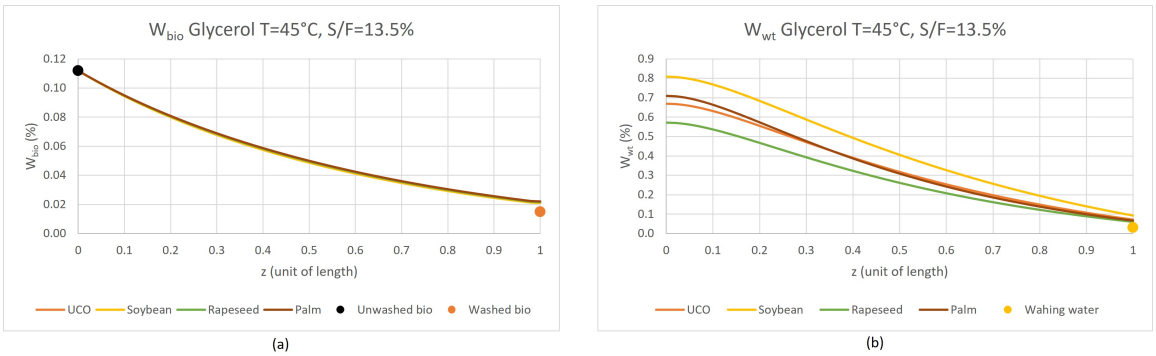

Figure 3.13: Glycerol concentration profile in (a) biodiesel and (b) washing water for different oils compared with typical process values (markers).

3.4 Sensitivity Analysis

After validating the model and analysing the impact of different working conditions such as temperature, solvent to feed ratio and ester composition, it is presented in this section the sensitivity analysis to evaluate the hydrodynamics of the column. Particularly: 1. the effect of contamination or incomplete reaction (small suspended particles or surfactants) - reflected through the interfacial tension; 2. the effect of the interface level - by changing the holdup, which is given by the dispersed phase to continuous phase ratio; 3. the effect of liquid atomisation/agitation intensity - which is simulated by the droplet diameter; 4. the effect of density of the dispersed phase. For this sensitivity analysis, the base conditions are 45 °C, a solvent to feed ratio of 13.5 vol.% and a biodiesel inlet mass flowrate at nominal capacity (reference).

Figures 3.14 to 3.17 show the impact of density in the solubility of the solutes in both phases for different temperatures and solvent to feed ratios. It is observed that decreasing the density is beneficial since it decreases the solubility of glycerol and water in the biodiesel. The solubility of methanol increases, however, the overall purity of the dispersed phase increases. As seen before, a higher temperature and solvent to feed ratio will increase the purity of the dispersed phase.

The parameter H_{so} was presented in Chapter 2 (page 19) and is proportional to the coalescence velocity. The impact of interfacial tension, droplet diameter, temperature, and solvent to feed ratio on this parameter were analysed. It was observed that the solvent to feed ratio had no effect on H_{so}, so the plot will not be shown. The impact of liquid atomisation or agitation of biodiesel was modelled by changing

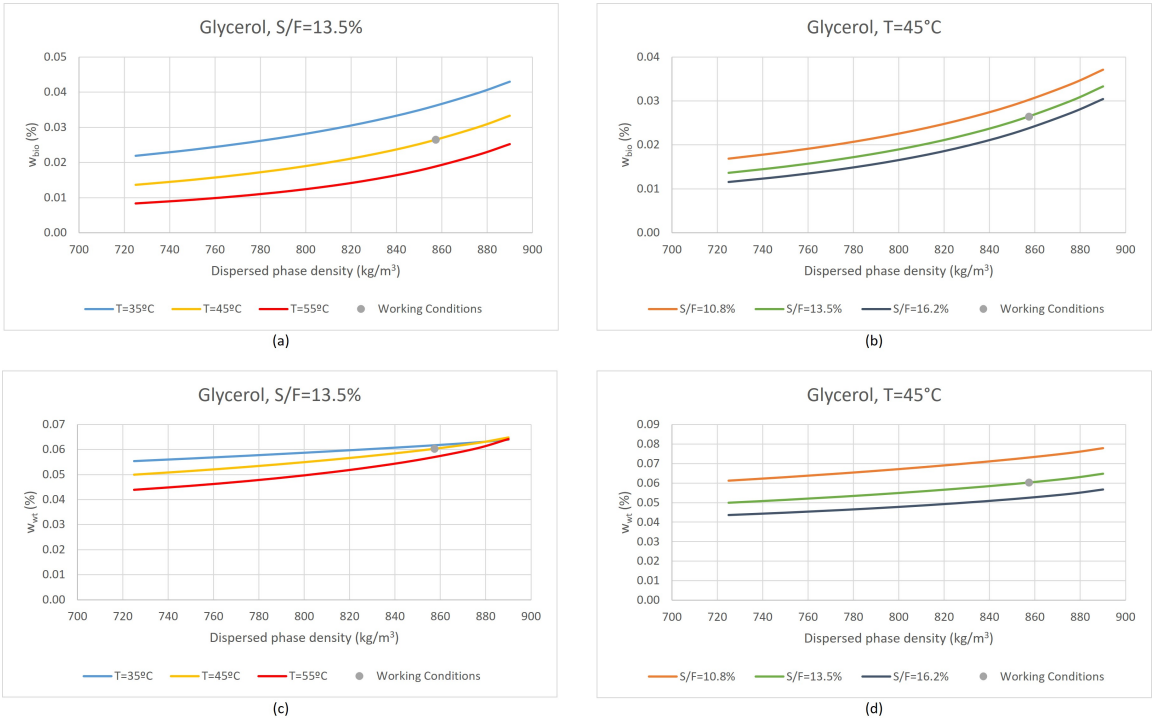

Figure 3.14: Impact of dispersed phase density in glycerol solubility in biodiesel, (a) and (b), and in water, (c) and (d), for different solvent to feed ratios and temperatures with a biodiesel inlet mass flowrate of reference.

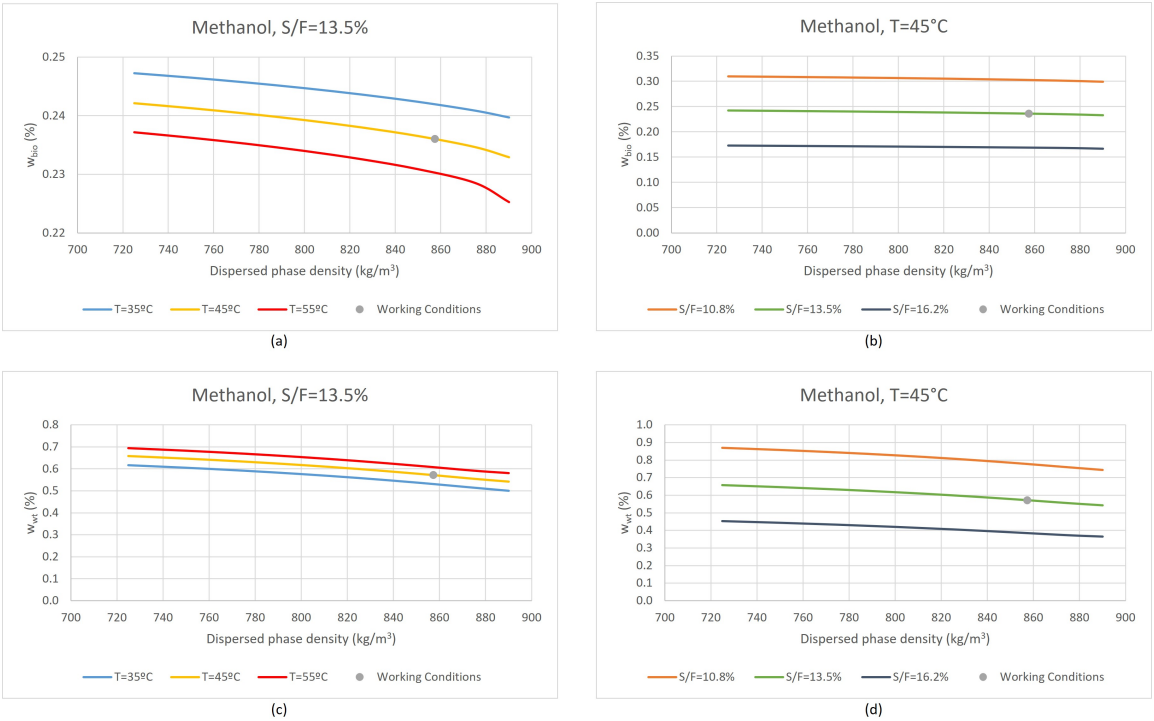

Figure 3.15: Impact of dispersed phase density in methanol solubility in biodiesel, (a) and (b), and in water, (c) and (d), for different solvent to feed ratios and temperatures with biodiesel inlet mass flowrate of reference.

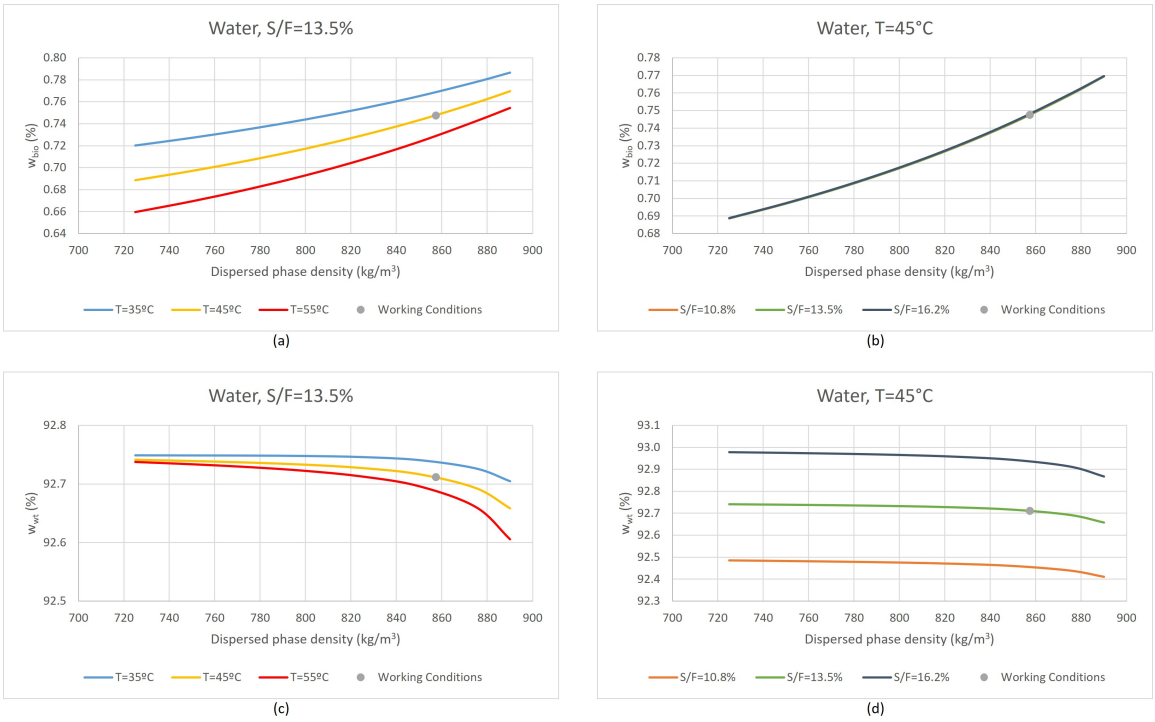

Figure 3.16: Impact of dispersed phase density in water solubility in biodiesel, (a) and (b), and in water, (c) and (d), for different solvent to feed ratios and temperatures with biodiesel inlet mass flowrate of reference.

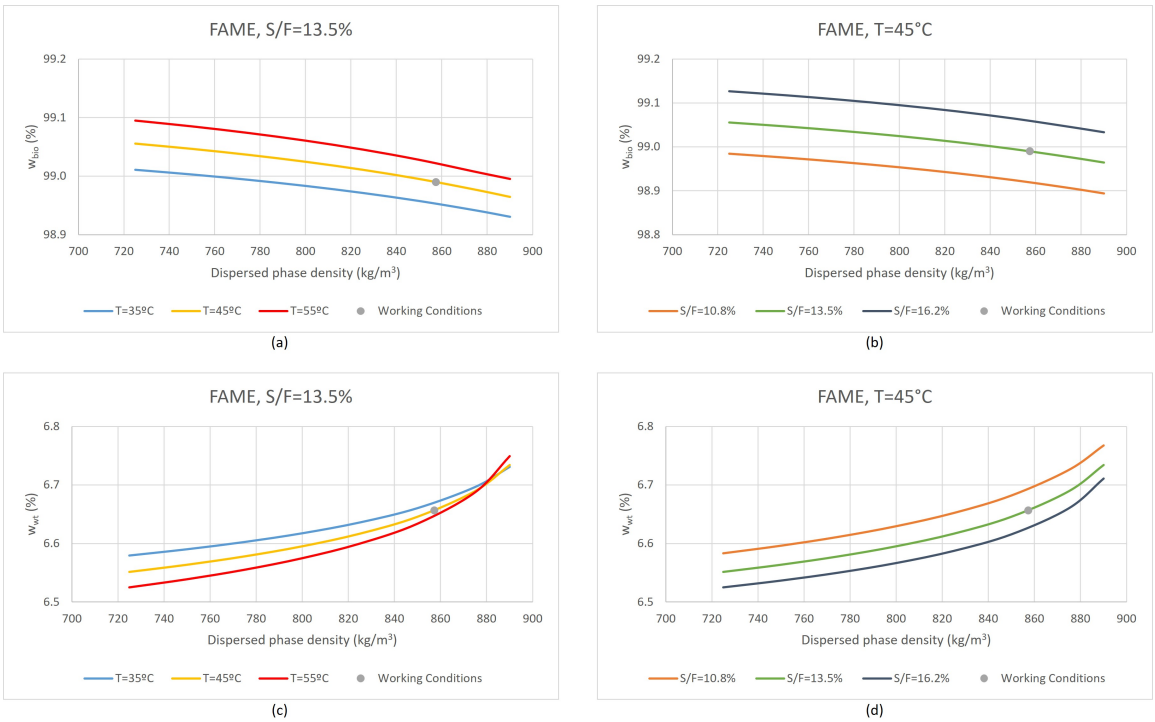

Figure 3.17: Impact of dispersed phase density in FAME solubility in biodiesel, (a) and (b), and in water, (c) and (d), for different solvent to feed ratios and temperatures with biodiesel inlet mass flowrate of reference.

the particle diameter (d_{32}). Figure 3.18 shows the effect of the interfacial tension and particle diameter on H_{so} for different temperatures. Here, it is possible to see that this parameter increases significantly with the diameter of the particles and also with the interfacial tension.

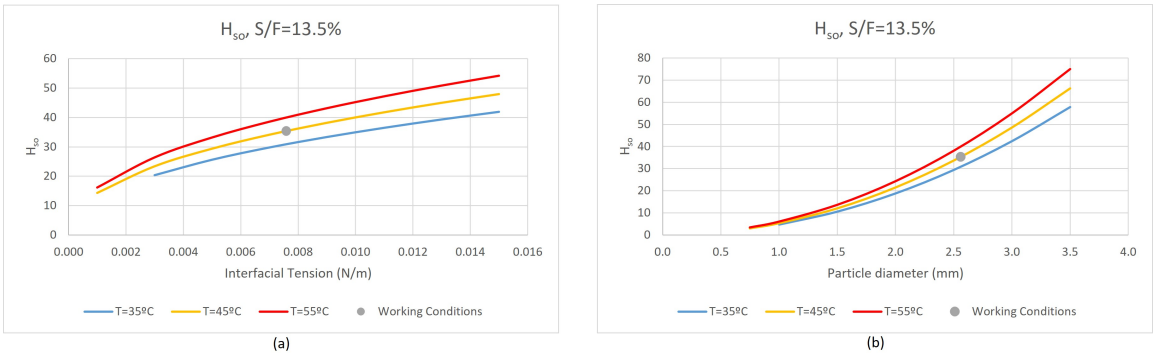

Figure 3.18: Impact of (a) interfacial tension, and (b) particle diameter, in dispersed phase coalescence velocity for different temperatures with a biodiesel inlet mass flowrate of reference.

If the droplets are too small ($d_{32} \approx$ 1.0 mm) they will have a similar behaviour as rigid spheres and will hinder the coalescence phenomenon [26]. This can promote the entrainment of washing water that will exit the column through the dispersed phase outlet. This undesirable phenomenon may occur due to small residence times after the centrifugation step that are not sufficient for the droplets to aggregate before the liquid atomisation of biodiesel that happens inside the column. On the other hand, for $d_{32} >$ 3.5 mm, $H_{so} >$ 53 which suggests insufficient droplet rise that may lead to a inefficient extraction [26]. Higher values of H_{so} will also promote phase inversion since there is early coalescence of the particles. This happens due to clogging problems in the distribution equipment of the dispersed phase that result in the increase of the droplets size if the inlet flowrate is kept constant. Lastly, the effect of temperature is noticeable, however, manipulating this variable to change the convergence velocity of the droplets will not be efficient.

For the impact of interfacial tension on H_{so}, higher values of interfacial tension will lead to insufficient droplet rise, however, contaminations usually decrease this value and not the opposite. In case of low interfacial values, this will promote droplet breakdown, since there is not enough tension to keep the droplets and, consequently, the interface level will decrease. This decrease in the interface level will increase the probability of phase inversion to occur, which can be seen in Figures 3.19 to 3.21.

Finally, the effects of the interfacial tension and the interface level on the hydrodynamics of the column were analysed and are shown in Figures 3.19 ($S/F =$ 13.5 % and $T =$ 45 °C), 3.20 ($S/F =$ 16.2 % and $T =$ 45 °C), and 3.21 ($S/F =$ 16.2 % and $T =$ 50 °C). In these plots, the vertical black line represents the value of the interface level calculated by the model for the working conditions; and the horizontal dashed line corresponds to the maximum recommended percentage of flooding, that is, the superficial velocity of either phase should be lower than 60 % of the flooding velocity of that phase [18]. It is also

important to note that the interfacial tension of the system is usually around 0.008 N/m.

Starting with Figures 3.19 and 3.20, the interface level (x axis) and the interfacial tension (legend) were fixed at a certain value and the simulation calculated the values of the flooding of the continuous phase (Equation (2.25), page 22) and dispersed phase (Equation (2.26), page 22). This process was repeated for different values of interfacial tension and interface level. The same method was applied to obtain Figure 3.21 but the biodiesel inlet mass flowrate was varied instead of the interfacial tension. Here, it is also shown a colour code corresponding to the probability of phase inversion. This was achieved by calculating the interface level for different values of holdup (from 0.0 to 1.0) with Equation (2.21) (page 21), and then by calculating χ with Equation (2.27) (page 22). Note the different intervals for the phase inversion parameter: $\chi < 0.3$ corresponds to the light phase, biodiesel, always dispersed; $\chi = 0.3 – 0.5$ light phase probably dispersed; and $\chi = 0.5 – 2.0$ either phase can be dispersed. As an example, for a holdup of 30 % the interface level is 12.1 meters and the phase inversion parameter is 0.268 (< 0.3). So, for an interface level of 12.1 meters the light phase is always dispersed (green zone).

These figures provide two different information: 1. which phase is more probable to be dispersed, according to the interface level; 2. for a given interfacial tension, it returns the flooding percentage of the continuous phase (- - -) and dispersed phase (—) calculated with Equations 2.25 (page 22) and 2.26 (page 22).

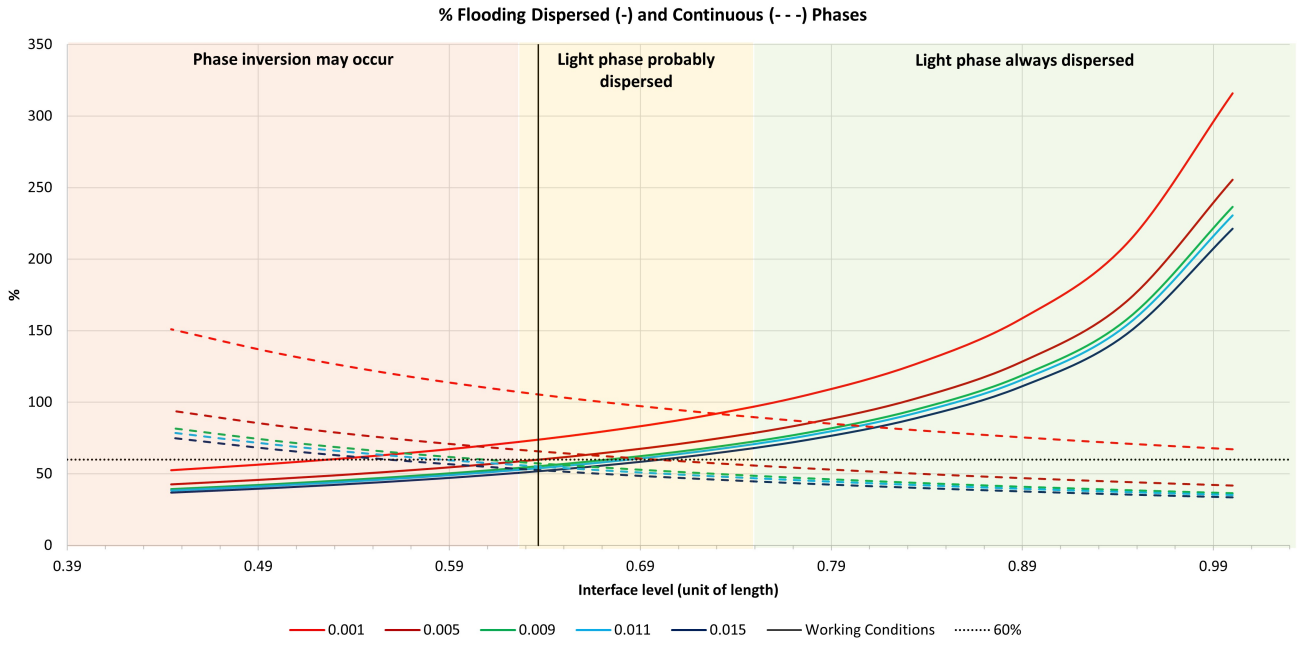

Figure 3.19: Impact of interfacial tension in flooding of both phases with an indicator of phase inversion with solvent to feed ratio of 13.5 %, 45 °C, and biodiesel inlet mass flowrate of reference.

Analysing Figure 3.19, and considering the normal values for interfacial tension (0.008 N/m), it is possible to see that the interface level should be lower than 0.70 length units so the flooding percentage

of either phase is below 60 % and higher than 0.63 length units to avoid phase inversion. From this figure, it is also observable that with contamination (which reflects on a lower interfacial tension, as explained above) the flooding percentage of both phases increases. The working conditions demonstrated that the current interface level corresponds to a flooding percentage within the recommend values in most situations. However, for low interfacial tensions, close to 0.001 N/m, both phases exceed this value, which is aggravated by increasing S/F (see Figure 3.20). That is, a higher contamination will increase the flooding percentage of both phases, which is not reversible by changing the solvent to feed ratio, nor the interface level for a given biodiesel inlet flowrate.

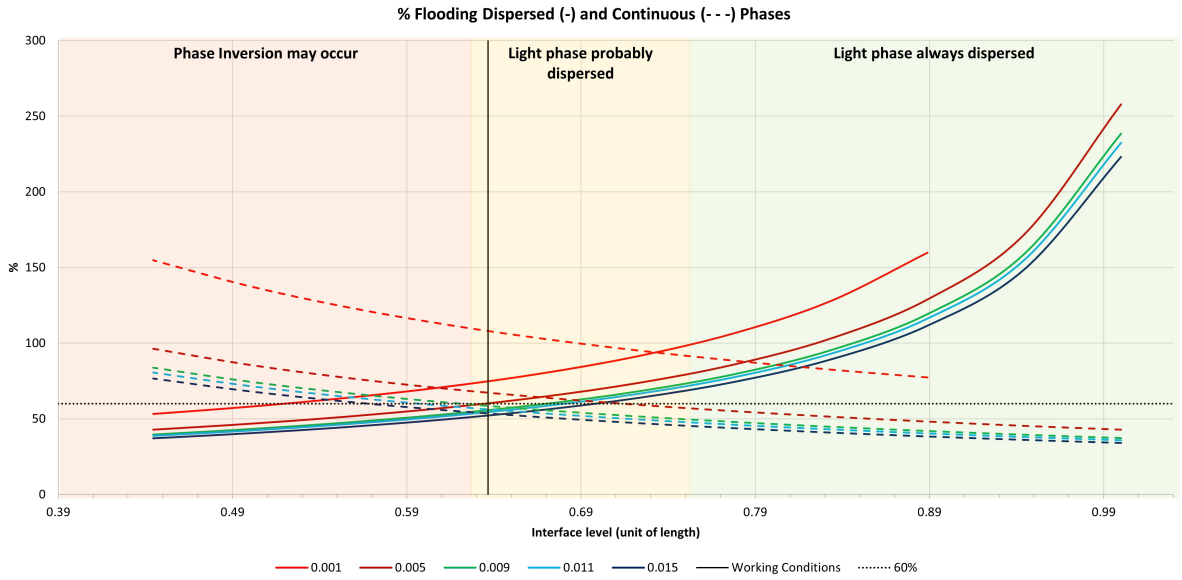

Figure 3.20: Impact of interfacial tension in flooding of both phases with an indicator of phase inversion with solvent to feed ratio of 16.2 %, 45 °C and biodiesel inlet mass flowrate of reference.

Given the analysis of Figures 3.19 and 3.20, the impact of the inlet flowrate of biodiesel was analysed. Figure 3.21 shows the flooding percentage of the continuous phase (- - -) and dispersed phase (—) for the biodiesel flowrates of reference, -10 %, -20 % and -36 % of the nominal value at 50 °C, solvent to feed ratio of 16.2 vol% and interfacial tension of 0.001 N/m. From this figure, reducing the inlet flowrate of biodiesel in 36 %, approximately 1/3 of the original value, reduces the flooding percentage of the continuous phase to roughly 60 %. Ideally, the interface level should be around 16% higher.

It is important to mention that the interface level predicted by the model for the base conditions is approximately 43 % higher than the measurement of the real plant at the time of the sample. This happens because the model does not account with the coalescence and breakage velocities of the droplets, which could only be achieved using a population balance model. Nevertheless, the model is capable of describing the hydrodynamic behaviour of the column and helps identifying which working conditions should be manipulated in order to keep the process under optimal conditions.

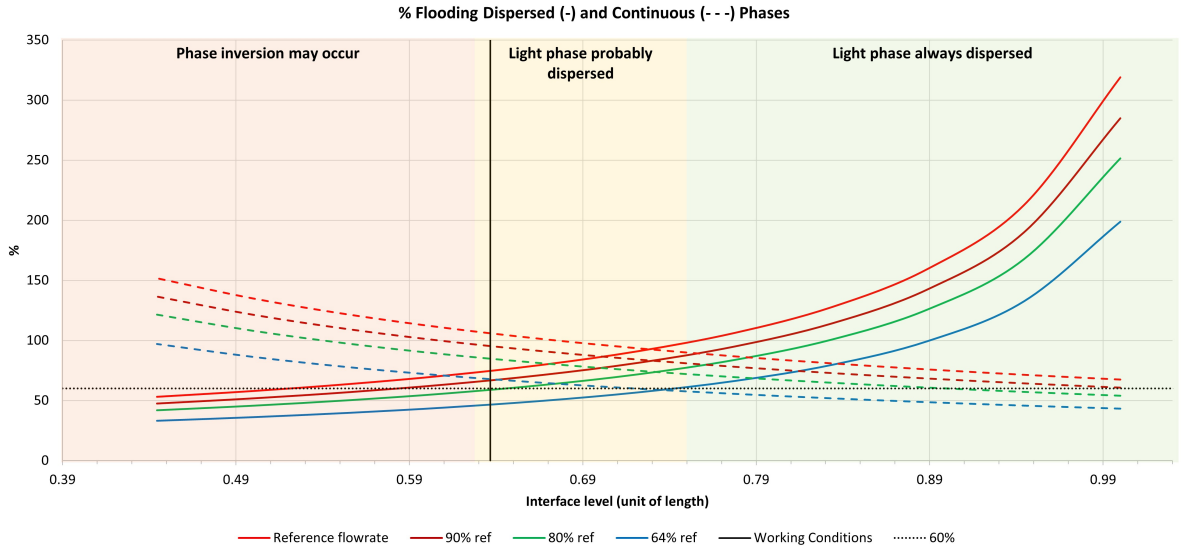

Figure 3.21: Impact of biodiesel inlet mass flowrate in flooding of both phases with an indicator of phase inversion with solvent to feed ratio of 16.2 %, 50 °C and interfacial tension of 0.001 N/m.

That being said, the suggested operating conditions are temperature at 50 °C and S/F of 16.2 vol%. In case of contamination, the biodiesel inlet flowrate should be lowered to 2/3 of its original value, the interface level should be increased in 16 % keeping the solvent to feed ratio at 16.2 vol%.

4

Control of Biodiesel Extraction Column

Contents

In this chapter the control approaches that are used in the biodiesel industry will be presented as well as the most commonly used control schemes in extraction columns. The biodiesel washing column was deeply analysed: first, several open-loop tests were executed in gPROMS® and then the linearisation of the system was performed in MATLAB® (with the System Identification toolbox). With the resulting transfer functions of the linearised system, it was possible to decide the variable pairings for this multivariable control system. Lastly, the controllers were tuned and the overall multiloop control was evaluated.

To simplify the notation, in this chapter, all input/output variables will be presented as deviation variables (so their nominal value is 0). For this chapter, the analysis was conducted with UCO, at 45 °C and a solvent to feed ratio of 13.5 %. The impact of the temperature on the system was not analysed here, the temperature is assumed to be constant.

4.1 Plantwide Control in the Biodiesel Industry

The majority of cases regarding process control in the biodiesel industry are based on plantwide control (PWC) and focus mainly on the transesterification reaction section. Since this step precedes the washing process, the main objective is to obtain raw biodiesel such that after the washing process, the resulting biodiesel product complies with the quality specifications [46, 47]. This control objective targets the fatty acids and mono-, di- and triglyceride compositions since the methanol and glycerol will be removed in the separation and washing phases. Figure 4.1 shows a representation of the main equipment units in a biodiesel plant as well as the typical controlled and manipulated variables.

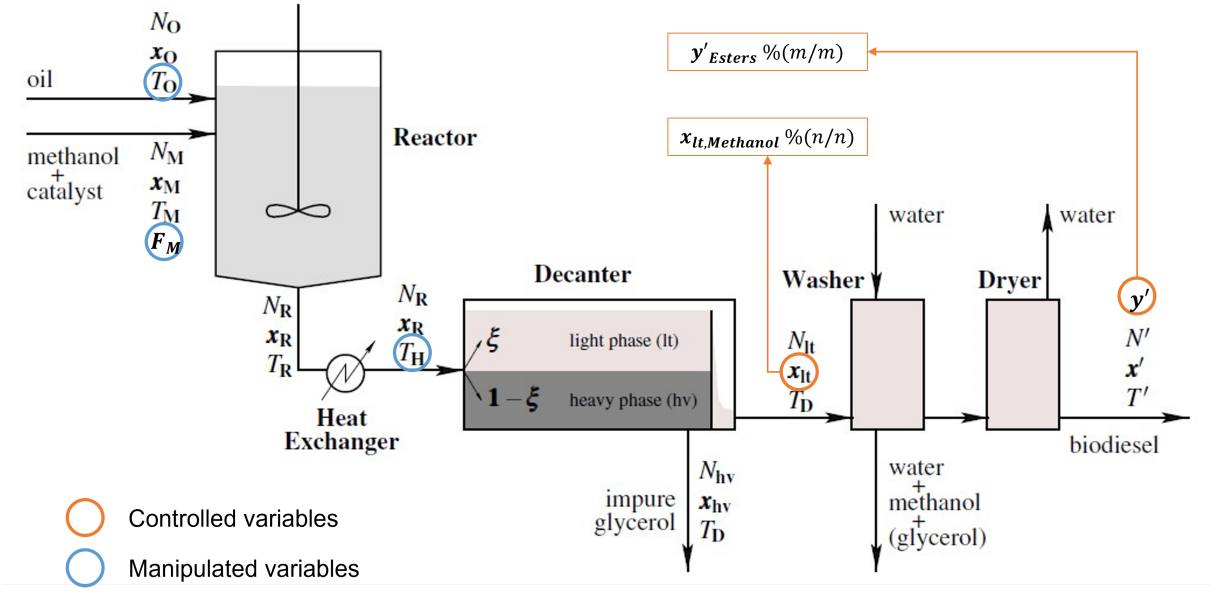

Figure 4.1: Simplified biodiesel plant and the respective controlled and manipulated variables [48].

The classical objectives of PWC for a biodiesel process include a stable production rate under normal operation with good disturbance rejection, safety concerns and environmental regulations, and obtain a product with a purity within specifications. According to the European Standard EN14214, Table 4.1, biodiesel wt% $>$ 96.5 % , for example [46, 47].

Table 4.1: European Standard EN14214 for FAME, glycerol and methanol content in biodiesel.

Solutes	EN14214 wt %
FAME	96.5 min
Glycerol	0.25 max
Methanol	0.2 max

It is also crucial to consider process and equipment constraints such as distillation column's maximum temperatures to avoid biodiesel and glycerol degradation; maintaining the respective ratios of feeds which is significantly important for methanol:FFAs and methanol:glycerides; methanol split ratios for the continuous stirred-tank reactors and the CSTR temperatures to ensure an optimal conversion [49]. Patle et al. in [49] suggest CV-MV pairings and evaluates the performance of the control system using the settling time (an indicator of smooth and safe operation of the plant), deviation from the production target (an indirect economic index), and total variation in the manipulated variables (an indicator of the control efforts required for the PWC structure to attain stable operation).

Patle et al. [49] developed an eight level control system consisting of 52 control loops where the example mentioned above is included. This system is based on the integrated framework of simulation and heuristics methodology and performed particularly well for disturbance rejection, keeping the biodiesel purity under control in accordance with EN14214.

As said before, there are not a lot of published work on control of biodiesel extraction columns, particularly with model predictive control. However, with the increasing tendency of incorporating lower-quality raw materials to make biodiesel [9, 10], the problems related with the oil composition that already have a big impact on the column will become more frequent. Therefore, the development of a control system with good disturbance rejection capabilities is necessary and urgent.

4.2 Control of an Extraction Column

Regarding extraction columns, most control models focus on the interface level between the two phases inside the column and outlet concentrations control [27, 50]. If this level is not adequately stabilised, the dispersed layer could entrain out of the column, leading to flooding, loss of solvent and product [27]. The manipulated variables (MV) used to control the holdup and outlet concentrations are usually the dispersed-phase flow rate, the continuous-phase feed/effluent flow rate and the rotor speed. The control

scheme using the continuous-phase effluent flowrate as MV instead of the feed flow rate demonstrated a monotonic behaviour, while the former showed overshoots, oscillatory behaviour and inverse response [27].

Another control scheme commonly used for extraction columns is the one presented in Figure 4.2 [51]. Here the level of the interface is controlled by manipulating the extract flowrate using a valve. Another important scheme present in this figure is the control of the solvent over feed ratio because it has a great impact on the solubility of the solutes.

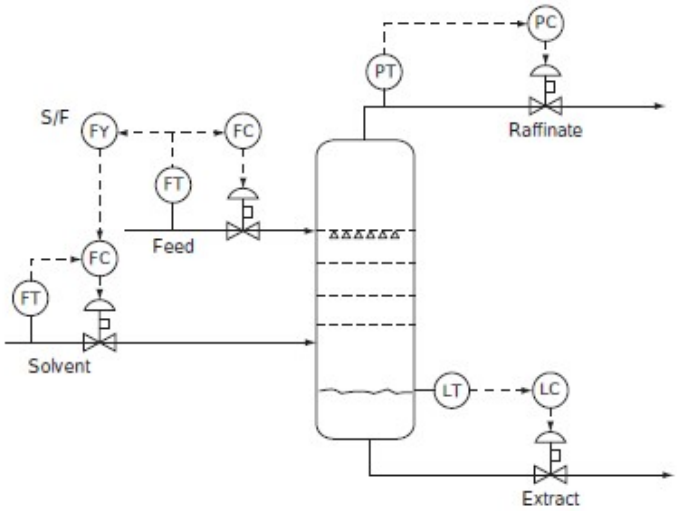

Figure 4.2: Liquid-liquid extraction column control scheme [51].

Patle et al. [49] implemented another control system, illustrated in Figure 4.3. Here, three control loops are implemented: the methanol composition of the biodiesel outlet stream is measured and the wash water flowrate is manipulated if the measured composition is out of the specified limits; the light phase level is controlled and the manipulated variable is the light phase outlet flow; and the heavy phase level is also measured and paired with the heavy phase outlet flow.

4.3 Open-loop Testing and System Linearisation

4.3.1 Open loop testing

Open-loop testing is a crucial procedure to analyse how the system reacts to certain disturbances. Having already an accurate model, input variables such as inlet flowrate, temperature and composition, are subject to intentional changes to observe how they will impact the output variables without the influence of a controller. This step provides useful information particularly for control purposes.

The impact of disturbances in input variables related to biodiesel formulation, such as interfacial ten-

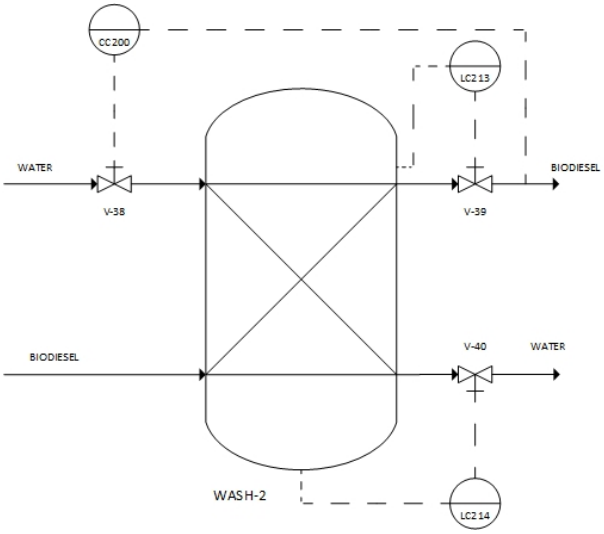

Figure 4.3: Control scheme of a biodiesel washing column with three control loops [49].

sion, density and viscosity, and inlet glycerol composition (that reflects a poor phase separation) on the glycerol composition (wt$\%$) of the biodiesel outlet stream, flooding percentage of both phases, holdup and in the phase inversion parameter (χ) were studied. It was also analysed the effect of step disturbances on the inlet and outlet mass flowrates of biodiesel and water on the output variables mentioned above. The input and output variables are listed in Table 4.2.

Table 4.2: List of input and output variables analysed for control of the extraction column.

Input	Output
Interfacial tension, σ	Biodiesel glycerol composition, $w_{\text{Gly}}^{\text{bd, out}}$
Density, ρ_d	Holdup, ϕ_d
Viscosity, μ_d	Flooding continuous phase, Fl_C
Glycerol composition in washing water, $w_{\text{Gly}}^{\text{wt, in}}$	Flooding dispersed phase, Fl_D
Glycerol composition in unwashed biodiesel, $w_{\text{Gly}}^{\text{bd, in}}$	Phase inversion parameter, χ
Biodiesel mass flowrate, Q_{bio}	
Water mass flowrate, Q_{wt}	

4.3.1.A Input Variables

Starting with the input variables related to biodiesel properties, step disturbances of varying magnitudes were tested and the behaviour of the output variables are presented in Figures 4.4 and 4.5. In these plots are also represented the European norm for the glycerol composition in biodiesel, EN14214, and the two lowest levels for the phase inversion parameter, χ, that are presented in Chapter 2.

The relative values of these changes were chosen according to plausible plant disturbances, that is,

the values for biodiesel density acknowledge the variety of UCO that can be used to produce biodiesel and their densities; the interfacial tension can drop to values close to -80 % of its normal value if contaminants are present, and a 300 % increase in glycerol composition on the washing water or feed streams is not unusual due to its low absolute value, for example.

- Interfacial Tension

  Analysing Figures 4.4 and 4.5, it can be observed that a decrease in the interfacial tension leads to a small decrease in the glycerol composition of the product, to a significant increase on the flooding of both phases and it has almost no effect on the holdup and on χ. Nonetheless, this is a crucial variable to analyse because it reflects the presence of contaminants in biodiesel. However, it is expected a decrease in holdup with the interfacial tension, since there will be less tension to form the droplets. This happens because the model does not incorporate population balance equations.

- Density

  It can be seen that an increase in the density produces a marginal increase in the glycerol composition of the biodiesel, a severe increase in the flooding of the continuous phase, a decrease in the flooding of the dispersed phase, and also a undesirable increase in holdup and χ. Hence, the phase inversion parameter even exceeds the value where phase inversion is more probable as seen in 3.

- Viscosity

  The effect of varying biodiesel viscosity in the controlled variables are minimal. This was not expected, however, biodiesel is the dispersed phase, so increasing its viscosity will not be as impactful as increasing the viscosity of the continuous phase, which would significantly affect the mass transfer. So, this variable will not be analysed further in this chapter.

- Glycerol composition in washing water

  The impact of disturbances in the glycerol composition of washing water is also minimal. Overall, the output variables have slight deviations from their steady-state values, hence, this variable will also not be analysed further in this chapter.

- Glycerol composition in feed

  Finally, these disturbances have a clear impact on the glycerol composition of the washed biodiesel, a +380 % increase is enough to make the product surpass the EN14214 limit of 0.25 wt%. This variable has a small impact in flooding, holdup and phase inversion. Since the inlet glycerol composition is low, around 0.025 wt%, a +380 % increase is not extremely high.

Figure 4.4: Open-loop testing for disturbances in interfacial tension, biodiesel density and biodiesel viscosity.

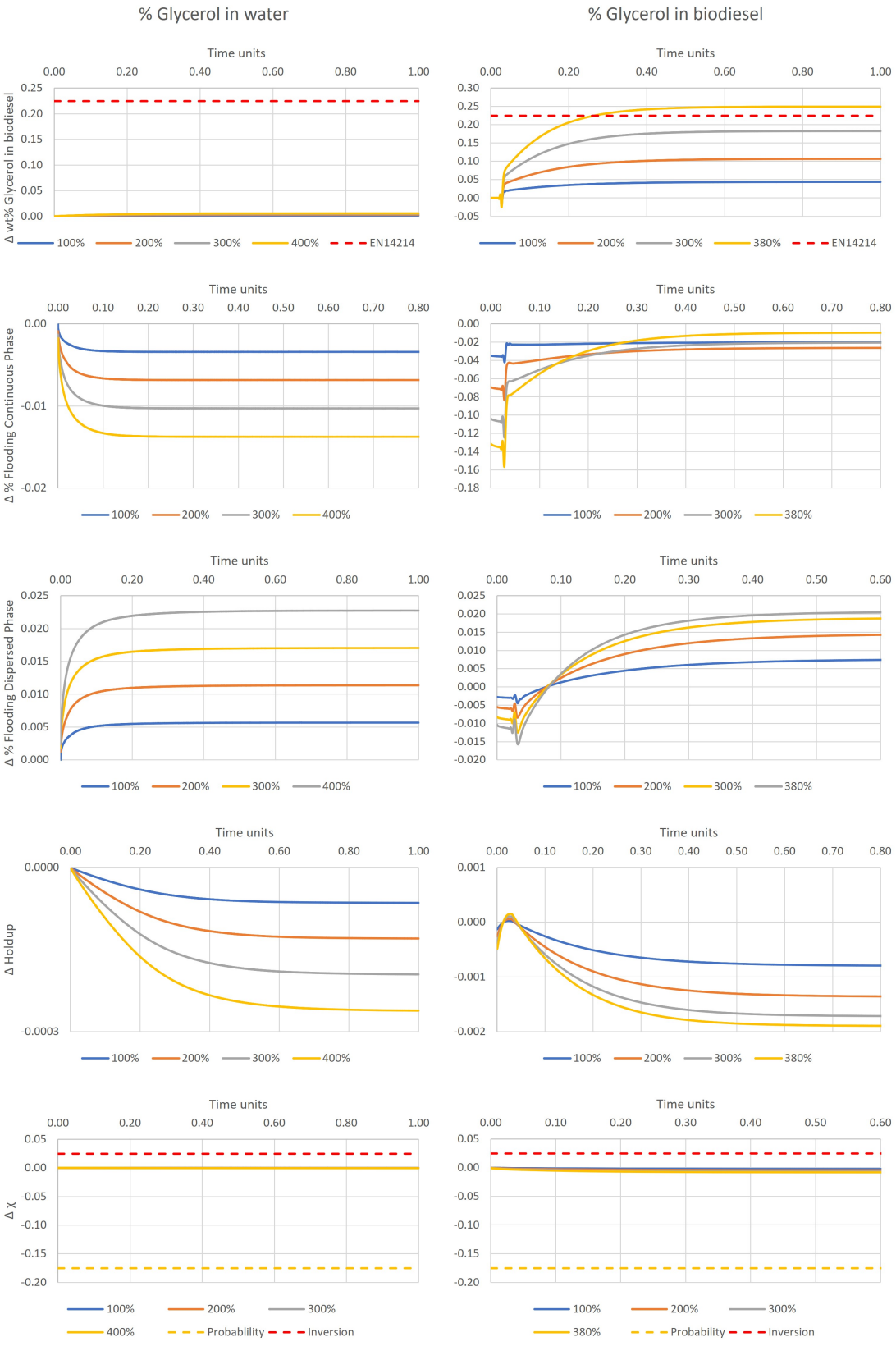

Figure 4.5: Open-loop testing for disturbances in glycerol composition in washing water and feed streams.

For the other input variables, step disturbances of -10 %, -5 %, 5 % and 10 % were implemented. The responses of the output variables to these tests are presented below in Figures 4.6 and 4.7.

- Biodiesel mass flowrate

  Starting with biodiesel flowrate and analysing Figures 4.6 and 4.7, it can be said that the inlet and outlet biodiesel streams have the exactly same impact on the output variables. This happens due to the limitations of the model, because the holdup is not considered to vary with time. An increase in the biodiesel flowrate will lead to an increase in all the analysed output variables, however, it has a larger impact on flooding, holdup and χ.

- Water mass flowrate

  For the water flowrate, the same phenomenon is observed, that is, the inlet and outlet streams have the same effect on the output variables which happens due to model limitations. These limitations are observed because the dynamic behaviour of the holdup was not considered.

  Here, an increase in the water flowrate will lead to an increase in the flooding of continuous phase, holdup and phase inversion parameter and to a decrease in the other two variables. Similarly to what was observed with the biodiesel flowrate, this input variable has a small impact in the glycerol composition of biodiesel, which suggests that if this output variable is controlled, it will require a more aggressive controller that will probably saturate the actuator in order to be more efficient.

4.3.2 System Linearization

In order to proceed with the development of a control system in MATLAB® it was necessary to linearise the system, that is, to obtain the transfer functions that best describe the behaviour of the system. This was performed with the *System Identification* toolbox from MATLAB®. All transfer functions had a fit to estimation data higher than 94 %. The transfer functions are presented in Appendix A.

4.4 Variable Pairing

Proper pairing of controlled and manipulated variables in a multiloop control scheme is essential. Incorrect pairings commonly lead to poor control system performance and reduced stability margins [52]. To analyse this multivariable process control problem, Bristol's Relative Gain Array (RGA) and Singular Value Analysis (SVA) methods will be used. Since manipulating both inlet and outlet flowrates for biodiesel and water would lead to a over-specified system, only the outlet streams will be used for control purposes. Weinstein et al. [27] demonstrated that manipulating the outlet instead of the inlet flowrate would lead to a more smooth behaviour of the system, minimizing overshoots, excessive oscilation and

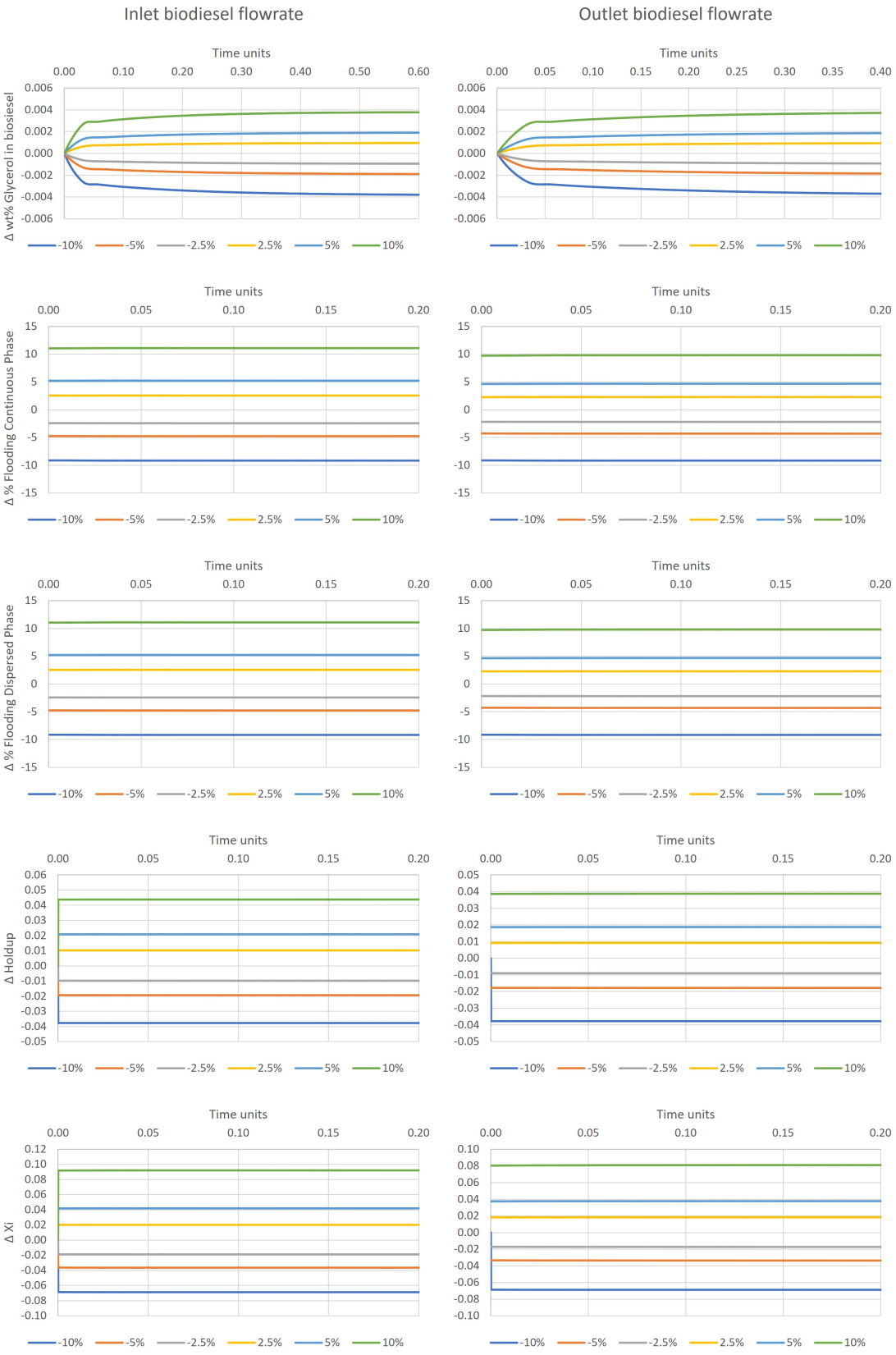

Figure 4.6: Open-loop testing for biodiesel inlet and outlet flowrates.

Figure 4.7: Open-loop testing for water inlet and outlet flowrates.

even reverse-response. Consequently, there can only exist two controlled variables (CV) which is not a problem because holdup, flooding percentages and the phase inversion parameter, χ are all strongly related. Therefore, the mass fraction of glycerol in biodiesel was always analysed with one more of the mentioned variables except χ since it is the least directly dependent on the level of the interface.

4.4.1 Relative Gain Array

The RGA method only requires steady-state information, that is the process gain matrix, K, and provides a measure of process interactions as well as a recommendation for variable pairing CV-MV. After calculating the steady-state gains of the process, summarised in Table 4.3 according to Equation (4.1), it was possible to calculate the relative gains [52].

$$K_{ij} = \left(\frac{\partial y_i}{\partial u_j}\right) \tag{4.1}$$

Table 4.3: Steady-state gain table for the manipulated variables.

K	Water outlet flowrate	Biodisel outlet flowrate
Biodiesel Glycerol Composition (wt%/(kg/h))	-9.33E(-06)	2.96E(-06)
Holdup (h/kg)	1.88E(-05)	3.02E(-05)
Flooding Continuous Phase (%/(kg/h))	5.14E(-03)	7.33E(-03)
Flooding Dispersed Phase (%/(kg/h))	-8.31E(-04)	9.24E(-04)

According to the definition [52] the relative gain, λ_{ij}, between a CV u_i and MV y_j is the dimensionless ratio of two steady-state gains:

$$\lambda_{ij} = \frac{(\partial y_i/\partial u_j)_u}{(\partial y_i/\partial u_j)_y} = \frac{\text{open-loop gain}}{\text{closed-loop gain}} \tag{4.2}$$

with $i = 1, 2, ..., n$ and $j = 1, 2, ..., n$. In Equation (4.2) $(\partial y_i/\partial u_j)_u$ is a partial derivative that is evaluated with all of the manipulated variables except u_j held constant, i.e. open-loop gain, K_{ij}. In the same way, $(\partial y_i/\partial u_j)_y$ is evaluated with all of the controlled variables except y_i held constant, the closed-loop gain which could be achieved in practice by adjusting the other manipulated variables using controllers with integral action [52]. For convenience, the relative gains are usually arranged in a matrix Λ, the Relative Gain Array. The relative gains can be calculated from the following equations for a 2×2 control scheme:

$$y_1 = K_{11}u_1 + K_{12}u_2 \tag{4.3}$$

$$y_2 = K_{21}u_1 + K_{22}u_2 \tag{4.4}$$

Solving Equation (4.4) for u_2, and holding y_2 constant at its nominal value (y_2 = 0):

$$u_2 = -\frac{K_{21}}{K_{22}} u_1 \tag{4.5}$$

Substituting Equation (4.5) into 4.3 gives:

$$y_1 = K_{11}\left(1 - \frac{K_{12}K_{21}}{K_{11}K_{22}}\right) u_1 \tag{4.6}$$

With the definitions of steady-state gain, Equation (4.1), and relative gain, Equation (4.2), an expression for the relative gain is obtained:

$$\lambda_{11} = \frac{1}{1 - \frac{K_{12}K_{21}}{K_{11}K_{22}}} \tag{4.7}$$

Therefore, the three Relative Gain Array matrices for the possible pairings are illustrated below:

Table 4.4: RGA matrix for the controlled variables biodiesel glycerol composition and holdup.

Λ	Water Outlet Flowrate	Biodiesel Outlet Flowrate
Biodiesel Glycerol Composition	**0.83**	0.17
Holdup	0.17	**0.83**

Table 4.5: RGA matrix for the controlled variables biodiesel glycerol composition and flooding of continuous phase.

Λ	Water Outlet Flowrate	Biodiesel Outlet Flowrate
Biodiesel Glycerol Composition	**0.82**	0.18
Flooding Continuous Phase	0.18	**0.82**

Table 4.6: RGA matrix for the controlled variables biodiesel glycerol composition and flooding of dispersed phase.

Λ	Water Outlet Flowrate	Biodiesel Outlet Flowrate
Biodiesel Glycerol Composition	**1.40**	-0.40
Flooding Dispersed Phase	-0.40	**1.40**

From Table 4.4 to Table 4.6 the suggested pairings are emphasised in bold. When $0 < \lambda < 1$ the closed-loop gain between y_i and u_i is larger than the open-loop gain. Thus, the interaction between the two loops is largest when $\lambda = 0.5$. For $\lambda > 1$, closing the second loop reduces the gain between u_i and y_i. Hence, there is interaction between the control loops. This degree of interaction increases with larger values of λ, being impossible to control both outputs independently as $\lambda \to \infty$ (Skogestad and Postlethwaite, 2005) [52]. Finally, for $\lambda < 0$ opening/closing one loop will have an adverse effect on the

behaviour of the other loop since the closed-loop and open-loop have opposite signs. Taken that into consideration, if $\lambda < 0$ than u_i and y_i should not be paired.

Based on these considerations, two variables should be paired only if $\lambda \geq 0.5$ [52].

Another important analysis for a control system is the *Stability Theorem*. This theorem is based on three assumptions [52]: for all transfer functions describing the process, each one of them must be stable, rational, and proper, that is, the order of the denominator must be at least as great as the order of the numerator; each of the n feedback controllers in the multiloop control system has integral action, and each individual control loop is stable when the other loops are opened. If these assumptions are satisfied, then the closed-loop system is unstable if:

$$\frac{|K|}{\Pi_{i=1}^{n} K_{ii}} < 0 \tag{4.8}$$

This theorem provides a sufficient condition for instability, that is, if the inequality is satisfied the closed-loop system will be unstable. However, if the condition is not satisfied, the closed-loop system may or may not be unstable. The values for the Stability Theorem for the three possible pairs are presented in Table 4.7.

Table 4.7: Values for the Stability Theorem for the three possible pairs containing: holdup, flooding of the continuous and dispersed phases.

Pair with the controlled variable:	Holdup	Flooding Continuous Phase	Flooding Dispersed Phase
Condition for instability (< 0)	1.20	1.22	0.71

As mentioned before, the RGA is a practical method to determine variable pairings, however it has a considerable disadvantage: it does not consider process dynamics, which is a weighting factor in the pairing decision. If the transfer function between y_1 and u_1 has a large time delay or time constant when compared to the other variables, y_1 will respond very slowly to variations in u_1. Hence, pairing y_1 with u_1 is not desirable and would not be possible to analyse with the RGA approach.

4.4.2 Singular Value Analysis

The SVA method is a powerful analytical technique that is used to select controlled, measured and manipulated variables, and can also help evaluate the robustness of a given control strategy. Similarly to the RGA it also suggests the best multiloop control configuration and is based on an analysis of steady-state gains from the process model. Starting with the steady-state gain matrix, it is necessary to determine the eigenvalues of K. If any of the eigenvalues are zero then K is a singular matrix and the

process is going to be laborious. If one eigenvalue is significantly smaller when compared to the others, then in order to control the process, very large changes in at least one of the manipulated variables will be required [52].

For the three possible pairings, the eigenvalues α of the K matrices are present in Table 4.8.

Table 4.8: Eigenvalues of the steady-state gain matrices K for the three possible parings.

Eigenvalues of K	Pairing with Holdup (wt%/(kg/h)^2)	Pairing with Flooding Continuous Phase (wt% ol%/(kg/h)^2)	Pairing with Flooding Dispersed Phase (wt% ol%/(kg/h)^2)
α_1	3.14E(-05)	7.30E(-03)	9.21E(-04)
α_2	-1.07E(-05)	0.00	-6.70E(-06)

Analysing Table 4.8, it is possible to identify two undesirable pairings. The possible pairing containing the controlled variable flooding of continuous phase has a singular matrix and the one controlling the flooding of dispersed phase has an eigenvalue significantly larger than the other (in absolute values).

It is also interesting to analyse the *singular values* of K. These are non-negative numbers that are defined as the positive square roots of the eigenvalues of the matrix resulting from K^TK, where K^T is the transpose matrix of K. The singular values were calculated and are presented in Table 4.9.

Table 4.9: Singular values of K for the three possible pairings containing the holdup, flooding of continuous phase and flooding of dispersed phase.

Singular Values of K	Pairing with Holdup	Pairing with Flooding Continuos Phase	Pairing with Flooding Dispersed Phase
σ_1	3.57E(-05)	9.0E(-03)	1.2E(-03)
σ_2	9.43E(-06)	-	-

The only possible pair with two non-negative singular values is the one containing the holdup. The matrix product K^TK for the other two pairs has one negative eigenvalue, hence having only one singular value. With the singular values it is now possible to calculate the Condition Number (CN), Equation (4.9). The CN of K is defined as the ratio of the largest and smallest nonzero singular values, assuming that K in non-singular [52].

$$CN = \frac{\sigma_1}{\sigma_2} \tag{4.9}$$

Where σ_1 is the largest singular value and σ_2 is the smallest. Since there is only one possible pairing with two singular values, its CN is:

Table 4.10: Condition number for the pairing biodiesel glycerol composition - water outlet mass flowrate, holdup - biodiesel outlet mass flowrate.

	Pairing with Holdup
Condition Number	3.78

If K is singular, then it is ill-conditioned and CN $= \infty$. The Condition Number provides useful information about the sensitivity of the matrix properties to variations in the elements of the matrices. A large CN implies that the process is poorly conditioned and thus will be difficult to control [52]. So, from Table 4.10, the CN for the given pairing is acceptable, not implying a particular difficult control situation.

Regarding the RGA and SVA, there is one significant difference that should be addressed. While the elements of RGA are independent of scaling, the same does not apply for the singular values and CN. So, normalising the steady-state gains according to Equation (4.10), the values from Table 4.11 were obtained for the normalised steady-state gains matrix, K^*.

$$K^*_{ij} = K_{ij} \frac{u'_{\text{max},j}}{y_{\text{max}}, i} \tag{4.10}$$

Table 4.11: Normalised steady-state gains.

K^*	Water outlet flowrate	Biodiesel outlet flowrate
Biodiesel Glycerol Composition	-0.47	0.97
Holdup	0.10	1.00
Flooding Continuous Phase	0.11	1.00
Flooding Dispersed Phase	-0.14	1.00

From the values of Table 4.11 the same procedure for the SVA was used and the values are summarised in Table 4.12.

Table 4.12: SVA analysis for the normalised values of K.

SVA*		Pairing with Holdup	Pairing with Flooding Continuous Phase	Pairing with Flooding Dispersed Phase
Eigenvalues	α_1^*	1.06	1.07	0.90
	α_2^*	-0.53	-0.54	-0.37
Singular Values	σ_1^*	1.42	1.41	1.45
	σ_2^*	0.39	0.40	0.23
CN*		3.60	3.52	6.37

From Table 4.12, all three pairings could be used to control the system. Table 4.13 summarises the variable pairing analysis.

Table 4.13: Variable pairing analysis from RGA and SVA methods.

Pairing Number	CV	MV	RGA	CN	CN*
1	wt% Gly HU	Q_{out} water Q_{out} biodiesel	0.83	3.78	3.60
2	wt% Gly Fl. C. %	Q_{out} water Q_{out} biodiesel	0.82	-	3.52
3	wt% Gly Fl. D. %	Q_{out} water Q_{out} biodiesel	1.40	-	6.37

Taking everything into account, pairing number 1 from Table 4.13 is the most recommended since all three methods gave satisfactory results. The control scheme is illustrated in Figure 4.8.

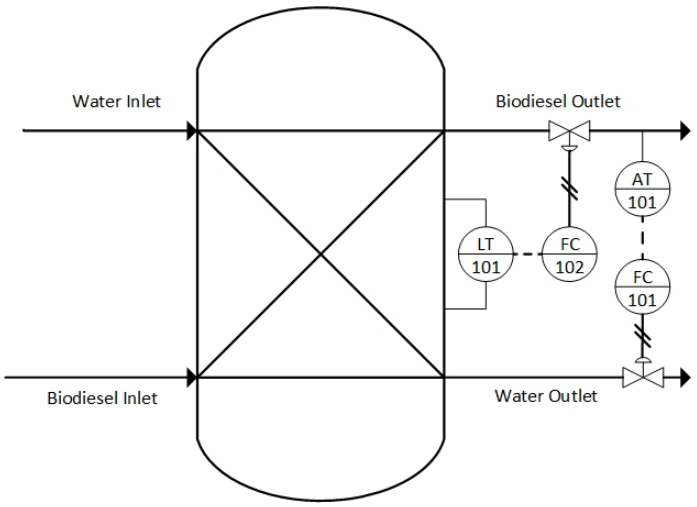

Figure 4.8: Control scheme for the biodiesel extraction column.

The nomenclature used in Figure 4.8 will be used to refer to the controllers in the next subsection.

4.5 Controller Tuning

Knowing which variables to pair, it is now necessary to tune the controllers. Each controller was tuned with the other loop opened and different approaches were tested and then compared. The tested controllers were evaluated based on integral error criterion in set-point tracking and disturbance rejection. The control system was also analysed in terms or relative stability with the concepts of Gain Margin (GM) and Phase Margin (°) (PM). All controllers were tuned in Mathematica® with Ziegler-Nichols (ZN), Internal Model Control (IMC) and Cohen-Coon (CC) tuning techniques available in the solver. Saturation was added to the MV, -10 % to 10 % for biodiesel mass flowrate and -20 % to 20 % for water mass flowrate.

Controller's performance can be compared based on integral error criteria. The controller can be optimised according to the closed-loop response for a specified disturbance or set-point change. The three most used integral error criteria are:

- Integral of the squared error (ISE)

$$\text{ISE} = \int_0^\infty e^2(t)dt \tag{4.11}$$

- Integral of the absolute value of the error (IAE)

$$\text{IAE} = \int_0^\infty |e(t)|dt \tag{4.12}$$

- Integral of the time-weighted absolute error (ITAE)

$$\text{ITAE} = \int_0^\infty t|e(t)|dt \tag{4.13}$$

Overall, the ISE method minimises overshoot and is more aggressive while the ITAE penalises long settling times and is more conservative. On the other hand, the IAE criterion tends to produce controller settings that are between those between for the ISE and ITAE criteria.

Before choosing the best controller, it is interesting to analyse another two parameters: the GM and the PM. These concepts are measures of relative stability that indicate how close the system is to become unstable [52]. Starting with the GM, it provides a measure of relative stability because it indicates how much the gain in the feedback loop can increase before the system reaches instability. Hence, a stability requirement is that GM should be higher than 1. On the other hand, the PM indicates how much time delay can be included in the feedback loop before instability will occur [52]. The values of the Gain and Phase Margins were calculated using MATLAB®.

4.5.1 FC101 - Composition controller

Starting with the FC101 controller, the Ziegler-Nichols and Internal Model Control (Skogestad) tuning methods were tested [52].

The ZN method for controller tuning is based in a trial-and-error procedure. First the ultimate gain and ultimate period are determined, that is, the gain value that produces continuous cycling for proportional-only control and its respective period. This method is further explained in Chapter 12 of Seborg et al. [52], including the controller settings. Finally, the tuned controller should be evaluated by introducing a small set-point change and fine-tuned, if necessary [52].

Only the PI and PID controller modes will be presented since a proportional-only controller is oscillatory and has an offset, which is undesirable.

IMC is a type of model-based design methods for controller tuning. This method is based on a designed process model and leads to analytical expressions for the controller settings. The IMC method is based on the simplified block diagram shown in Figure 4.9 *(b)*. Here, the process model, $\tilde{G}$, and the process output, P, are used to compute the model response, $\tilde{Y}$ in the diagram. The model response is subtracted from the actual response, $Y - \tilde{Y}$, and the result is used as input to calculate the error for the IMC controller, G_c^*.

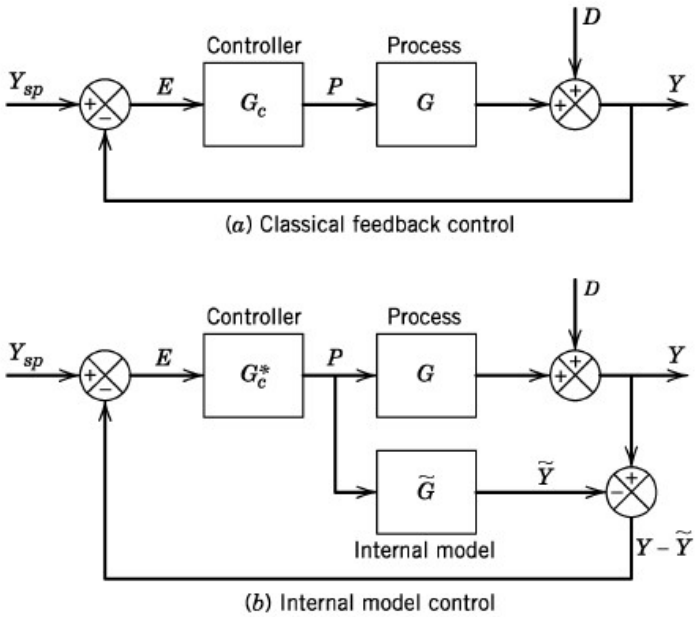

Figure 4.9: Classical feedback control and IMC [52].

The IMC controller is designed according to the tuning settings shown in Chapter 12 of Seborg et al. [52]. The selection of τ_C was done according to Skogestad guidelines, that is $\tau_C = \theta$, where θ is the "effective" delay. The IMC for more complicated models calculates θ as half of the second largest time

constant [53].

The controller settings for the different tuning methods are presented in Table 4.14 with the values of GM and PM. The controller is in parallel and the derivative mode has a filter N.

Table 4.14: Controller settings for the controller FC101 according to ZN and IMC tuning methods and Gain and Phase Margins.

Tuning Method		ZN		IMC	
Controller mode		PI	PID	PI	PID
	K_P	-2.05E06	-273E06	-2.24E06	-1.07E09
Controller	K_I	-7.21E07	-1.60E08	-6.36E07	-1.41E11
Settings	K_D	-	-1.16E04	-	-8.08E05
	N	-	100	-	100000
Relative	GM	68	1392	67	2
Stability	PM	34	23	37	47

To evaluate the controller performance, a set-point change of -10 % was tested. The responses of the controlled and manipulated variables to this set-point change are presented in Figure 4.10 and Figure 4.11. In Figure 4.10, the IMC PID controller stabilises at around 1.2 time units.

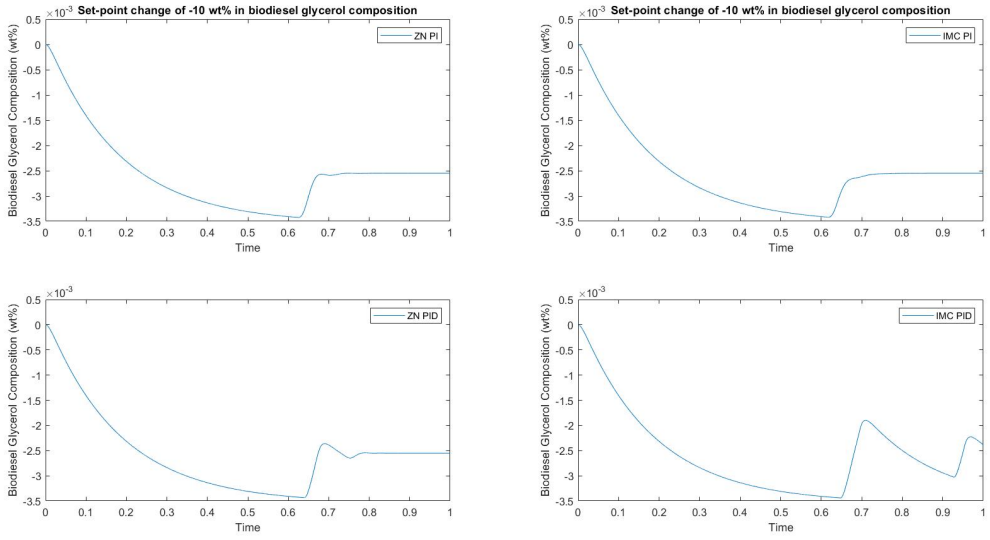

Figure 4.10: Response of the controlled variable biodiesel glycerol composition to a set-point change of -10 % for a controller with different tuning methods.

The integral error criteria for the set-point tracking shown in Figures 4.10 and 4.11 is presented in Table 4.15.

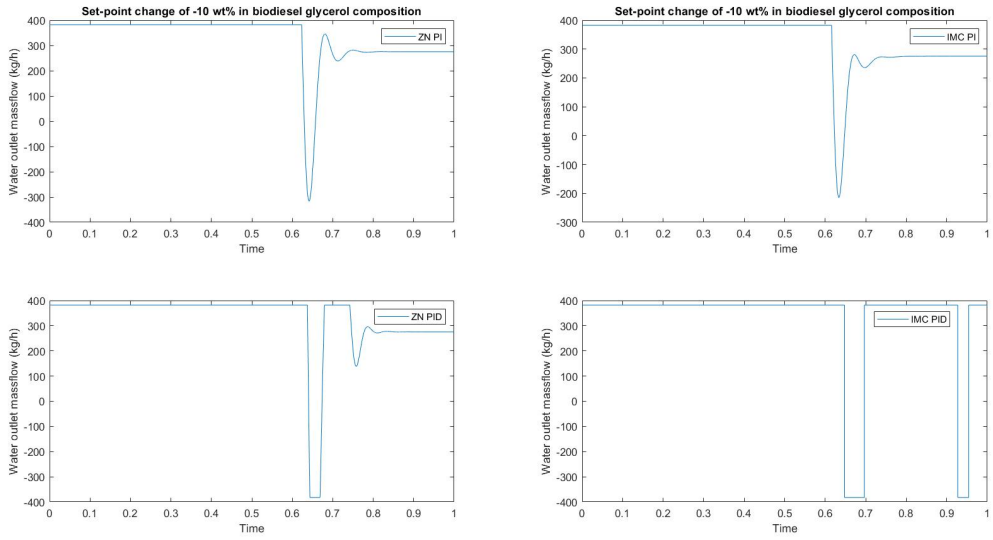

Figure 4.11: Response of the manipulated variable water outlet mass flowrate to a set-point change of -10 % in biodiesel glycerol composition (wt %) for a controller with different tuning methods.

Table 4.15: Integral error criteria for controller FC101 relative to a set-point change.

Tuning Method	ZN		IMC	
Controller Mode	PI	PID	PI	PID
IAE	5.04E(-04)	5.19E(-04)	5.04E(-04)	6.11E(-04)
ISE	5.80E(-07)	5.89E(-07)	5.76E(-07)	6.31E(-07)
ITAE	1.41E(-04)	1.52E(-04)	1.41E(-04)	2.28E(-04)

Analysing Figures 4.10 and 4.11, and Table 4.15 it is notable that adding derivative action to this controller increases instability and decreases its performance when compared to a proportional-integral controller. Thus, from the table, the PI controller tuned with IMC has slightly better performance than the other tuning methods.

Now for the disturbance rejection, a disturbance of -80 % in the interfacial tension was applied to the system. The responses of the controlled and manipulated variables are illustrated in Figures 4.12 and 4.13. The integral error criteria is presented in Table 4.16.

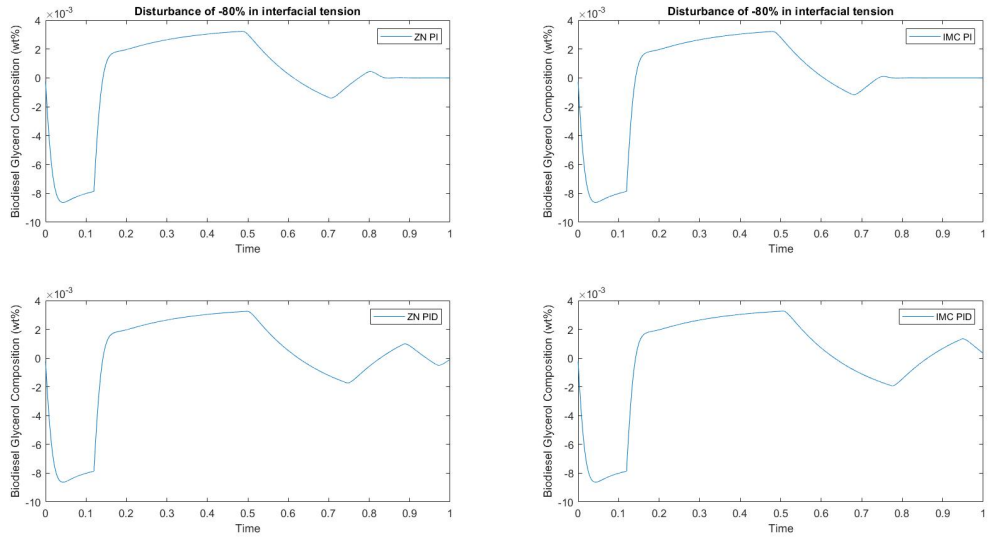

Figure 4.12: Response of the controlled variable biodiesel glycerol composition to a disturbance of -80 % in interfacial tension for a controller with different tuning methods.

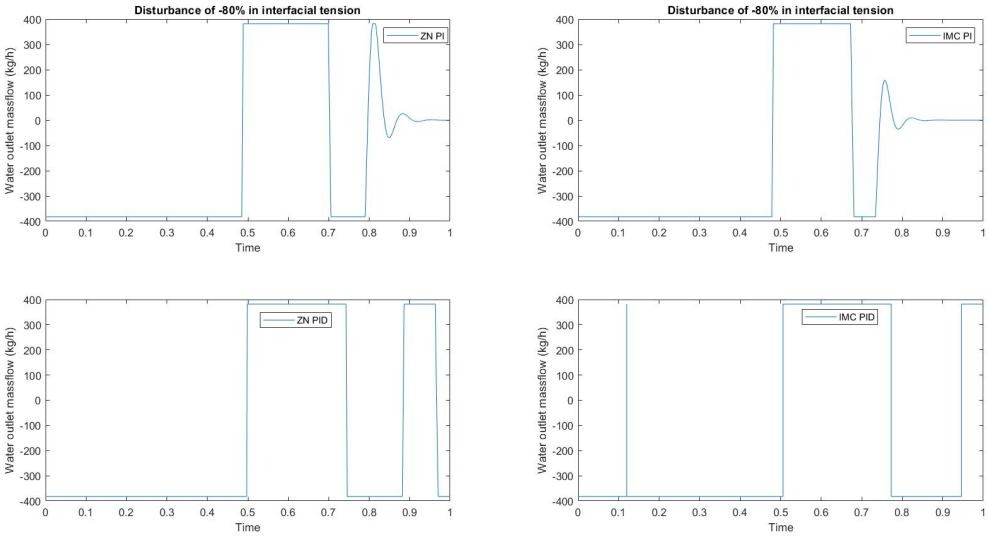

Figure 4.13: Response of the manipulated variable water outlet mass flowrate to a disturbance of -80 % in interfacial tension for a controller with different tuning methods.

Table 4.16: Integral error criteria for controller FC101 relative to a disturbance in interfacial tension.

Tuning Method	ZN		IMC	
Controller Mode	PI	PID	PI	PID
IAE	2.20E(-03)	2.37E(-03)	2.12E(-03)	2.47E(-03)
ISE	1.05E(-05)	1.08E(-05)	1.34E(-05)	1.10E(-05)
ITAE	5.66E(-04)	7.01E(-04)	5.15E(-04)	7.88E(-04)

Analysing Figures 4.12 and 4.13, and Table 4.16, it is observable that, similarly to the set-point change, the PI controllers have a better performance than the PID controllers. This behaviour was expected because adding derivative action to a controller increases its sensibility. The increase in sensibility will result in a greater controller output when the deviation is changing, which will depend on the error rate of change. In 4.12 all plots stabilise, even the ones below. Since both large errors, as well as errors that persist for long time periods are undesirable, the IAE criterion was the deciding factor for the selection of the best controller settings for FC101. So, the PI controller tuned with IMC settings was chosen for controller FC101.

4.5.2 FC102 - Liquid-level controller

Similarly to FC101, the controller FC102 was also tuned with two different methods. Both ZN and IMC tuning approaches were tested, however, the IMC tuning technique failed to return a viable controller. This happened due to the denominator dynamics of the transfer function that characterises the effect of the biodiesel outlet flowrate on the holdup,

$$G(s) = \frac{1.664s + 6.588}{s^2 + 55080s + 218000}$$

Here, the s^2 term is much smaller than the term 218000 and so, when $s \to 0$ the denominator has no dynamics (it becomes constant). *Mathematica*© could not develop a controller with IMC because it is based in zero-pole cancellation and the system had no denominator dynamics for small s values. So, the Cohen-Coon tuning method was used instead of IMC.

This method is similar to ZN method, however, its settings are determined to get a minimum offset and a standard decay ratio of 1/4. A 1/4 decay ratio refers to a response that has decreasing oscillations in such a manner that the second oscillation has 1/4 the amplitude of the first oscillation. The settings for these controllers are shown in Woolf [54].

Applying the ZN and CC tuning methods to the controller, the controller settings in Table 4.17 are obtained.

Table 4.17: Controller settings for the controller FC102 according to ZN and CC tuning methods and Gain and Phase Margins.

Tuning Method		ZN		CC	
Controller mode		PI	PID	PI	PID
Controller Settings	K_P	3.02E04	4.03E04	5.76E04	5.34E04
	K_I	1.64E06	3.65E06	9.21E06	5.18E06
	K_D	-	111	-	91.7
	N	-	100	-	1000
Relative Stability	GM	∞	∞	∞	∞
	PM (°)	156	∞	125	∞

Again, to evaluate the different controllers a set-point of -10 % in holdup was studied, Figures 4.14 and 4.15, and a disturbance of +3.5 % in biodiesel density was also analysed, Figures 4.16 and 4.17. Here, it is possible to see that the holdup changes immediately to any input change because its equation does not have dynamics. This is a limitation of the model that was already addressed.

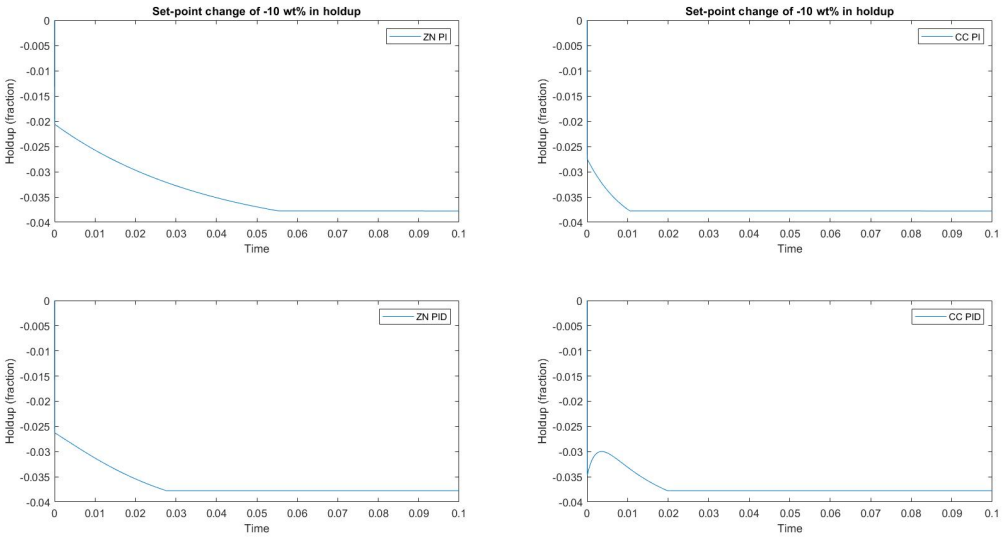

Figure 4.14: Response of the controlled variable holdup to a set-point change of -10 % for a controller with different tuning methods.

The integral error criteria for the set-point change and disturbance rejection are summarised in Tables 4.18 and 4.19, respectively.

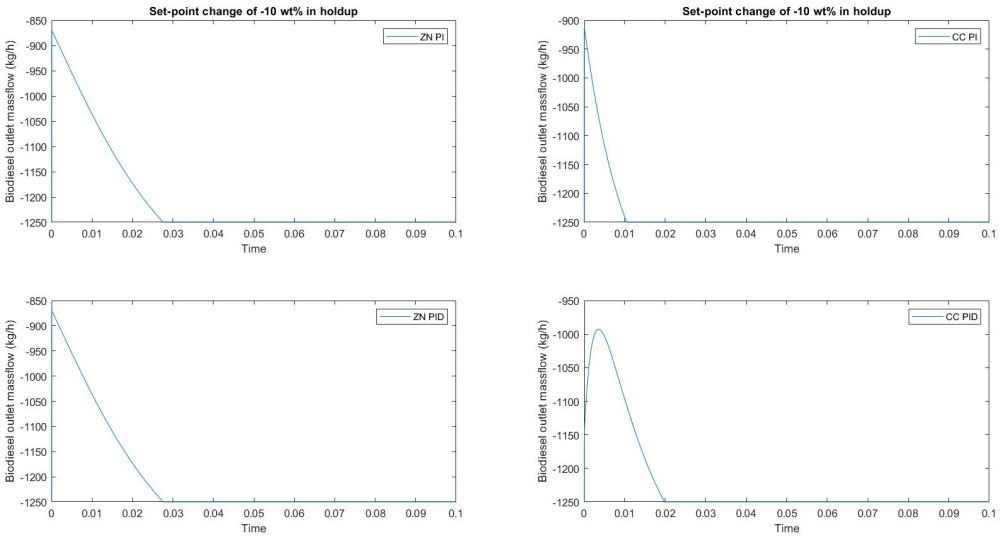

Figure 4.15: Response of the manipulated variable biodiesel outlet mass flowrate to a set-point change of -10 % in holdup for a controller with different tuning methods.

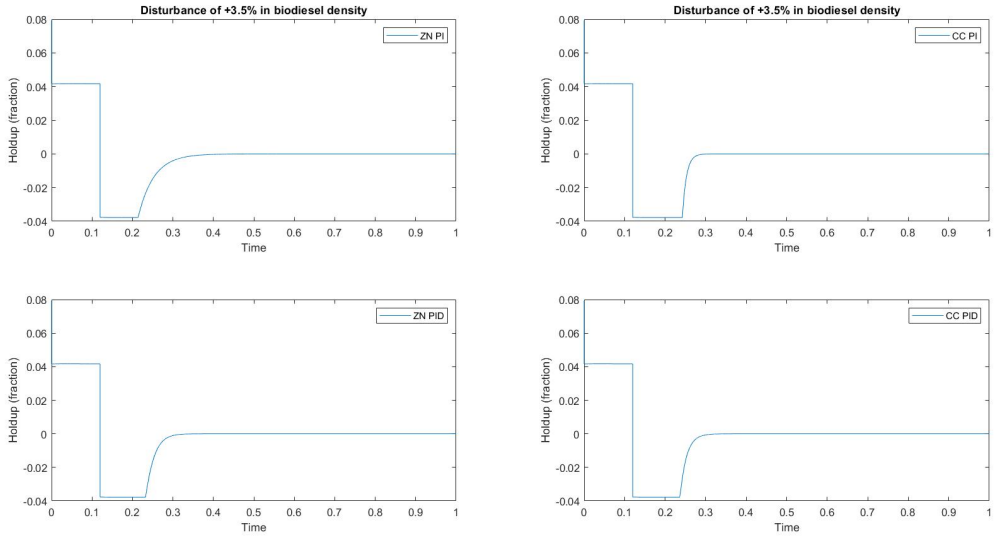

Figure 4.16: Response of the controlled variable holdup to a disturbance of +3.5% in biodiesel density for a controller with different tuning methods.

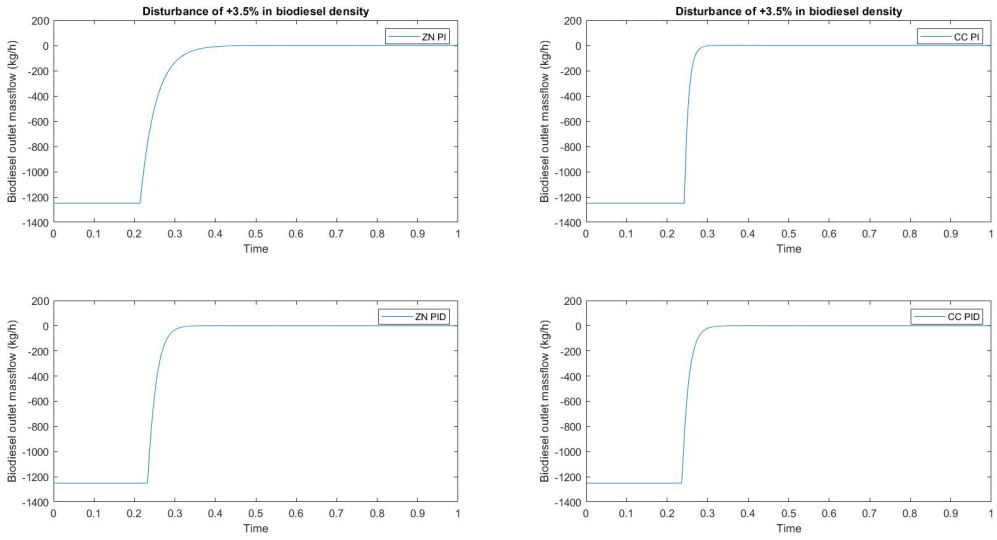

Figure 4.17: Response of the manipulated variable biodiesel outlet mass flowrate to a disturbance of +3.5 % in biodiesel density for a controller with different tuning methods.

Table 4.18: Integral error criteria for controller FC102 relative to a set-point change in holdup.

Tuning Method	ZN		CC	
Controller Mode	PI	PID	PI	PID
IAE	5.74E(-03)	5.51E(-03)	5.42E(-03)	5.46E(-03)
ISE	3.65E(-05)	3.14E(-05)	2.96E(-05)	3.03E(-05)
ITAE	2.69E(-03)	2.69E(-03)	2.69E(-03)	2.69E(-03)

Table 4.19: Integral error criteria for controller FC102 relative to a disturbance in biodiesel density.

Tuning Method	ZN		CC	
Controller Mode	PI	PID	PI	PID
IAE	1.00E(-02)	1.00E-02	1.00E-02	1.00E(-02)
ISE	3.70E(-04)	3.84E-04	3.91E-04	3.87E-04
ITAE	1.26E(-03)	1.24E-03	1.23E-03	1.24E-03

Analysing both tables, and taking the IAE criterion as the deciding factor, the PI controller tuned with CC rules has a slightly better performance when compared with the other ones. Hence, this was the chosen controller settings.

4.5.3 Decouplers

Having the two closed-loops with both controllers tuned, it is necessary to add decouplers to minimise interaction between the closed-loops. In this subsection the decouplers will be tuned and then in the *Multiloop Control System* section the behaviour of the system with and without decouplers will be presented.

Decouplers are controllers that can be added in multivariable control cases in order to reduce control loop interactions [52]. The input signal to each decoupler is the output signal from a feedback controller. So, considering the 2 $\times$ 2 decoupling control system of Figure 4.18 [52], the ideal decouplers are given by Equations 4.14 and 4.15.

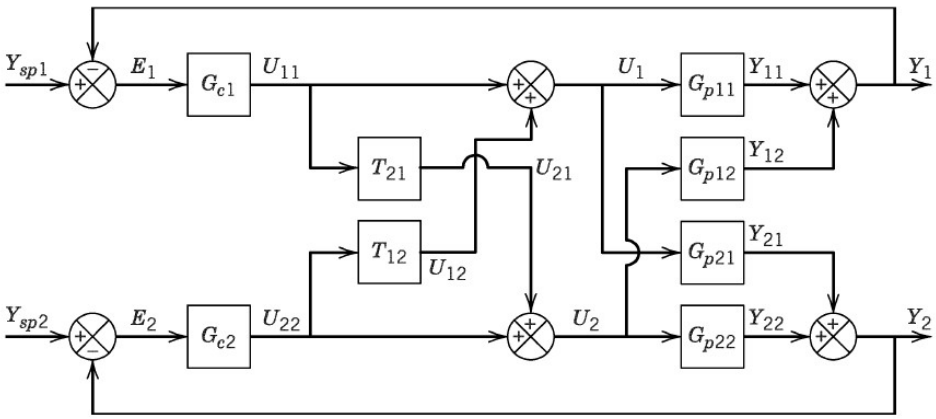

Figure 4.18: Decoupling control system of a 2 $\times$ 2 process [52].

$$T_{21} = -\frac{G_{p21}}{G_{22}} \tag{4.14}$$

$$T_{21} = -\frac{G_{p12}}{G_{11}} \tag{4.15}$$

Applying these equations to the extraction column, the following transfer functions are obtained.

$$T_{\text{HU-Water}} = \frac{-0.8514s^4 - 4.691E04s^3 - 9.991E05s^2 - 6.137E06s - 1.155E07}{1.664s^4 + 7.435E04s^3 + 1.609E06s^2 + 9.89E06s + 1.855E07} \tag{4.16}$$

$$T_{\text{Gly-Biodiesel}} = \frac{-7.395E(-05)s^4 - 0.02508s^3 - 2.139s^2 - 26.82s - 87.25}{6.192E(-07)s^4 - 0.005889s^3 - 0.8153s^2 - 49.93s - 263.1} \tag{4.17}$$

However, when analysing the transfer function of the decoupler $T_{\text{Gly-Biodiesel}}$ has a real right-half plane pole which makes it unstable. So, instead of using ideal decouplers, static decouplers will have to be used instead. Static decouplers are calculated similarly to Equations 4.14 and 4.15 but instead of the process transfer functions, only the steady-state gains are used. The static decouplers used are presented in Table 4.20.

Table 4.20: Static decouplers used to minimised closed-loop interactions.

Static Decouplers	
$T_{\text{HU-Water}}$	-0.6225
$T_{\text{Gly-Biodiesel}}$	0.3324

4.6 Multiloop Control System

Having the multiloop with decouplers, it is interesting to evaluate if and how the system benefited from the addition of the closed-loops and decouplers. Starting with set-point tracking, Figures 4.19 and 4.20 illustrate the response of the system to set-point changes in both controlled variables.

In Figure 4.19 for the closed-loop (in blue) it is possible to identify strong closed-loop interactions. When the set-point for the glycerol outlet composition decreases, the water flowrate immediately increases to its maximum value which leads to an increase in holdup that quickly returns to its original value due to a decrease in the biodiesel flowrate. With the saturation of the biodiesel flowrate, the glycerol outlet composition goes to a lower value and then increases to its new set-point due to a decrease in the water outlet flowrate, at around 0.31 time units. This decrease causes the holdup do change again but it is immediately corrected by an increase in the biodiesel flowrate. As it is possible to see, the addition of decouplers was able to eliminate the peaks in the holdup and minimise the changes in the biodiesel outlet flowrate.

In Figure 4.20 for the closed-loop (in blue), the interactions between the closed-loops are even stronger due to the dynamics of the system. A lower set-point for the holdup is achieved rapidly with an immediate decrease in the biodiesel flowrate. This causes a strong disturbance in the glycerol outlet composition that is corrected with the saturation of the water outlet flowrate with a long settling time. Again, the addition of decouplers was able to minimise the action of the actuators and reduced the

settling time of the glycerol outlet composition.

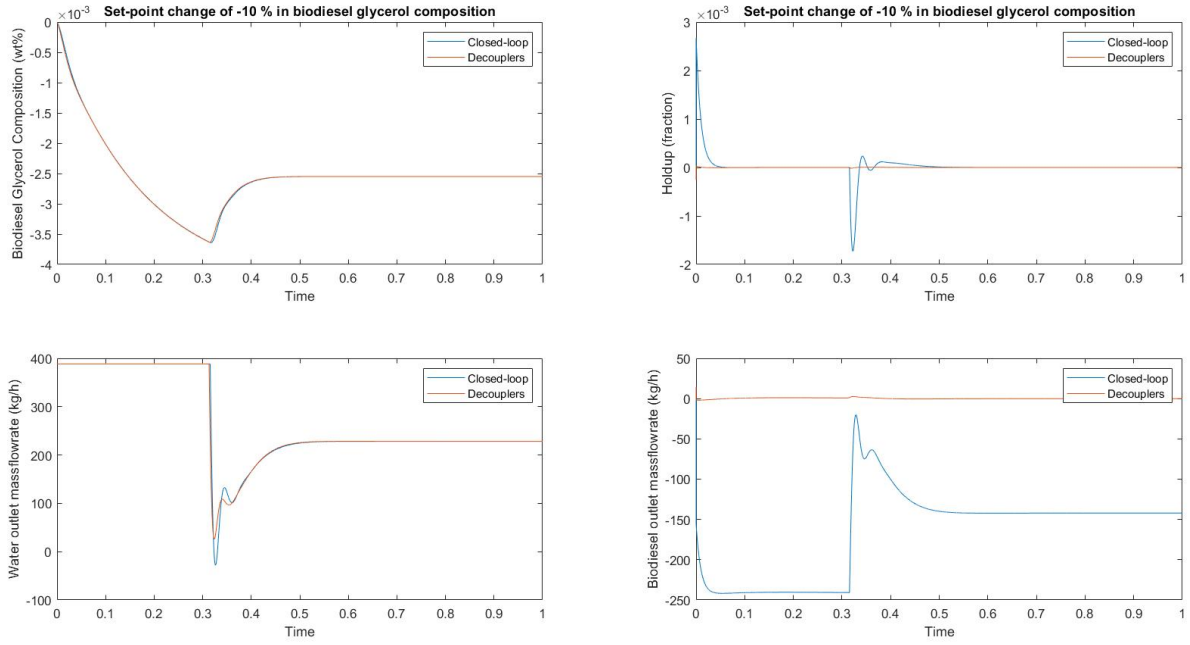

Figure 4.19: Evolution of the controlled and manipulated variables to a set-point change of -10 % in biodiesel glycerol composition (wt %).

The response of the open-loop, closed-loop, and closed-loop with static decouplers systems to disturbances in interfacial tension, biodiesel density and feed glycerol composition are presented in Figures 4.21 to 4.24.

The presence of the peaks in these figures with closed-loop control should be addressed. This behaviour happens due to strong interactions between closed-loops, as explained before for the plots for set-point tracking. For disturbances in interfacial tension, the glycerol outlet composition decreases and the water outlet flowrate is immediately decreased to its minimum value. This causes a decrease in holdup that is rapidly adjusted by an increase in the biodiesel outlet flowrate. However, a higher biodiesel flowrate increases the glycerol outlet composition that is corrected with an increase (saturation) of the water flowrate at around 0.4 time units. This increase causes a peak in holdup that required the biodiesel flowrate to decrease. Once again, this change led to a decrease in glycerol outlet composition with the stabilization of the water outlet flowrate. This had a small impact in the holdup and, consequently, in the biodiesel flowrate.

For a disturbance in biodiesel density, there is an immediate increase in holdup that saturates the biodiesel outlet flowrate at its minimum value. The increase in glycerol outlet flowrate verified at the beginning of the simulation also saturated the water outlet flowrate at its maximum. The holdup stabilises for some time period due to the saturation of the manipulated variables. The glycerol outlet composi-

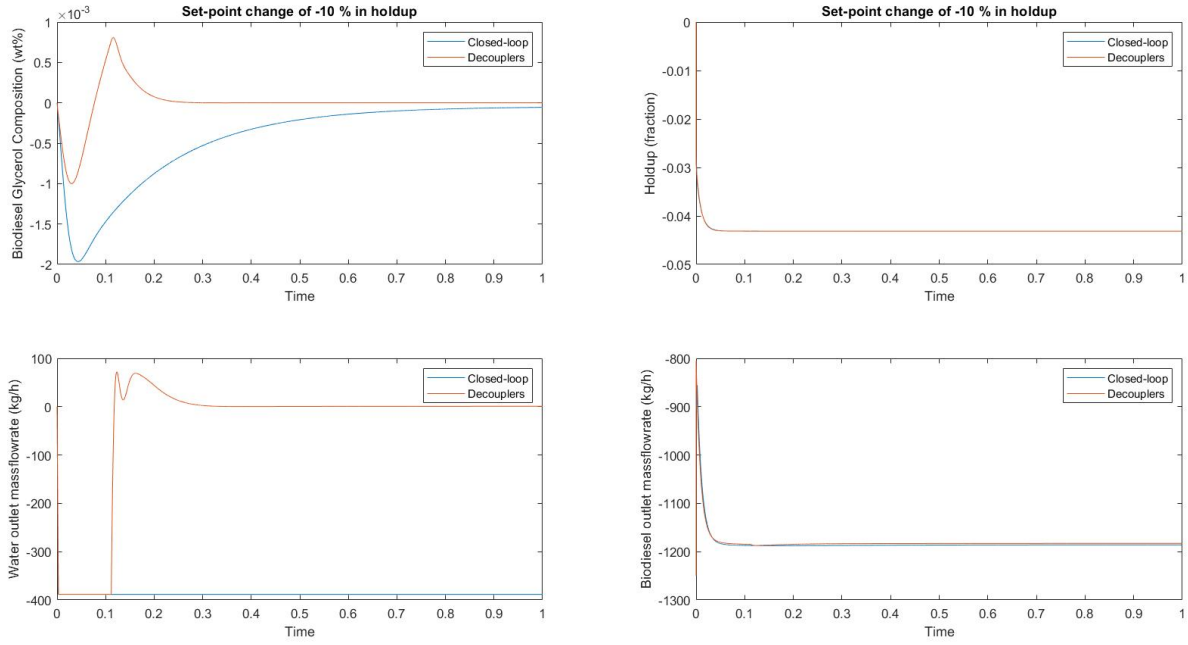

Figure 4.20: Evolution of the controlled and manipulated variables to a set-point change of -10% in holdup.

tion starts to decrease which then saturates the water outlet flowrate at its minimum value, decreasing the holdup and increasing the biodiesel flowrate until it reaches saturation. After that, both controlled variables start to stabilise, which is also observed in the manipulated variables.

Finally, a disturbance in the glycerol inlet composition increases the glycerol outlet flowrate with delay. In order to stop this, the water outlet flowrate saturates at its maximum value and stays saturated. This immediate response causes the holdup to increase but it is quickly regulated by a decrease in biodiesel flowrate.

It is noticeable that the addition of decouplers to the control system was beneficial because, for set-point tracking, it was able to reduce settling-time, excessive oscillation and overshoots, and even reducing the duration of the actuator saturation. For disturbance rejection, the control of holdup greatly improved with the reduction of settling-time and lower overshoots; the control of biodiesel glycerol composition was not ideal due to an increase in oscillation, however the overshoots were minimised. Additionally, it was also observable that the closed-loop interactions were reduced by adding decouplers, and that they were successful in reducing excessive controller action.

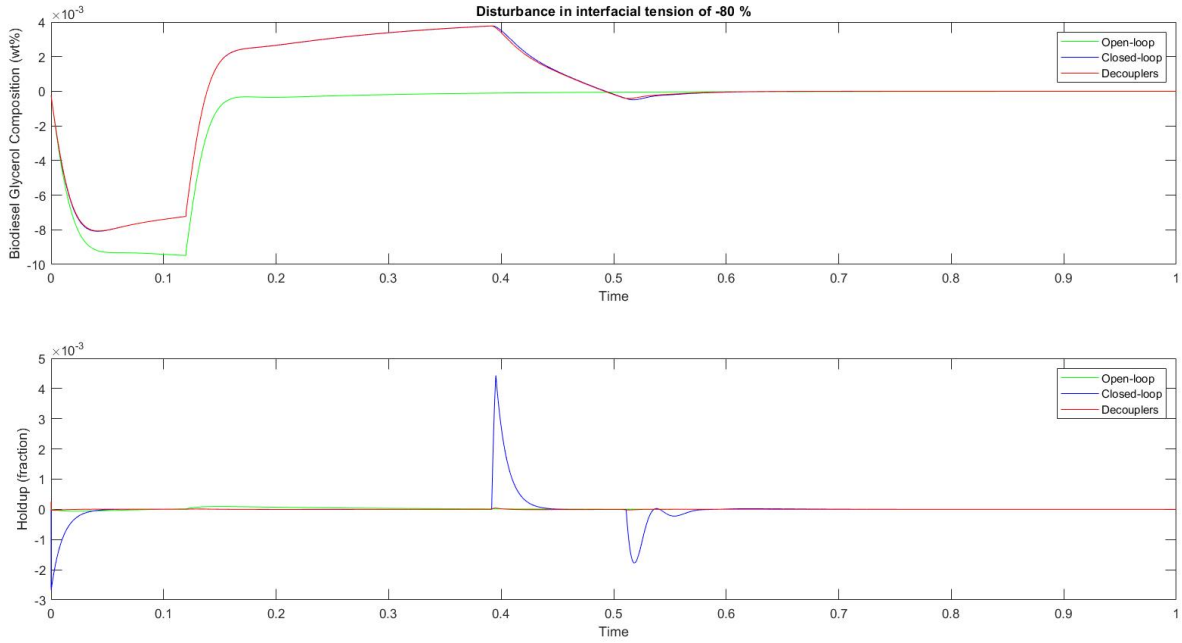

Figure 4.21: Evolution of the controlled variables: biodiesel glycerol composition (wt%) and holdup fraction to a disturbance in interfacial tension of -80 %.

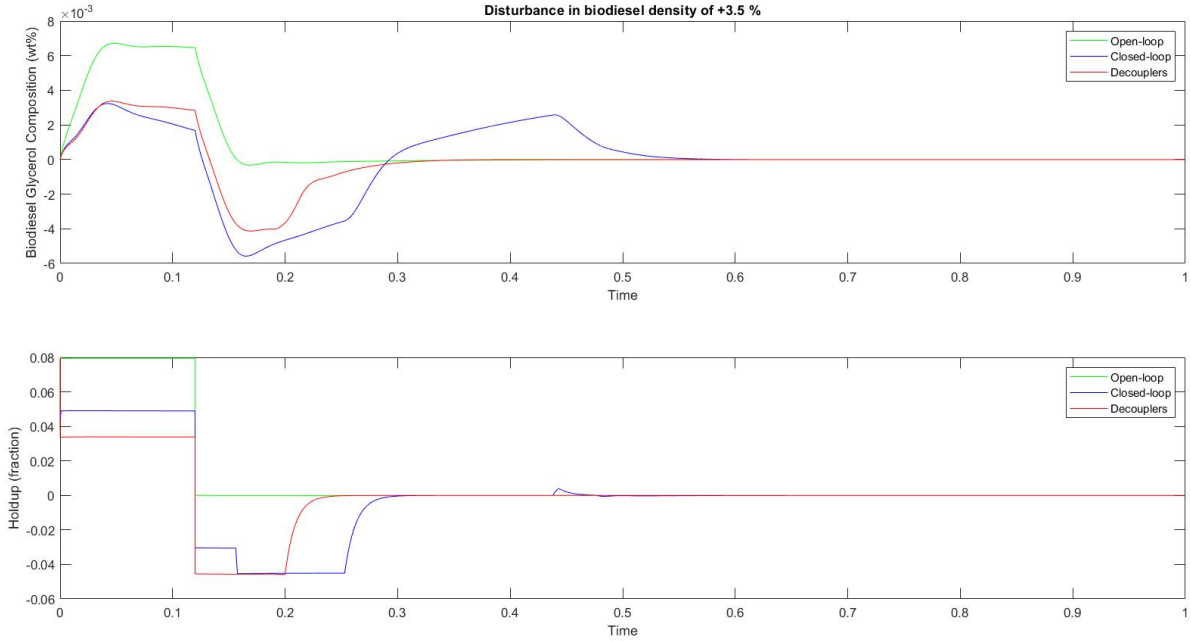

Figure 4.22: Evolution of the controlled variables: biodiesel glycerol composition (wt%) and holdup fraction to a disturbance in biodiesel density of +3.5 %.

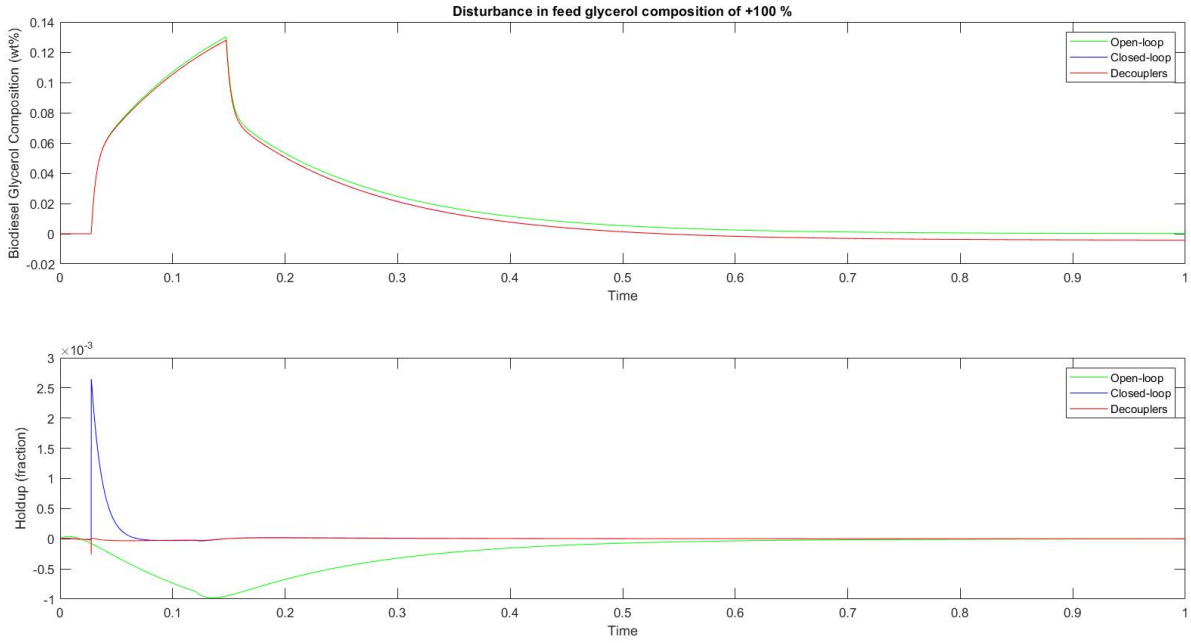

Figure 4.23: Evolution of the controlled variables: biodiesel glycerol composition (wt%) and holdup fraction to a disturbance in feed glycerol mass composition of +100 %.

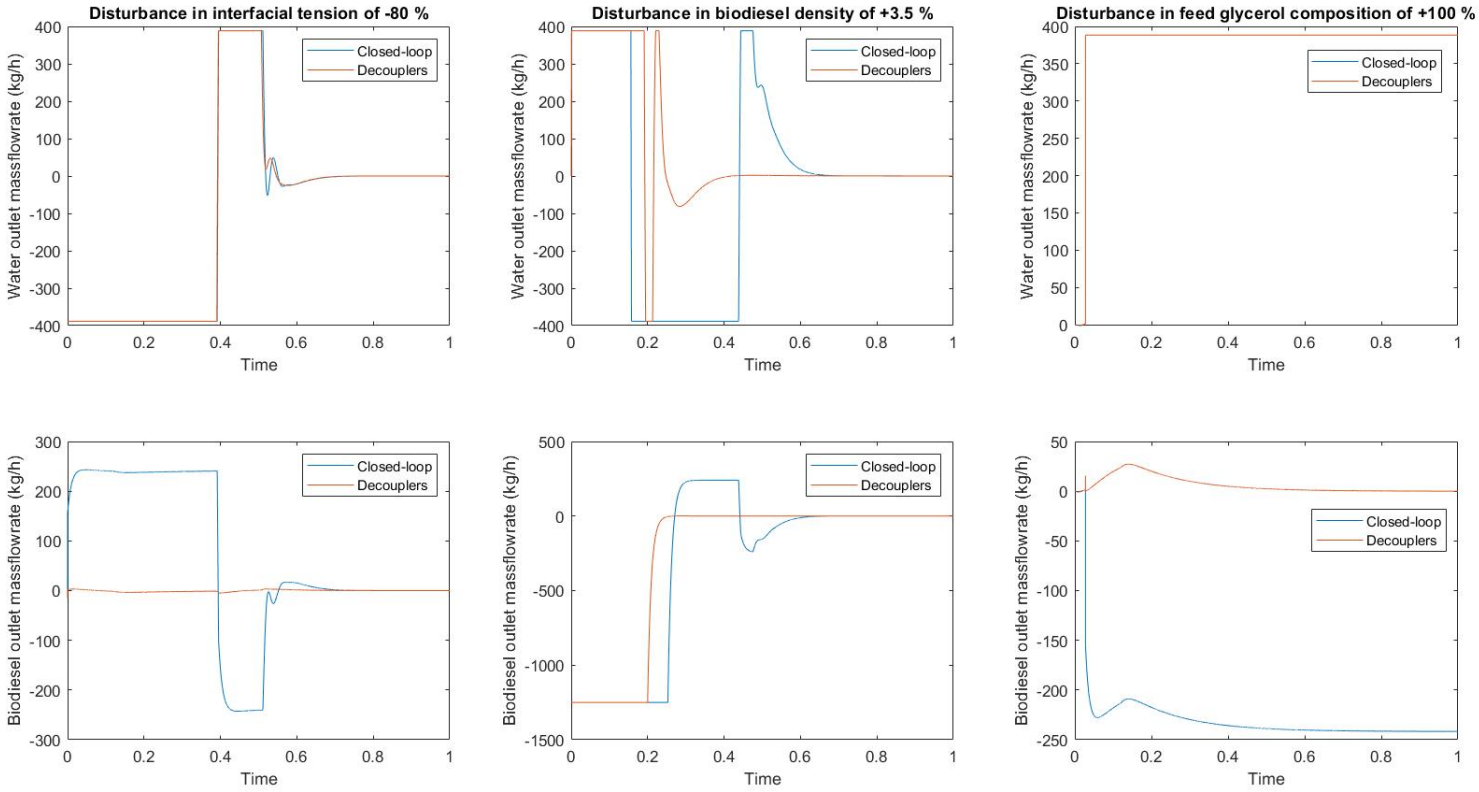

Figure 4.24: Evolution of the manipulated variables: water and biodiesel outlet mass flowrates (kg/h) to disturbances in interfacial tension, biodiesel density and feed glycerol composition.

5

Conclusion and Future Work

The present work focused on the development of a dynamic model for a biodiesel washing column which was motivated by a real problem in an industrial unit of a biodiesel production plant. The usage of biodiesel from virgin oils is expensive, so the incorporation of used cooking oils has been growing in the last decade and is expected to keep this trend. This alternative is economically and environmentally advantageous, however, the contamination present in these used oils present a challenge in the production of biodiesel due to their quality, and quantity of impurities. The development of a dynamic model for the column helps to predict and avoid certain problems related to these impurities.

A dynamic rate-based model for the liquid-liquid extraction column was build, where phenomena such as flooding, convergence velocity, holdup, and phase inversion were considered. The properties of biodiesel, density, viscosity, were also estimated. The model was validated with industrial data provided by an industrial partner and the model accurately predicted the solubility of the solutes in the washed biodiesel. The effects of temperature, solvent to feed ratio, and biodiesel inlet flowrate on the system were tested and are in accordance with the real plant. A sensitivity analysis was performed to evaluate the impact of the presence of impurities (biodiesel interfacial tension) or different types of oils (biodiesel density) might have on the performance of the column. Additionally, other operating variables were also analysed such as interface level, and glycerol inlet composition that was not removed in the decanter. It was observed that at 50 $^{\circ}$C and for a solvent to feed ratio of 16.2 % the column had a better performance. In case of contamination, an approach to manipulate the working conditions was suggested in order to avoid flooding and phase inversion.

Finally, the system was further analysed in order to implement a 2 $\times$ 2 control scheme. The best suggested pairing was Glycerol outlet composition in biodiesel - water outlet flowrate, and holdup - biodiesel outlet flowrate. The controllers were then tuned with the Internal Model Control and Cohen-Coon methods, respectively. The addition of static decouplers was successful in minimizing strong loop interactions. Overall, the control system has a good performance for set-point tracking and disturbance rejection.

The development of a dynamic model of a liquid-liquid extraction column for a biodiesel/water system is innovative, more so with an implemented control system. It was not possible to develop a drop population balance model for this column due to lack of time, however, the development of this extremely detailed model could help surpass some of the observed limitations in the rate-based model. Furthermore, the implementation of a Model Predictive Control scheme would be highly interesting and undoubtedly useful to have a process running under the optimal working conditions.

Bibliography

[1] "Why biodiesel?" https://www.biodiesel.org/what-is-biodiesel/why-biodiesel, Accessed in 20-07-2021.

[2] S. Chattopadhyay and R. Sen, "Fuel properties, Engine performance and environmental benefits of biodiesel produced by a green process," Applied Energy, vol. 105, pp. 319–326, 2013.

[3] S. Živković and M. Veljković, "Environmental impacts the of production and use of biodiesel," Environmental Science and Pollution Research, vol. 25, no. 1, pp. 191–199, 2018.

[4] "Biodiesel benefits and considerations," https://afdc.energy.gov/fuels/biodiesel_benefits.html, Accessed in 21-07-2021.

[5] "Economics of Biofuels — US EPA," https://www.epa.gov/environmental-economics/economics-biofuels, Accessed in 04-08-2021.

[6] H. Huang, M. Khanna, H. Önal, and X. Chen, "Stacking low carbon policies on the renewable fuels standard: Economic and greenhouse gas implications," Energy Policy, vol. 56, pp. 5–15, 2013.

[7] A. Demirbas, "Political, economic and environmental impacts of biofuels: A review," Applied Energy, vol. 86, no. 1, pp. 108–117, 2009.

[8] "International Energy Data, Monthly Update," https://knoema.com/EIAINTL2018May/international-energy-data-monthly-update#, Accessed in 05-08-2021.

[9] A. v. Grinsven, E. v. d. Toorn, R. v. d. Veen, and B. Kampman, "Used Cooking Oil (UCO) as biofuel feedstock in the EU," Tech. Rep., 2020.

[10] M. Ellen Smith, B. Flach, K. Bendz, and S. Lieberz, "Biofuels Annual," United States Department of Agriculture, Tech. Rep., 2012.

[11] A. Tafesh and S. Basheer, "Pretreatment Methods in Biodiesel Production Processes," in Pretreatment Techniques for Biofuels and Biorefineries. Springer Berlin Heidelberg, 2013, ch. 18.

[12] J. V. Gerpen, B. Shanks, R. Pruszko, D. Clements, and G. Knothe, “Biodiesel Production Technology,” National Renewable Energy Laboratory, Tech. Rep., 2004.

[13] M. Ramos, A. P. S. Dias, J. F. Puna, J. Gomes, and J. C. Bordado, “Biodiesel Production Processes and Sustainable Raw Materials,” energies, vol. 4408, no. 12, pp. 1–30, 2019.

[14] R. Pruszko, “Biodiesel production,” in Bioenergy. Elsevier, 2020, no. 2004, ch. 23, pp. 491–514.

[15] Y. Zhang, M. A. Dubé, D. D. McLean, and M. Kates, “Biodiesel production from waste cooking oil: 1. Process design and technological assessment,” Bioresource Technology, vol. 89, no. 1, pp. 1–16, 2003.

[16] J. F. Granjo, B. P. Duarte, and N. M. Oliveira, “Integrated production of biodiesel in a soybean biorefinery: Modeling, simulation and economical assessment,” Energy, vol. 129, pp. 273–291, 2017.

[17] E. G. Azevedo and A. M. Alves, Engenharia de Processos de Separação, 3rd ed., IST Press, Ed., 2017.

[18] T. C. Frank, L. Dahuron, B. S. Holden, D. Prince, William, A. F. Seibert, and L. C. Wilson, “Liquid-Liquid Extraction and Other Liquid-Liquid Extraction Operations and Equipment,” in Perry’s Chemical Engineers’ Handbook, 2008, no. 11, pp. 15–1 – 15–105.

[19] S. Mohanty, “Modeling of liquid-liquid extraction column: A review,” Reviews in Chemical Engineering, vol. 16, no. 3, pp. 199 – 248, 2000.

[20] J. D. Seader, E. J. Henley, and D. K. Roper, Separation Process Principles, 4th ed., J. Wiley and Sons LTD, Ed., 2016.

[21] A. M. Sereno, T. F. Anderson, and A. G. Medina, “Dynamic simulation of liquid-liquid operations using simple non-linear models,” Computers and Chemical Engineering, vol. 11, no. 2, pp. 177–185, 1987.

[22] A. C. G. Braz, “Profitability Increase of a Formaldehyde Production Plant,” Ph.D. dissertation, Instituto Superior Técnico, 2019.

[23] Ramesh K., Aziz N., Abd Shukor S.R., and Ramasamy M., “Dynamic Rate-Based and Equilibrium Model Approaches for Continuous Tray Distillation Column,” Journal of Applied Sciences Research, vol. 3, no. 12, pp. 2030–2041, 2007.

[24] H. J. Bart, H. Jildeh, and M. Attarakih, “Population Balances for Extraction Column Simulations—An Overview,” Solvent Extraction and Ion Exchange, vol. 38, no. 1, pp. 14–65, 2020.

[25] D. Ramkrishna, Population Balances: Theory and Applications to Particulate Systems in Engineering. Academic Press, 2000.

[26] J. C. Godfrey and M. J. Slater, Liquid-Liquid Extraction Equipment, 1994.

[27] O. Weinstein, R. Semiat, and D. R. Lewin, "Modeling, simulation and control of liquid-liquid extraction columns," Chemical Engineering Science, vol. 53, no. 2, pp. 325–339, 1998.

[28] M. Faulde, E. Siemes, D. Wöll, and A. Jupke, "Fluid dynamics of microgel-covered drops reveal impact on interfacial conditions," polymers, vol. 10, no. 8, pp. 1 – 16, 2018.

[29] J. Mackowiak, Fluid Dynamics of Packed Columns, 1st ed. Springer, 2010.

[30] S. Bhatia, "Biodiesel," in Advanced Renewable Energy Systems, 2014, ch. 22, pp. 573–626.

[31] N. K. Patel and S. N. Shah, Biodiesel from Plant Oils. Elsevier Inc., 2015.

[32] Y. C. Su, Y. A. Liu, C. A. Diaz Tovar, and R. Gani, "Selection of prediction methods for thermophysical properties for process modeling and product design of biodiesel manufacturing," Industrial and Engineering Chemistry Research, vol. 50, no. 11, pp. 6809–6836, 2011.

[33] L. Gouveia, A. C. Oliveira, R. Congestri, L. Bruno, A. T. Soares, R. S. Menezes, N. R. Filho, and I. Tzovenis, Biodiesel from microalgae. Elsevier Ltd., 2017.

[34] D. Babu and R. Anand, Influence of fuel injection timing and nozzle opening pressure on a CRDI-assisted diesel engine fueled with biodiesel-diesel-alcohol fuel. Elsevier Ltd., 2019.

[35] M. Mofijur, M. G. Rasul, N. M. Hassan, H. H. Masjuki, M. A. Kalam, and H. M. Mahmudul, "Assessment of physical, chemical, and tribological properties of different biodiesel fuels," in Clean Energy for Sustainable Development: Comparisons and Contrasts of New Approaches. Elsevier, 2017, ch. 14, pp. 441–463.

[36] M. J. Pratas, S. V. Freitas, M. B. Oliveira, S. C. Monteiro, Á. S. Lima, and J. A. Coutinho, "Biodiesel density: Experimental measurements and prediction models," Energy and Fuels, vol. 25, no. 5, pp. 2333–2340, 2011.

[37] L. Zong, S. Ramanathan, and C. C. Chen, "Erratum: Fragment-based approach for estimating thermophysical properties of fats and vegetable oils for modeling biodiesel production processes," Industrial and Engineering Chemistry Research, vol. 49, no. 6, pp. 3022–3023, 2010.

[38] H. G. Rackett, "Equation of State for Saturated Liquids," Journal of Chemical and Engineering Data, vol. 15, no. 4, pp. 514–517, 1970.

[39] R. Ceriani, C. B. Gonçalves, and J. A. Coutinho, “Prediction of viscosities of fatty compounds and biodiesel by group contribution,” Energy and Fuels, vol. 25, no. 8, pp. 3712–3717, 2011.

[40] A. Plus, A. Properties, A. E. Suite, A. Technology, T. C. Park, and O. Systems, “Part Number : Aspen Physical Property System 11 . 1 September 2001,” Engineering, pp. 2–18, 2001.

[41] F. Jufu, L. Buqiang, and W. Zihao, “Estimation of Fluid-fluid Interfacial Tensions of Multicomponent Mixtures,” Chemical Engineering Science, vol. 41, no. 10, pp. 2673–2679, 1986.

[42] D. S. Abrams and J. M. Prausnitz, “Statistical thermodynamics of liquid mixtures: A new expression for the excess Gibbs energy of partly or completely miscible systems,” AIChE Journal, vol. 21, no. 1, pp. 116–128, 1975.

[43] R. C. Reid, T. K. Sherwood, and R. E. Street, The Properties of Gases and Liquids, 4th ed., 1959.

[44] K. Sivaramakrishnan and P. Ravikumar, “Determination of cetane number of biodiesel and it’s influence on physical properties,” ARPN Journal of Engineering and Applied Sciences, vol. 7, no. 2, pp. 205–211, 2012.

[45] R. O. Dunn, “Cold flow properties of biodiesel: A guide to getting an accurate analysis,” Biofuels, vol. 6, no. 1-2, pp. 115–128, 2015.

[46] A. S. Brásio, A. Romanenko, J. Leal, L. O. Santos, and N. C. Fernandes, “Nonlinear model predictive control of biodiesel production via transesterification of used vegetable oils,” Journal of Process Control, vol. 23, no. 10, pp. 1471–1479, 2013.

[47] A. S. Brásio, A. Romanenko, N. C. Fernandes, and L. O. Santos, “First principle modeling and predictive control of a continuous biodiesel plant,” Journal of Process Control, vol. 47, pp. 11–21, 2016.

[48] A. S. Brásio, A. Romanenko, and N. C. Fernandes, “Simulation and advanced control of the continuous biodiesel production process,” Springer Proceedings in Mathematics and Statistics, vol. 224, pp. 127–146, 2018.

[49] D. S. Patle, Z. Ahmad, and G. P. Rangaiah, “Plantwide control of biodiesel production from waste cooking oil using integrated framework of simulation and heuristics,” Industrial and Engineering Chemistry Research, vol. 53, no. 37, pp. 14 408–14 418, 2014.

[50] B. Grosman and D. R. Lewin, “Automated nonlinear model predictive control using genetic programming,” Computers and Chemical Engineering, vol. 26, no. 4-5, pp. 631–640, 2002.

[51] “Process Control,” in Chemical Process Equipment, second edi ed., J. R. Couper, W. R. Penney, J. R. Fair, and S. M. Walas, Eds., 2010, ch. 3, pp. 31–51.

[52] D. Seborg, T. Edgar, D. Mellicamp, and F. Doyle III, Process Dynamics and Control, 3rd ed., 2011.

[53] S. Skogestad, “Probably the best simple PID tuning rules in the world,” Journal of Process Control, pp. 1–28, 2001.

[54] P. Woolf, “9.3: PID Tuning via Classical Methods - Engineering LibreTexts,” https://eng.libretexts.org/Bookshelves/Industrial_and_Systems_Engineering/Book%3A_Chemical_Process_Dynamics_and_Controls_(Woolf)/09%3A_Proportional-Integral-Derivative_(PID)_Control/9.03%3A_PID_Tuning_via_Classical_Methods, Accessed in 14-10-2021.

A

Transfer Functions for the linearised system

The transfer functions that described the behaviour of the linearised system are shown in Table A.1 for the outlet flowrates, and Tables A.2 to A.4 for the variables related to biodiesel properties.

Table A.1: Transfer functions for the outlet flowrates and output variables.

Transfer Functions	Q_{out} water	R^2	Q_{out} biodiesel	R^2
Biodiesel Glycerol Composition (wt%)	$\frac{6.192\text{E}(-07)s-0.005975}{s^2+121.6s+644.9}$	99.7 %	$\frac{7.395\text{E}(-05)s^2+0.01609s+0.1353}{s^3+137.3s^2+8362s+4.404\text{E}04}$	97.9 %
Flooding Continuous Phase %	$\frac{359.9s^2+3.15\text{E}04s+2.836\text{E}05}{s^3+6.751\text{E}04s^2+5.975\text{E}06+5.519\text{E}07}$	99.5 %	$\frac{358.3s+2.501\text{E}04}{s^2+4.925\text{E}04+3.412\text{E}06}$	99.1 %
Flooding Dispersed Phase %	$\frac{-58.41s^2-4657s-3.88\text{E}04}{s^3+6.209\text{E}04+5.083\text{E}06+4.668\text{E}07}$	99.5 %	$\frac{77.49s+4937}{s^2+8.695\text{E}04s+5.342\text{E}06}$	96.9 %
Holdup (fraction)	$\frac{0.8514s^2+14.77s+52.96}{s^3+4.469\text{E}04s^2+7.903\text{E}05+2.815\text{E}06}$	99.7 %	$\frac{1.664s+6.588}{s^2+5.508\text{E}04+2.18\text{E}05}$	99.9 %
Phase Inversion Parameter	$\frac{1.343s+18.27}{s^2+3.652\text{E}04+5.283\text{E}05}$	95.4 %	$\frac{2.305s+171}{s^2+4.212\text{E}04+3.109\text{E}06}$	99.4 %

Table A.2: Transfer functions for the interfacial tension and output variables.

Transfer Functions	Interfacial Tension (N/m)	R^2
Biodiesel Glycerol Composition (wt%)	$\frac{0.04171s^3+89.82s^2+1.365\text{E}04s+9.367\text{E}04}{s^3+158.7s^2+9404s+5.426\text{E}04}$	96.7 %
Flooding Continuous Phase %	$\frac{-5642s^4-1.263\text{E}06s^3-1.92\text{E}08s^2-1.205\text{E}10s-1.169\text{E}11}{s^4+224.5s^3+3.408\text{E}04s^2+2.163\text{E}06s+2.103\text{E}07}$	95.7 %
Flooding Dispersed Phase %	$\frac{-2295s^3-3.249\text{E}05s^2-2.374\text{E}07s-2.127\text{E}08}{s^3+141.5s^2+1.043\text{E}04s+9.376\text{E}04}$	95.3 %
Holdup (fraction)	$\frac{1.313s-11.59}{s^2+90.95s+634.3}$	98.6 %
Phase Inversion Parameter	$\frac{13.08s+10.25}{s^2+95.77s+760.4}$	97.3 %

Table A.3: Transfer functions for the biodiesel density and output variables.

Transfer Functions	Biodiesel Density (kg/m^3)	R^2
Biodiesel Glycerol Composition (wt%)	$\frac{0.01097s^3+0.7538s^2+264s+2494}{s^4+188.1s^3+2.431\text{E}04s^2+1.365\text{E}06s+1.193\text{E}07}$	95.5 %
Flooding Continuous Phase %	$\frac{0.5138s^5+141.7s^4+4.154\text{E}04s^3+5.192\text{E}06s^2+3.555\text{E}08s+2.807\text{E}09}{s^5+276.8s^4+8.082\text{E}04s^3+1.015\text{E}07s^2+6.894\text{E}08s+5.451\text{E}09}$	94.4 %
Flooding Dispersed Phase %	$\frac{-0.07315s^4-13.59s^3-2046s^2-1.126\text{E}05s-8.302\text{E}05}{s^4+187.7s^3+2.804\text{E}04s^2+1.583\text{E}06s+1.179\text{E}07}$	97.4 %
Holdup (fraction)	$\frac{0.002646s^3+0.5172s^2+41.69s+298.2}{s^3+195.5s^2+1.574\text{E}04s+1.127\text{E}05}$	95.8 %
Phase Inversion Parameter	$\frac{0.005962s^3+0.9461s^2+59.67s+421.3}{s^3+158.5s^2+9974s+7.053\text{E}04}$	96.9 %

Table A.4: Transfer functions for the feed glycerol composition and output variables.

Transfer Functions	Feed Glycerol Composition (wt%)	R^2
Biodiesel Glycerol Composition (wt%)	$e^{-0.0277s}\frac{3007s+7.68\text{E}04}{s^2+253.2s+1883}$	96.4 %
Flooding Continuous Phase %	$e^{-2.0283s}\frac{3765s^3+2.217\text{E}05s^2+3.179\text{E}06s-1.274\text{E}07}{s^4+411.8s^3+2.222\text{E}04s^2+5.155\text{E}05s+2.801\text{E}06}$	94.7 %
Flooding Dispersed Phase %	$e^{-0.003s}\frac{-261.3s+2562}{s^2+74.5s+607.5}$	95.2 %
Holdup (fraction)	$\frac{2.369s-211.3}{s^2+81.64s+549.6}$	98.8 %
Phase Inversion Parameter	$\frac{-109.1s-3871}{s^2+342.9s+2579}$	97.8 %